Bifurcation analysis of a system of Morris-Lecar neurons with time delayed gap junctional coupling

by

Ilya Kobelevskiy

A thesis
presented to the University of Waterloo
in fulfillment of the
thesis requirement for the degree of
Master of Mathematics
in
Applied Mathematics

Waterloo, Ontario, Canada, 2008

I hereby declare that I am the sole author of this thesis. This is a true copy of the thesis, including any required final revisions, as accepted by my examiners.

I understand that my thesis may be made electronically available to the public.

Abstract

We consider a system of two identical Morris-Lecar neurons coupled via electrical coupling. We focus our study on the effects that the coupling strength, γ, and the coupling time delay, τ, cause on the dynamics of the system.

For small γ we use the phase model reduction technique to analyze the system behavior. We determine the stable states of the system with respect to γ and τ using the appropriate phase models, and we estimate the regions of validity of the phase models in the γ, τ plane using both analytical and numerical analysis.

Next we examine asymptotic of the arbitrary conductance-based neuronal model for $\gamma \to +\infty$ and $\gamma \to -\infty$. The theory of nearly linear systems developed in [30] is extended in the special case of matrices with non-positive eigenvalues. The asymptotic analysis for $\gamma > 0$ shows that with appropriate choice of γ the voltages of the neurons can be made arbitrarily close in finite time and will remain that close for all subsequent time, while the asymptotic analysis for $\gamma < 0$ suggests the method of estimation of the boundary between "weak" and "strong" coupling.

Acknowledgements

I would like to acknowledge and express my gratitude to my supervisor Sue Ann Campbell. Her helpful suggestions, motivation for research, guidance through the study process and help with involvement in student research group meetings made this thesis possible. I would like to thank the faculty and staff of the Department of Applied Mathematics of University of Waterloo for a friendly and supportive research atmosphere, and for the knowledge and experience that I have obtained here. I would like to thank the faculty and staff of Lomonosov Moscow State University for the basis of mathematical education that I have obtained there. Finally, I would like to thank my family and friends for their moral support during the development of the present thesis.

Contents

List of Tables

List of Figures

Chapter 1

Introduction

The present thesis is devoted to the analysis of gap-junctional coupling between neurons. Neurons can exchange signals between each other via two qualitatively different mechanisms - electrical coupling realized by gap-junction connections and chemical coupling provided by neurotransmitters. Early studies of neurons assumed that most of the information in higher mammals is transmitted by chemical coupling. However, newer studies suggest that gap-junctional connections in higher mammals occur more frequently than was initially assumed [1].

To begin we briefly review the literature on gap-junctional coupling. Recent studies have verified the existence of gap junctional connections in neocortex, auditory cortex and hippocampus of higher mammals including humans [1, 2, 3, 12, 13, 14, 15]. In many cases electrical and chemical coupling occur together [1, 3, 12, 28]. Electrical coupling frequently occurs between neurons of similar type [2, 12, 27] and sometimes between the neurons of different types [15]. In the case when electrical coupling occurs between the same type of neurons, it is believed to contribute to *synchronization* of the neuronal behavior [2, 13, 27]. Chemical and electrical coupling often occur together, and in these cases they can lead to complicated behavior, for example, bistable synchronous and anti-synchronous behavior patterns were observed in GABAergic neurons [28].

Finally, we note that electrical coupling can occur between neurons separated by distances from $50\mu m$ [14] up to $\approx 1000\mu m$ [12]. The latter relatively large distance may cause an effect of *time delay* in the signal transmission. The strength of the electrical coupling can vary as well. Scientists distinguish *weak* and *strong* coupling. Weak coupling is usually understood as infinitesimal coupling, or coupling that is small enough in order to be considered as a small parameter in the perturbational analysis. *Strong* hence denotes any coupling that cannot be considered as *weak*. Some aspects of the relationship between strong and weak coupling in gap-junctional coupled neurons were studied in [38].

An increased interest in electrical coupling in the biological literature motivated us to study the effects of the coupling strength and time delay on an electrically coupled neuronal network. In order to address this question, we choose to study

a simple network of two identical electrically coupled neurons. Each neuron is modeled by the Morris-Lecar neuronal model, which is a simple neuronal model having biophysical meaning. Another advantage of Morris-Lecar model is the fact that it can demonstrate two different classes of neuronal excitability.

We will analyze electrical coupling in the dynamical systems framework. The analysis is done with respect to all values of the coupling strength. Despite the fact that negative and large positive values of coupling strength are physically impossible, inclusion of those values in our study helps to better understand the dynamics in the physical parameter range, and hence contributes to the development of a general theory.

Analysis of neural systems with time delay is important and yet not fully developed mathematical problem. Variation of the time delay can cause various effects on the system, including oscillator death or attractor switching (see [6]). [6] provides an overview of the possible effects of delays on the neural systems. Type I and type II excitable systems with time delays were studied in [4] using the Terman-Wang and Fizhugh-Nagumo models. However, in this and some other papers on neural networks with time delays neurons are considered to be non-oscillating in the uncoupled state, while we will consider inherently oscillating neurons. This setup leads to analysis of phase models with time delay in the case of weak coupling. Studies in this area were recently done by Smith in [34]. However, in his paper Smith considers Fithzugh-Nagumo model, which is of type II only. The present thesis hence complements the analysis done in [34] and [4].

In the present thesis we also go beyond weak coupling and perform asymptotic analysis on an arbitrary conductance-based model for large positive and negative values of the coupling strength. It turns out that this analysis contributes to the theory of nearly linear systems developed in [30], provides a way to estimate a boundary between weak and strong coupling for an arbitrary gap junctionally coupled model, and contributes to the understanding of the effects of gap junctional coupling on synchronization.

The present thesis has the following structure. In **chapter 2** we provide the physical background to the problem. We describe the way in which the neuron generates and transmits signals, types of neuronal excitability, possible ways of modeling neurons, derivation and properties of the Morris-Lecar model, mechanisms and ways of mathematical modeling of electrical and chemical coupling. The mathematical definition of the problem to be studied concludes the chapter.

Chapter 3 is devoted to analysis of the coupled Morris-Lecar system in the case of *weak* coupling. We approach the problem using an *invariant manifold reduction* technique, and hence reduce the complete coupled Morris-Lecar system to the corresponding phase model. Next we determine the stable periodic solutions by analysis of the phase model with respect to the values of the coupling strength and time delay.

In **Chapter 4** the coupled Morris-Lecar system is analyzed numerically. We determine the structure of equilibrium points, analyze the bifurcation diagram of

the non-delayed Morris-Lecar model using XPPAUT software, and then analyze the bifurcation diagrams of the delayed Morris-Lecar model using DDE-BIFTOOL. Numerical analysis verifies the correctness of the analysis done in chapter 3 and provides an estimate of the region of validity of the phase model.

In **Chapter 5** we analyze the special case of large values of the coupling strength using asymptotic analysis, and **Chapter 6** summarizes results of the present thesis and suggest directions of possible future work.

Chapter 2

Physical background

In this chapter we will provide a short physical background to the area of our research.We start with the definition and general description of a typical neuron and its properties following [37] and [26]. Next we examine the principles of mathematical modeling of neuronal signal generation and transmission. We consider the underlying principles and assumptions of single-compartment conductance-based models. This part mainly follows [7] and [33].

The general information discussed above provides a basis which allows us to proceed to a detailed description of the model we are going to work with: the Morris-Lecar model. We begin our examination of the model with a study of the experiments and methods that led to the derivation of the model; mainly the original paper of Morris and Lecar [29] and a recent summary article written by Lecar [25] will be considered. Next we non-dimensionalize the model and discuss the mathematical properties of the non-dimensionalized version following the analysis of Rinzel and Ermentrout [32].

At the end of the present chapter we discuss types of connections between neurons. A short overview of possible connection types is followed by a more detailed examination of the electrical type of connection and its mathematical modeling. The content of the chapter provides a motivation for the problem that is going to be studied throughout this thesis. Thus, the full problem formulation completes the present chapter.

2.1 Structure of a typical neuron. Signal generation and transmission in neurons.

I would like to start this section with an elegant definition of the neuron given by Llinas in [26]:

"Neurons are the cells that underlie the function of the nervous system including the brain, spinal cord, peripheral sensory systems and enteric (gut) nervous

system. The anatomical variation of these neurons is large, but the general morphology allows these cells to be classed as 'neurons' (coined in 1891 by Wilhelm von Waldeyer)".

Following the definition above, consider the typical neuron morphology.

2.1.1 Structure of a single neuron

Figure (2.1) provides the schematic structure of a neuron. The important functional parts are labeled on the figure. A short description of each part and its functionality is provided below. More detailed descriptions of selected parts of the neuron and their role are given in the following subsections.

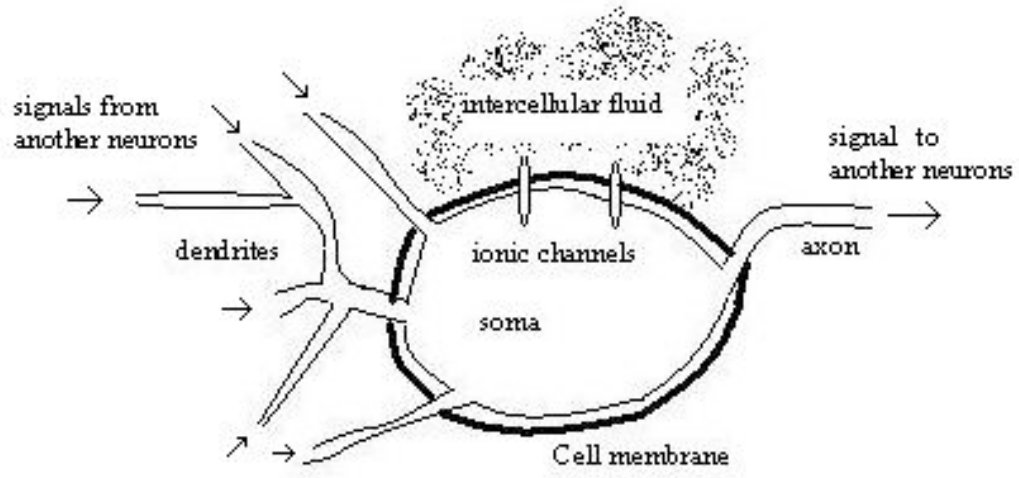

Figure 2.1: Typical neuron morphology

The *soma* is the central cell body of the neuron. It contains the neuron's genetic material. The soma is responsible for maintaining the neuron's vital activity, processing incoming currents and generation of a response signal. The soma is surrounded by the *cell membrane*, which bounds the soma and defines the intracellular area. The cell membrane contains the *ionic channels*, which are responsible for transmission of ions and play an important role in the generation of electrical signals by the neuron. The *dendrites* are branch-like protrusions which come out of the cell body. A typical cell has a large number of the dendrites which are highly branched. Dendrites are responsible for delivering information from the other neurons and receptors to the cell. The *axon* is a long fiber-like extension of the soma. It is responsible for the transmission of a signal to another neuron. The space outside of the neuron is filled by the *intercellular fluid*.

It worth mentioning that not all neurons necessarily fit into the scheme presented here (see [26] for more detailed overview and for the possible exceptions). Nevertheless, the structure of the vast majority of neurons can be represented by the scheme provided, and we will consider only such neurons in this thesis.

2.1.2 Signal generation and procession in neuron.

On the intracellular level signals are transmitted mostly in electrical form. The neuron receives an input current from the other neurons and receptors via its dendrites, processes this input electrical current and generates some output. An output is then transmitted via the neuron's axon in the form of a self-regenerating electrical wave, also known as an *action potential* or *spike*. Before describing the process of the signal transmission and generation, let us discuss the electro-chemical mechanism of the neuron first.

Consider a neuron in its steady state, i.e. with an absence of any input. Both the interior and exterior of the neuron contain some number of charged ions.[1] The concentrations of ions of each type outside and inside of the neuron are different. This difference in concentrations causes a voltage drop or potential difference across the cell membrane, which is typically -50 to -80 mV depending on the type of neuron being examined. This steady state voltage drop is also known as the *resting potential* or the *equilibrium potential* of a neuron.

The energy for maintaining nonzero equilibrium potential is produced by a mechanism which is called a *biological ionic pump*. The biological ionic pump transfers the ions from one side of membrane to another using the power produced by burning sugar and molecular oxygen.

However, there is a mechanism which acts against the biological ionic pump. The cell membrane could let in some particular types of ions through *ionic channels*. Each ionic channel (or gate) is responsible for its particular type of ion and could vary between an open and closed state depending on the membrane voltage and other biological properties.

When an ionic channel is open, the ions governed by this channel are able to cross the membrane in the direction of their concentration and electro-chemical gradients. As the ions flow through an open channel, it changes both the membrane potential and the distribution of concentrations on the sides of the membrane. As the membrane voltage reaches a certain value, electro-chemical and concentration gradients become balanced, and ionic flow stops. This membrane voltage is called *equilibrium* or *reversal* potential for the type of ions under consideration. The term reversal is used because when the membrane potential passes through the

[1] The types of ions involved in the electrical process are different and could vary depending on the type of neuron being considered. However, potassium (K^+), sodium (Na^+), chloride (Cl^-) and calcium (Ca^{++}) ions typically make the most noticeable contribution in neuronal electro-chemical processes.

equilibrium potential of a certain ion type the direction of flow of that type of ion *reverses*. As long as we consider a particular type of neuron with the preset structure of ionic channels and pumps, the equilibrium potentials of each type of ions involved in the process are determined by that structure. It is possible to compute the equilibrium potential of each type of ion by evaluating its concentration gradient using the principles of statistical mechanics and finding the corresponding membrane potential. Equilibrium potentials for each type of ion involved in the process are different. As was mentioned above, in the absence of any external input the biological ionic pump and the ionic channels balance each other, keeping the neuron at its resting potential.

At this point I would like to make a comment about some common terminology. If the equilibrium potential of some type of ion is greater than the *resting potential* of the neuron, then the flow of ions of that type would try to increase the membrane potential in case of the corresponding ionic channel being opened. The current caused by this type of the ion is called *excitatory* or *depolarizing* current. The current depolarizes the cell membrane by making its potential more positive and excites the cell membrane by releasing the energy stored by the biological ionic pump.[2] Otherwise the current is called *hyperpolarizing* or *recovery* current. We follow [23] with this terminology, and we will use it consistently throughout the thesis.

Now we are ready to consider a neuron that is receiving some signal. The electrical current coming to the neuron by its dendrites or via experimental electrode is also called *applied* or *injected current*. Depending on its nature, injected current could either decrease or increase membrane potential. Consistent with the terminology above, the current that is decreasing membrane potential is called *hyperpolarizing* or *inhibitory* current, while the current that is increasing membrane potential is called *depolarizing* or *excitatory*.

Let us first consider the case where the injected current is given by a single pulse. When a pulse is not big enough, the cell membrane responds with an exponentially decaying RC-type voltage perturbation and then returns to its rest state. However, if the injected current is big enough to make the membrane voltage exceed its *threshold* value (typically around -55 mV), the neuron generates a single pulse which is then propagated without weakening along all the branches of the axon. Generation and maintenance of this pulse is provided via the mechanism described above, by realizing the energy stored by the biological ionic pump through the voltage-dependent ionic currents. Figures (2.2) and (2.3) provide an illustration of the behavior described above. Figure (2.2) shows four square wave signals that were applied to a neuron which was initially at its resting potential(-50 mV for the neuron under consideration). Current stimuli of 20 and 40 μA were not strong enough to increase the voltage beyond its threshold value and the neuron responded with an RC-type signal. However, currents of 60 and 80 μA were strong enough

[2]Recall that ionic pump attempts to keep membrane potential at a negative value. In other words it is constantly hyperpolarizing membrane until it reaches its equilibrium potential.

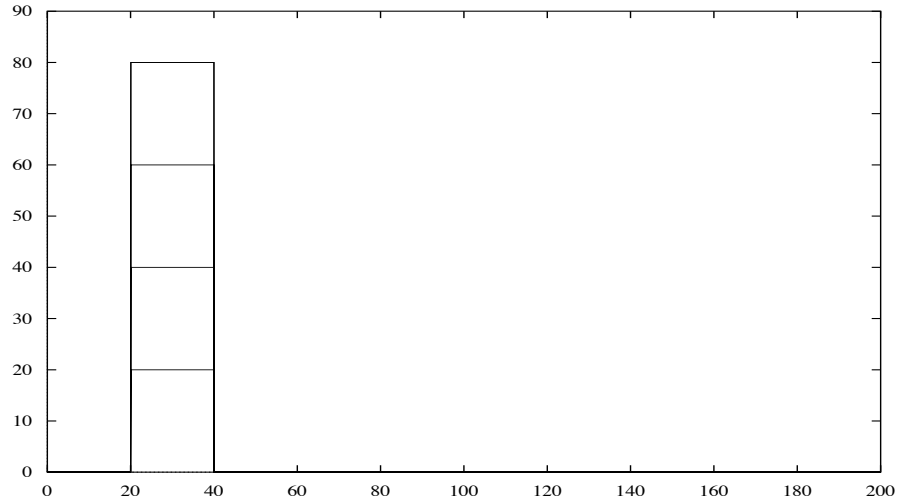

Figure 2.2: Injected pulses

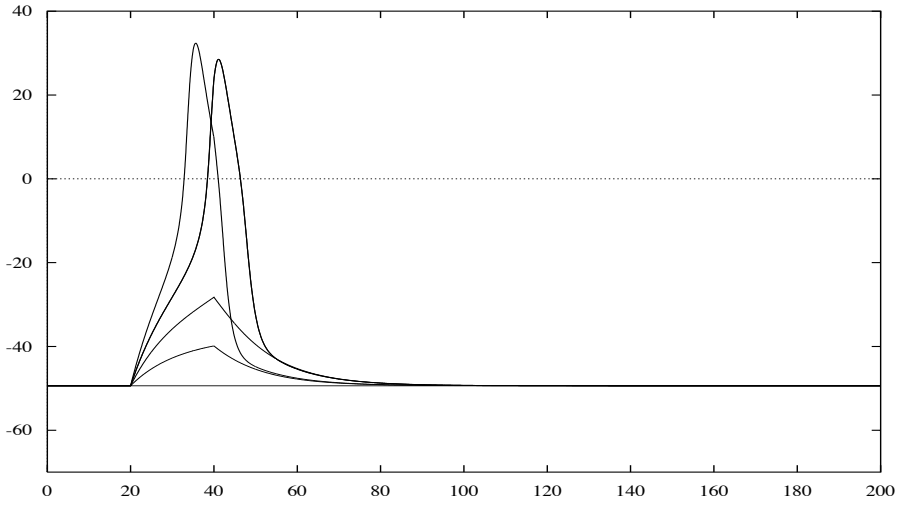

Figure 2.3: Responses of the neuron to the pulses injected

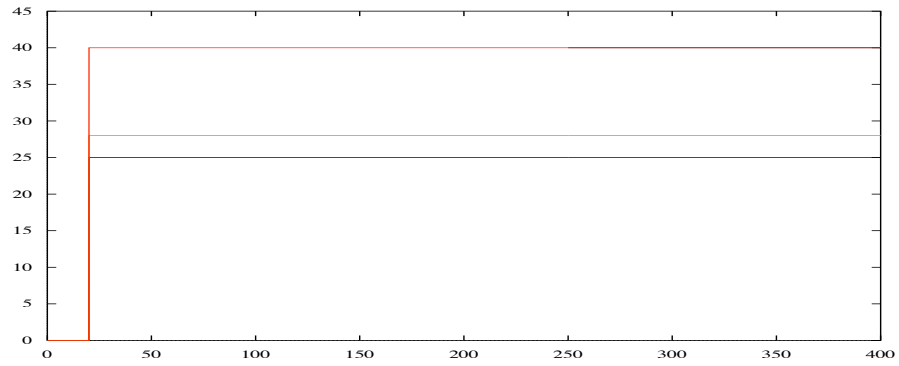

Figure 2.4: Input applied to a neuron

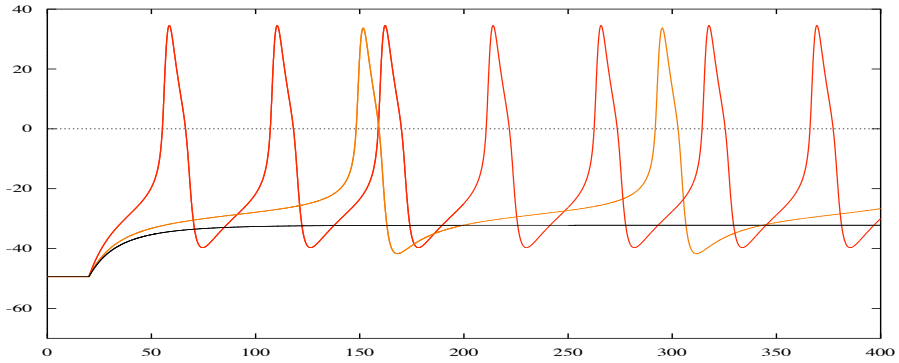

Figure 2.5: Response of the type I

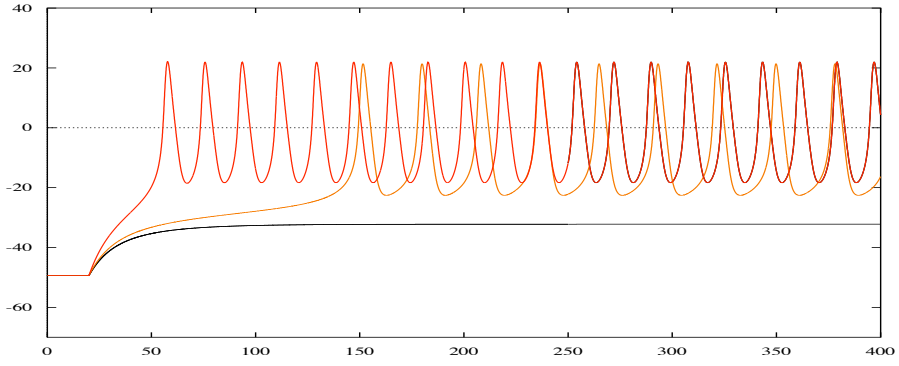

Figure 2.6: Response of the type II

to increase the voltage beyond its threshold value. The neuron responded with an action potential which consisted of the rapid overshoot over zero potential following by a rapid hyperpolarization. Figures (2.2) and (2.3) were created by numerical simulation of the Morris-Lecar neuron model with the XPPAUT software. The set of physical parameters was taken to be equal to the set used in the original simulations in [29].

Let us now consider the case where the signal is not a singular pulse but a sustained constant input. If the input signal I is above the threshold value, the neuron could demonstrate various and very rich behavior, depending on its type and the nature of the incoming signal. One of the possible responses is an *oscillatory response*. I would like to discuss oscillatory phenomena more fully, since it is important for the research done in the present thesis. Oscillations are the periodic in time series of spikes or sine-like waves. Depending on the neuron being considered, the scientists distinguish between two different types of oscillations, which are called *type I* and *type II* oscillations, respectively. This classification was first observed and introduced by Hodgkin in his work [18]. Let us illustrate the difference between those two types by consideration of an example.

Figures (2.5) and (2.6) provide the response of neurons exhibiting type I and type II oscillations to the same applied stimulus, which is provided on figure (2.4). As the applied current passes its threshold value, the type I neuron starts oscillations with the small frequency. As the input increases, the oscillation frequency increases as well. However, the oscillator frequency could be made arbitrarily small by an appropriate choice of the strength of the applied current.

The oscillator of type II demonstrates qualitatively different behavior. Oscillations are set at some *fixed* frequency, which cannot be made any smaller. If the value of the applied current gets close to its threshold value, it may affect the time required for oscillations to start. However, the steady state frequency of oscillations does not get below some nonzero value.

The difference between type I and type II oscillations could be observed more clearly by considering the relationship between the period of oscillations and the value of the applied current I. Figures (2.7) and (2.8) provide period vs I graphs for type I and type II oscillations respectively. These plots were created by numerical continuation with respect to I of the periodic solution of the Morris-Lecar equations. As we will see in the subsequent section, the Morris-Lecar equations are a mathematical model of a neuron, which can describe both type I and type II neurons depending on its parameter values. In the case of type I oscillation, the period of oscillations approaches infinity as I approaches its threshold value I_{tr}, whereas in the case of type II oscillation the period remains finite at $I = I_{tr}$. Note the different scales in the y axis of each graph.

Oscillations of both types are observed experimentally in neural networks. More theoretical information on signal processing and generation can be found in [7] or [23] , while papers [19] and [29] provide interesting experimental observations of neuronal behavior. Despite the fact that the figures provided to illustrate the

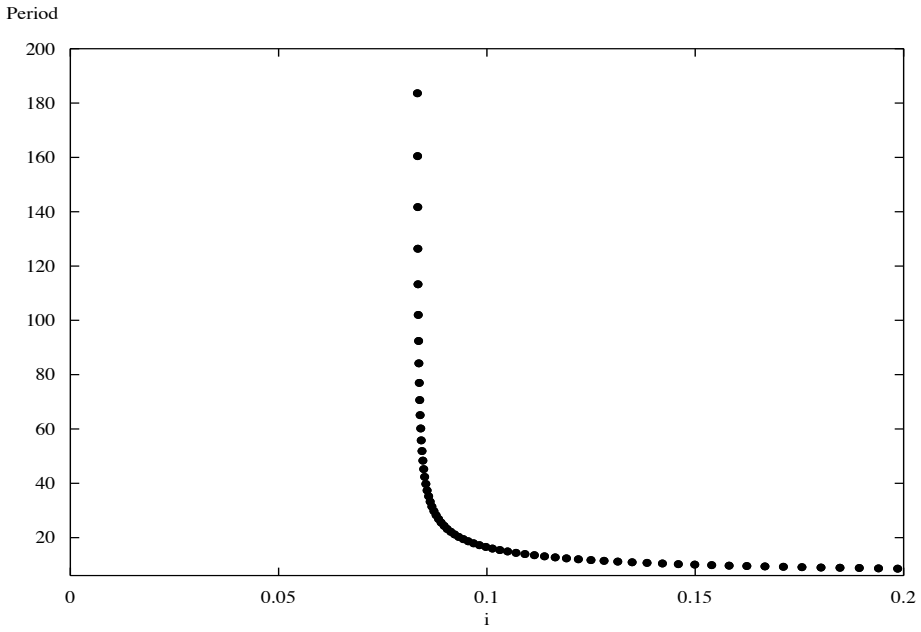

Figure 2.7: Period vs I plot for the type I oscillation

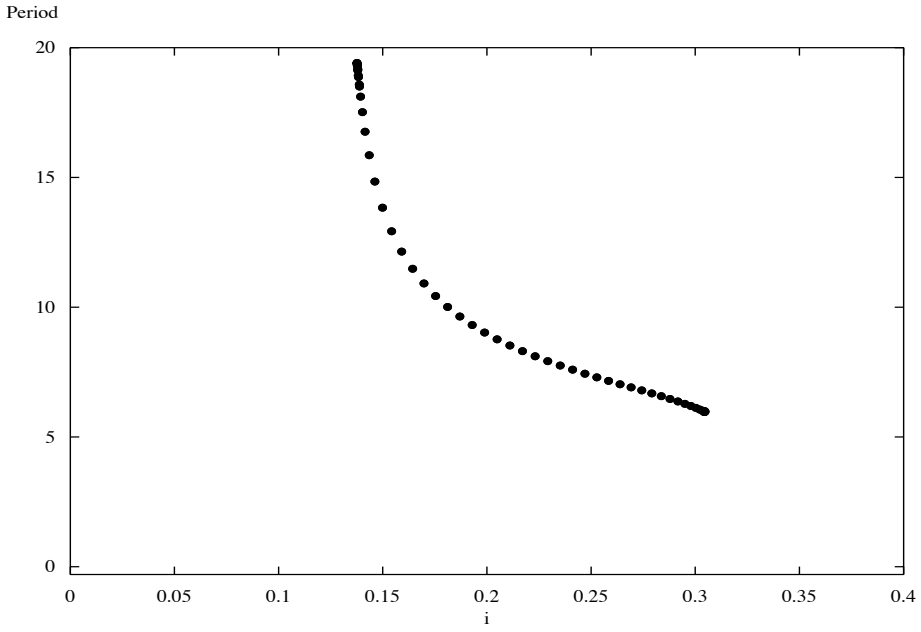

Figure 2.8: Period vs I plot for the type II oscillation

present section were created by numerical simulation of the mathematical model of the neuron, actual neurons demonstrate qualitatively the same behavior. However, experimental data cannot be included in the present thesis due to the copyright reasons. It can be found in [19], [11] or [18].

2.2 Neuron as a mathematical model.

There are several different approaches to mathematical modeling of signal generation and transmission in neurons. Among the most widely recognized are integrate-and-fire, spiking, soliton and conductance-based models. More detailed information on integrate-and fire and spiking models can be found in [7], while [16] provides an insight to the key concepts of soliton models. In this thesis we will consider only single-compartment conductance-based models. These are the simplest neural models where the parameters can be interpreted biophysically and measured experimentally.

2.2.1 General overview of underlying principles and derivation of single-compartment conductance-based models.

The basic foundations of conductance-based models were developed by Allan Lloyd Hodgkin and Andrew Huxley. Their original paper [19] was published in 1952 and introduced the first conductance-based model named in the honor of its inventors. The authors received the 1963 Nobel Prize in Physiology or Medicine for that work. [19] provides general ideas and methods to further work in the area. These ideas were generalized and further developed over the next 50 years. The formalization of the Hodgkin and Huxley point of view is nowadays known as the *conductance-based* approach to modeling neurons.

The electro-chemical mechanism of processing input current and signal generation in a neuron is replaced by a simplified electrical circuit in this method. The neuron membrane is modeled by a capacitor, while ionic gates and biological ionic pump are each represented by a conductance-battery pair. The electrical scheme of a neuron governed by n different ionic gates is shown in figure (2.9).

The conductance (inverse of resistance) g_i describes the state of i-th ionic gate. The closed ionic gate is modeled by $g_i = 0$, while the non-closed state of the ionic gate is described by some nonzero g_i, with a maximal value $\bar{g}_i$ corresponding to the ionic gate being completely open. It is always assumed that all ionic gates act independently from each other. The state of each gate could depend only on membrane potential and some other biological parameters, but not on the states of other ionic gates. Thus, $g_i = g_i(V, [\sigma_1, .., \sigma_n])$.

Battery V_i determines the strength and direction of i-th ionic flow. Thus, V_i is equal to the *reversal potential* of ions of i-th type, and the direction of the battery

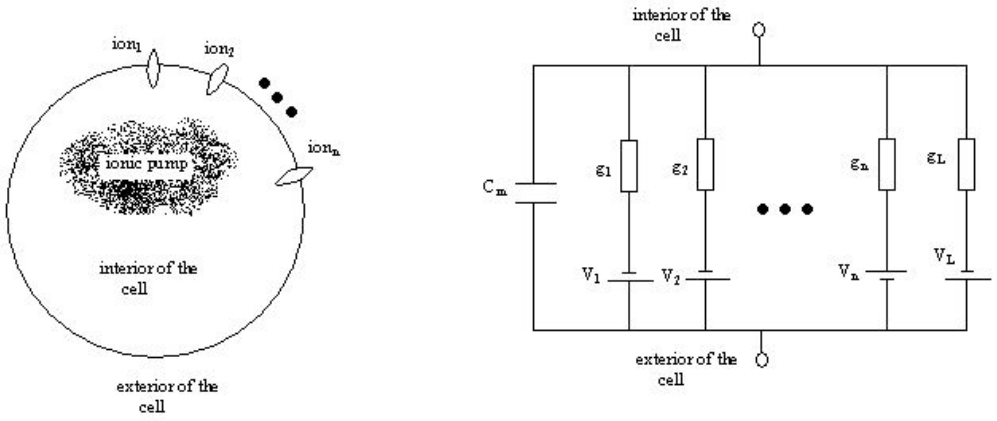

Figure 2.9: Neuron as an electrical ciruit

corresponds to the direction of ionic flow for the membrane voltage above and below the *reversal potential* respectively.

The biological ionic pump is modeled by the battery and resistor pair as well, and is typically included in a *leakage* current with equilibrium voltage V_L and conductance g_L. This leakage current represents ionic channels not included in the model as separate conductances, and the biological ionic pump itself.

According to Kirchhoff's law, the voltage of the circuit provided on the figure above is described by the following equation:

$$C\frac{dV}{dt} = I - g_L(V - V_L) - \sum_{i=1}^{N} g_i(V)(V - V_i). \tag{2.1}$$

The term I in the equation above represents the input signal, which is the *applied current* introduced in subsection 2.1.2. In order to complete the model above, it is necessary to specify each g_i as a function of V and possibly some other biological parameters of the system. For simplicity we will only consider g_i depending only on V. More specific models where conductances depend also on the concentration of various ions can be found in [7],[23]. Typically g_i are defined in the following form (from [33]):

$$g_i(V) = \bar{g}_i a^x b^y, \quad \text{or} \quad g_i(V) = \bar{g}_i a \tag{2.2}$$

where $\bar{g}_i$ is a constant corresponding to the maximal conductance of the ionic channel being considered, x and y are some fixed integers, while variables a and b describe the dynamics of the ionic channel being opened and closed. a and b are called "activation" and "inactivation" *gating variables* respectively. They are dimensionless and their values lie between 0 and 1.

The ionic channel is assumed to be voltage dependent. In other words, for each membrane voltage V there is fixed state (or conductance) of the ionic channel associated with this particular voltage V. However, as the membrane voltage changes

to some new voltage V', the ionic channel does not go to a state associated with V' instantaneously, but takes some time either for its "activation" or "inactivation". Variables a and b (or only variable a) describe this dynamics. It is assumed that the kinetics of variables a and b are first order, they are governed by the following equations:

$$\begin{array}{rcl} da/dt &=& [a_\infty(V)-a]/\tau_a(V) \\ db/dt &=& [b_\infty(V)-b]/\tau_b(V) \end{array} \quad ,or \quad \begin{array}{rcl} da/dt &=& \lambda_a(V)[a_\infty(V)-a] \\ db/dt &=& \lambda_b(V)[b_\infty(V)-b] \end{array} . \tag{2.3}$$

The functions $a_\infty(V)$ and $b_\infty(V)$ describe the state of the ionic channel associated with each voltage V, while variables $\tau_a(V)$ and $\tau_b(V)$ determine the time required for the ionic channel to activate or deactivate. Sometimes it is more convenient to use the inverse of $\tau_i(V)$: $\lambda_i(V) = 1/\tau_i(V)$. Variable $\lambda_i(V)$ is then referred to as the *rate constant* for activation or inactivation of the i-th ionic channel.

The choice of equation describing the ionic channel and the powers x and y, as well as the choice of functions $a_\infty, b_\infty, \tau_a$ and τ_b could be explained thermodynamically and in terms of statistical mechanics(for example, see [23] pages 146-152). However, the final word is always given by experiments. The parameters and the type of function are chosen in order to fit experimental observations of the neuron being modeled. Typically functions $a_\infty(V)$ and $b_\infty(V)$ have a sigmoid form, while functions $\tau_{a,b}(V)$ are bell-shaped.

Since experiments are extremely important in deriving and improving conductance-based models, we refer to some of them later. Thus, in the conclusion of this overview I would like to provide a brief description of two common experiments on neurons.

• *Voltage-clamp* experiment. The neuron membrane is held under the constant voltage drop V during this type of experiment. The effect of a constant voltage drop independently of the current through the cell membrane is achieved by adding a feedback loop. Thus, an experimentalist could observe and measure the currents flowing through the cell membrane under the various fixed membrane potentials.

• *Current-clamp* experiment. In this type of experiment an applied current is provided to the neuron by an injected electrode in the form of a sustained constant input. An experimentalist could measure the voltage of the cell membrane during this type of experiment, and thus determine the response of the cell membrane to each particular value of an input current.

There is the possibility of blocking certain types of ionic currents by adding special chemicals to the extracellular fluid during both types of experiments described above. Thus, altogether experiments provide a powerful tool for determining an appropriate explicit model for each particular neuron.

Remark: Conductance-based models are divided into two types - *single-compartment* and *multi-compartment* models. The term *single-compartment* means that the potential difference between the interior and the exterior of the cell is assumed to be the same everywhere on the cell membrane. The membrane voltage drop can

therefore be described by a single variable V, and the whole cell can be modeled by an equation of type (2.1).

However, if we would like to take into consideration the difference between ionic concentrations in different parts of the cell, we may want to use a *multi-compartment* type model in order to achieve better plausibility. The general idea of a multi-compartment model is same as idea described above. Each part of the cell is modeled like a single-compartment model, then terms describing interaction between different parts of a cell are introduced. We are not going to consider multi-compartment models in this thesis, but more information on that topic can be found in [7].

2.3 Morris-Lecar model - underlying assumptions, derivation and non-dimensionalization, typical behavior

The Morris-Lecar model was first introduced in 1981 by Lecar and Morris [29]. The model was intended to describe a barnacle giant muscle fiber. We will start describing the model by briefly reviewing the way it was originally derived.

2.3.1 Underlying assumptions.

Studies of the barnacle giant muscle fiber done in 1969-1979 showed that it could be represented by a conductance system consisting of two voltage dependent ionic channels - Ca^{++} and K^+ channels respectively. These channels are considered to be independent of each other. The authors followed this assumption and tried to describe a neuron by the following set of equations:

$$\begin{cases} C\dot{V} = -\bar{g}_L(V - V_L) - \bar{g}_{Ca}M(V - V_{Ca}) - \bar{g}_K W(V - V_K) + I, \\ \dot{M} = \bar{\lambda}_M \lambda_M(V)\left[M_\infty(V) - M\right], \\ \dot{W} = \bar{\lambda}_W \lambda_W(V)\left[W_\infty(V) - W\right]. \end{cases} \tag{2.4}$$

As we have shown before, system (2.4) is in the general form of a model representing an arbitrary neuron governed by two independent voltage dependent conductances.

Here I is the applied current($\mu A/cm^2$), C represents membrane capacitance ($\mu F/cm^2$), V is membrane potential (mV), while $\bar{g}_L$,$\bar{g}_{Ca}$ and $\bar{g}_K$ give the maximum instantaneous conductance values for the leak, Ca^{++} and K^+ pathways of the circuit respectively (mS/cm^2). As it was mentioned above, the conductances g_{Ca} and g_K govern the voltage dependent ionic pathways, and g_L represents the pathways for the natural leakage of the current.

V_L,V_{Ca} and V_K are the equilibrium potentials, corresponding to the leak, Ca^{++} and K^+ conductances respectively (mV).

The variables M and W represent the fraction of open Ca^{++} and K^+ channels respectively (dimensionless). $M_\infty(V)$ and $W_\infty(V)$ are the fractions of open Ca^{++} and K^+ channels at the steady state, while $\lambda_W(V)$ and $\lambda_M(V)$ are rate constants for opening Ca^{++} and K^+ channels (s^{-1}). For the barnacle giant fiber the functions $M_\infty(V)$, $\lambda_M(V)$, $W_\infty(V)$ and $\lambda_W(V)$ were modeled by the following explicit expressions:

$$\begin{array}{rcl} M_\infty(V) & = & 0.5\{1+\tanh[(V-V_1)/V_2]\}, \\ \lambda_M(V) & = & \cosh[(V-V_1)/2V_2], \\ W_\infty(V) & = & 0.5\{1+\tanh[(V-V_3)/V_4]\}, \\ \lambda_W(V) & = & \cosh[(V-V_3)/2V_4]. \end{array} \tag{2.5}$$

Here V_1 and V_3 are defined to be the potentials at which $M_\infty(V)$ and $W_\infty(V)$ respectively are equal to 0.5, V_2 and V_4 correspond to the reciprocal slope of voltage dependance of $M_\infty(V)$ and $W_\infty(V)$, and $\bar{\lambda}_M$, $\bar{\lambda}_W$ are maximum rate constants for Ca^{++} and K^+ channel opening.

System (2.4) served as the basis for the research which led to the development of the Morris Lecar model. Furthermore, the authors of the model combined experiments with numerical simulations of (2.4) in order to determine the contribution of each ionic current, characterize the barnacle giant fiber behavior and find a way to simplify the system without losing information. Let us consider the experiments first.

2.3.2 Experimental observations.

Experiments were done in three stages - with Ca^{++} current being blocked, K^+ current being blocked, and with both currents being active. The researchers investigated the voltage behavior of the cell membrane under *current clamp*. A neuron was separated from the organism and placed in a special liquid containing some concentrations of Ca^{++} and K^+ ions. These concentrations were varied during experiments with different species of barnacle giant fiber. Blocking of ionic currents was done by adding special components to the liquid. Observations showed the following results:

K^+ *conductance*. With the Ca^{++} conductance blocked, the membrane responded to injected current with an RC-type perturbation. As the injected current was increased, a slight difference from RC circuit behavior was observed, which was attributed to nonlinear effects in K^+ conductance. When the injected current was stopped, the membrane voltage returned almost exponentially to its resting voltage.

Ca^{++} *conductance*. With the K^+ conductance blocked, the membrane demonstrated more complex behavior. A small injected current still resulted in an RC type response. However, as the injected current passed some threshold value, bistability in the membrane voltage was observed. The membrane voltage rapidly increased to $+20mV$ and stayed in its new state with slow depolarization. Even after the injected current was removed, the voltage did not go straight to its resting state.

It simply underwent a small drop caused by the removal of the injected current, and stayed in its new stable state for up to hundreds of milliseconds (or several seconds) and then finally returned to its resting value.

K^+ and Ca^{++} conductances together. The behavior of a system containing both K^+ and Ca^{++} ions was essentially different from the behavior of a one-conductance system. When the injected current passed some threshold value, the voltage started to oscillate. Oscillations were observed over a wide range of injected current values and could be damped or continuous depending on the values of experimental parameters (such as $\bar{g}_L$ and $\bar{g}_{Ca}$). The oscillations usually stopped after the injected current was blocked, however, this was not always the case. One more important observation was that the fiber was extremely sensitive to the concentration of Ca^{++} in the liquid surrounding the neuron.

At this point I would like to discuss some important aspects of these experiments:

The experiments have shown that the barnacle giant fiber exhibits oscillations over a wide range of values of injected current and other biophysical parameters. The oscillations had different amplitudes and shapes for different realizations of the experiment. The authors attributed this effect to the variability of $\bar{g}_L$ from preparation to preparation, and to the fact that $\bar{g}_L$ seemed to be changing in time after the neuron was separated from the organism. However, the experiments showed that oscillatory behavior is typical for the fiber over a wide parameter range and that it seemed to be created by the combined action of K^+ and Ca^{++} currents. In order to verify or deny this assumption, it was necessary to check if the observed data could be explained by system (2.4). Thus, let us proceed to the numerical simulation and analysis of (2.4).

2.3.3 Analysis of the mathematical model.

Let us consider (2.4) in the case when one of the conductances is blocked. The case of the Ca^{++} current being blocked is described by $\bar{g}_{Ca} = 0$, while the case of the K^+ current being blocked could be described by $\bar{g}_K = 0$. In both cases (2.4) reduces to the form:

$$\begin{array}{l} \left\{ \begin{array}{l} C\dot{V} = -\bar{g}_L(V - V_L) - \bar{g}_i\mu(V - V_i) + I \\ \dot{\mu} = \bar{\lambda}_\mu\lambda_\mu(V)[\mu_\infty(V) - \mu] \end{array} \right. , \\ \text{where} \quad \mu = W, i = K \quad \text{or} \quad \mu = M, i = Ca. \end{array} \tag{2.6}$$

Let us consider the structure of the equilibrium points of (2.6). They can be found by setting the left hand sizes of (2.6) to zero. We obtain that

$$\left\{ \begin{array}{l} 0 = -\bar{g}_L(V - V_L) - \bar{g}_i\mu(V - V_i) + I \\ 0 = \bar{\lambda}_\mu\lambda_\mu(V)[\mu_\infty(V) - \mu] \end{array} \right. , \Rightarrow \left\{ \begin{array}{l} V = \frac{I + \bar{g}_L V_L + \bar{g}_i\mu_\infty(V)V_i}{\bar{g}_L + \bar{g}_i\mu_\infty(V)} \\ \mu = \mu_\infty(V) \end{array} \right. .$$

It follows that the number of equilibrium points is determined by the equation

$$V = (I + \bar{g}_L V_L + \bar{g}_i\mu_\infty(V)V_i)/(\bar{g}_L + \bar{g}_i\mu_\infty(V)). \tag{2.7}$$

The main difference between the cases $i = Ca$ and $i = K$ is that the Ca current is excitatory, while the K^+ current is recovery. In other words, $V_{Ca} > V_L$, while $V_K < V_L$ for all realizations of the experiment. The parameters $\mu_{i,\infty}(V)$ do not differ sufficiently for $i = Ca$ and $i = K$. It turns out that for $V_i < V_L$ equation (2.7) has a unique root, while for $V_i > V_L$ it can have up to three roots (see [29] for details). This explains the phenomena observed in experiments with one of the currents being blocked. For the Ca^{++} current being blocked the mathematical model has a unique equilibrium point to which it returns after the RC response, while the model without the K^+ current exhibits bistable behavior depending on the value of the injected current.

Let us consider the model equations for the K and Ca^{++} conductances acting together. Numerical simulations of the full third-order system (2.4) have shown voltage oscillations for some range of parameters and injected current. However, the third-order system is hard to work with, since it does not admit the geometrical analysis which can be done in $\mathbb{R}^2$. Experimental observations of relaxation times for the variables W and M have shown that M responds to a voltage change much faster than W. Thus, it seemed physically reasonable to consider a reduced system only with the variables V and W, assuming that $M = M_\infty(V)$. However, this reduction needs mathematical justification. It turns out that third order system (2.4) can be transformed to the second-order system with the little change of its dynamical properties. Let us provide a proof of this fact.

2.3.4 Reduction to two dimensions.

Tikhonov's theorem provides the conditions under which the dynamics of an n-dimensional system can be described by an m-dimensional subsystem. Tikhonov's theorem was originally published in [35] (in Russian), the English translation is available in [31]. In this subsection we will provide the preliminary setup and the statement of Tikhonov's theorem following [31], and then we will apply the theorem to system (2.4).

Consider the following n-dimensional dynamical system:

$$\begin{cases} \frac{dp_i}{dt} = f_i(t,p,q), & i = 1..m \\ \varepsilon_j(p,q)\frac{dq_j}{dt} = F_j(t,p,q_j), & j = 1..n-m \end{cases} \tag{2.8}$$

We require the functions $\varepsilon_j(p,q)$ to satisfy the following conditions: $\varepsilon_j \le \varepsilon_j(\delta)$ for some parameter δ, and $\lim\limits_{\delta\to 0} \varepsilon_j(\delta) = 0$.

Let $\bar{q}_j = \psi_j(t,p)$ be the root of the equation $F_j(t,p,q_j) = 0$.

• The root is called stable if there exists $r_0 > 0$, such that the function

$$F(t,p,q_j) = \sum_{j=1}^{m} [q_j - \psi_j(t,p)]\, F_j(t,p,q_j)$$

is negative for all t, p, q such that $q_j \neq \psi_j(t,p)$ and $r = \sqrt{\sum_{j=1}^{m} \left[q_j - \psi_j(t,p)\right]^2} < r_0$.

• The region of influence of the stable root $\bar{q} = (\bar{q}_1, .., \bar{q}_{n-m}) | \bar{q}_j = \psi_j(t,p)$ is given by the set of points (t_0, p_0, q_0) in $\mathbb{R}^{n+1}$ which satisfy the following property:

$$signF(t_0, p_0, q) = signF(t_0, p_0, q_0)$$

for all q between q_0 and $\bar{q}$ (i.e. $q_j^0 \leq q_j < \psi_j(t_0, p_0)$, if $q_j^0 < \psi_j(t_0, p_0)$ or $\psi_j(t_0, p_0) < q_j \leq q_j^0$, if $q_j^0 > \psi_j(t_0, p_0)$ $j = 1..(n-m)$).

Tikhonov's theorem

If the initial point (t, p_i^0, q_i^0) is contained in the region of influence of the stable root $q_j = \psi(t, p_i)$ of the system (2.8), then as $\delta \to 0$ the integral curve $(t, p_i(t,\delta), v_j(t,\delta))$ corresponding to the initial point (t, p_i^0, q_i^0) approaches the limit $(t, \hat{p}_i(t), \psi_j(t, \hat{p}_i))$ uniformly in the region $t \geq t_1 > t_0$, where $\hat{p}(t) = (\hat{p}_1, .., \hat{p}_m)^T$ is the solution of the degenerate system

$$\begin{array}{l} \frac{d\hat{p}_i}{dt} = f_i(t, \hat{p}_i, \psi_j(t, \hat{p}_i)), \qquad i = 1..m. \\ \hat{p}_i(0) = p_i^0 \end{array}$$

Thus, Tikhonov's theorem provides explicit conditions under which an n dimensional system can be reduced to an m dimensional subsystem. It turns out that Tikhonov's theorem is applicable to system (2.4), which can be rewritten in the following form:

$$\left\{ \begin{array}{l} C\dot{V} = -\bar{g}_L(V - V_L) - \bar{g}_{Ca} M (V - V_{Ca}) - \bar{g}_K W (V - V_K) + I \\ \dot{W} = \bar{\lambda}_W \lambda_W(V) \left[W_\infty(V) - W\right] \\ \left[1/(\bar{\lambda}_M \lambda_M(V))\right] \dot{M} = \left[M_\infty(V) - M\right] \end{array} \right. . \tag{2.9}$$

Let us define $\varepsilon(v) = 1/(\bar{\lambda}_M \lambda_M(V))$, and $\delta = 1/\bar{\lambda}_M$. Then the one-parameter family $\varepsilon(\delta)$ satisfies the condition $\lim_{\delta \to 0} \varepsilon_j(\delta) = 0$.

The root of of the third equation of (2.9) is given by $\bar{M} = M_\infty(V)$ and

$$F(t, V, M) = -\left[M_\infty(V) - M\right]^2 < 0, \qquad M \neq M_\infty(V)$$

The form of function $F(t, V, M)$ implies that the root $\bar{M}$ is stable and that the region of influence of that root is equal the whole $\mathbb{R}^4$ (Since $signF(t_0, V_0, W_0, \bar{M}) = signF(t_0, V_0, W_0, M_0) \equiv -1 \quad \forall (t_0, V_0, N_0, M_0) \in \mathbb{R}^4$).

Tikhonov's theorem implies that as $\bar{\lambda}_M \to +\infty$, solutions of the reduced $2 - D$ system uniformly approach those of the full third-order system (2.4) for any initial conditions $(V_0, M_0, W_0) \in \mathbb{R}^3$, where the reduced system has following form:

$$\left\{ \begin{array}{l} C\dot{V} = I - \bar{g}_L(V - V_L) - \bar{g}_{Ca} M_\infty(V)(V - V_{Ca}) - \bar{g}_K W (V - V_K) \\ \dot{W} = \lambda_W(V) \left[W_\infty(V) - W\right] \end{array} \right. \tag{2.10}$$

Thus, for large values of $\bar{\lambda}_M$ system (2.10) gives a good approximation of the full third order system (2.4). This reduction is crucial since second order systems can

be analyzed by an examination of the properties of the vector fields on the plane. More specifically, two dimensional vector fields and two-dimensional phase planes are essentially different from higher order vector fields and phase spaces, since in the plane any *simple closed curve* subdivides it into two disjoint open regions: "inside" and "outside" of the curve. This statement follows from the *Jordan Curve Theorem* and is not true for the higher dimensional spaces. It provides a basis for a powerful mathematical apparatus which is used for examining the dynamical systems on the plane only (from [8], see pages 327-330 for more detailed explanation and further references in the area). Reduced system (2.10) is referred as the *Morris-Lecar model*.

Note that Tikhonov's theorem is applicable to the variable W as well as for the variable M. However, $\bar{\lambda}_W$ is typically much less then $\bar{\lambda}_M$ in the experimental observations of Morris and Lecar. Thus, the reduction of the variable M is justified, but we may expect that variation of parameter $\bar{\lambda}_W$ could highly affect the dynamics of our system, since for large values of $\bar{\lambda}_W$ the system shrinks to the first order equation in V. For the rest of the thesis we are going to study the behavior of the Morris-Lecar system (2.10).

2.3.5 Non-dimensionalization.

The non-dimensionalized form of Morris-Lecar equations is more convenient to work with, since it is independent of the choice of physical units. We will follow [32] with the non-dimensionalization procedure. Consider the Morris-Lecar model:

$$\begin{cases} C\dot{V} = I - \bar{g}_L(V - V_L) - \bar{g}_{Ca}M_\infty(V)(V - V_{Ca}) - \bar{g}_K W(V - V_K) \\ \dot{W} = \lambda_W(V)\left[W_\infty(V) - W\right] \end{cases} \tag{2.11}$$

The first equation contains $\bar{g}_i$ and V_i as dimensional parameters in each of the ionic currents. Let us divide the equation by the factor $V_{Ca}\bar{g}_{ref}$. V_{Ca} is chosen in order to normalize the equilibrium ionic voltages, so that we will have $v_{Ca} = 1$ in dimensionless form. We could do so since equilibrium voltages usually do not change a lot in different realizations of the model. In particular, V_{Ca} is never equal to zero. However, for the conductances it is more convenient to normalize everything towards some reference value. This is done since, depending on the process being modeled, conductances can vary a lot. For example, sometimes it is convenient to choose one of conductances to be equal zero in order to block it, as we have seen in subsection 2.3.3. Thus, conductances are normalized towards the reference value $\bar{g}_{ref}$ which is chosen to be $\bar{g}_{ref} = 4mS/cm^2$.(The value of $\bar{g}_{ref}$ is equal to the value of $\bar{g}_{Ca}$ in one of the original experiments of Morris and Lecar [29]). New dimensionless variables are $v = V/V_{CA}$ and $w = W$, while the dimensionless parameters are $g_i = \bar{g}_i/\bar{g}_{ref}$, $v_i = V_i/V_{Ca}$, $i = I/(V_{Ca}\bar{g}_{ref})$. After division we obtain the following:

$$(C/\bar{g}_{ref})\dot{v} = i - g_L(v - v_L) - g_{Ca}M_\infty(v)(v - 1) + g_K w(v - v_K).$$

$C/\bar{g}_{ref}$ is the only dimensional constant left in the first equation of system (2.11). Noting that it has the dimension of time, we let $\tilde{t} = C/\bar{g}_{ref}$ be our scale in time. Then $t = \hat{t}/\tilde{t}$ is dimensionless time. Let the derivative with respect to t be denoted by $'$, while the derivative with respect to $\hat{t}$ be denoted by $\dot{}$. Substitution of the dimensionless time into the second equation of (2.11) gives us the following:

$$(1/\tilde{t})w' = \bar{\lambda}_W \lambda_W(V)\left[W_\infty(V) - W\right].$$

The only dimensional parameter left in the right side of the equation is $\bar{\lambda}_W$. Recall that $\lambda_W(V) = \cosh[(V - V_3)/2V_4]$. Thus, let $\phi = \bar{\lambda}_W \tilde{t}$ be new dimensionless rate constant of opening K^+ channels. This substitution concludes the non-dimensionalization. In new variables complete system has following form:

$$\begin{cases} v' = i - g_L(v - v_L) - g_{Ca} m_\infty(v)(v-1) - g_K w(v - v_K) \\ w' = \phi\lambda(v)\left[w_\infty(v) - w\right] \end{cases}, \quad \text{where}$$
$$m_\infty(v) = 0.5\{1 + \tanh[(v - v_1)/v_2]\} \tag{2.12}$$
$$w_\infty(v) = 0.5\{1 + \tanh[(v - v_3)/v_4]\}$$
$$\lambda(v) = \cosh[(v - v_3)/2v_4]$$

Comment: We write $\lambda(v)$ instead of $\lambda_w(v)$, since λ is the only rate constant left, and so the index w is unnecessary.

2.3.6 Analysis of the behavior of the reduced model.

Table 2.1: Values of parameters used in the Morris-Lecar equations

Values of parameters which are the same for both type I and type II oscillators			
Parameter	Name	Value	
v_{Ca}	Calcium equilibrium potential	1	
v_K	Potassium equilibrium potential	-0.7	
v_L	Leak equilibrium potential	-0.5	
g_K	Potassium ionic conductance	2	
g_L	Leak ionic conductance	0.5	
ϕ	Potassium rate constant	$\frac{1}{3}$	
v_1	Calcium activation potential	-0.01	
v_2	Calcium reciprocal slope	0.15	
v_3	Potassium activation potential	0.1	
v_4	Potassium reciprocal slope	0.145	
Values of parameters that differ for type I and type II oscillators			
Parameter	Name	Type I value	Type II value
g_{Ca}	Calcium ionic conductance	1	0.5
i	Applied current	0.09	0.15

In subsections 2.3.1-2.3.4 we have shown that the third order Moris-Lecar system can be reduced to a two-dimensional system which exhibits qualitatively the same

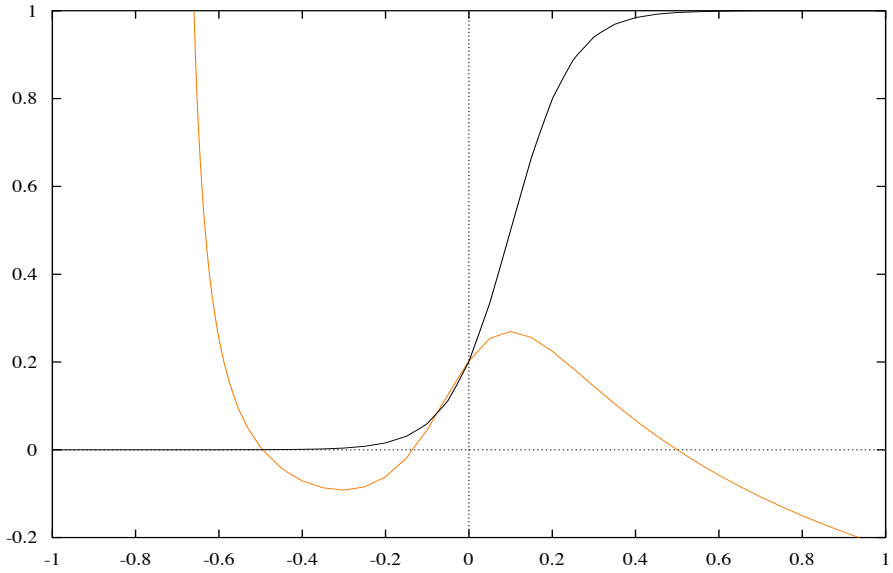

Figure 2.10: Nullclines of the Moris-Lecar system for $g_{ca} = 1$ and $i = 0$

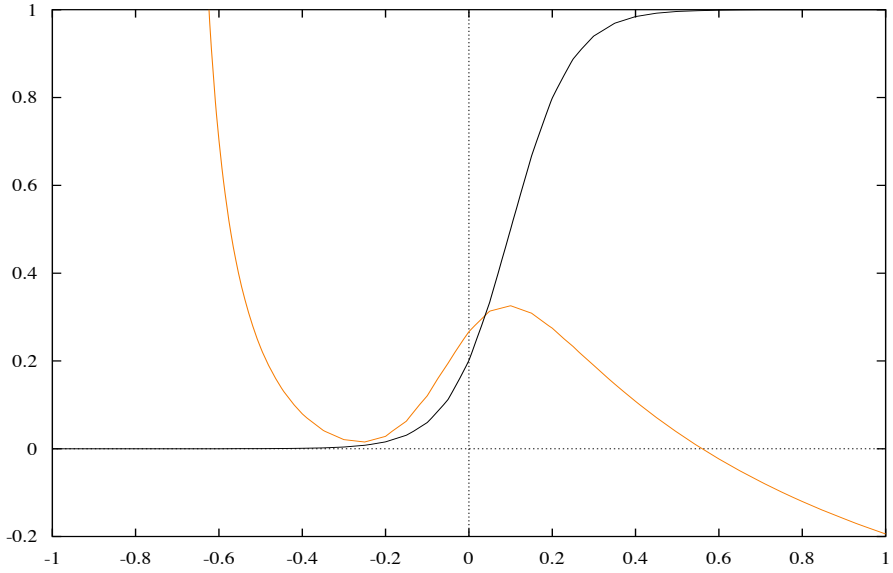

Figure 2.11: Nullclines of the Moris-Lecar system for $g_{ca} = 0.5$ and $i = 0.09$

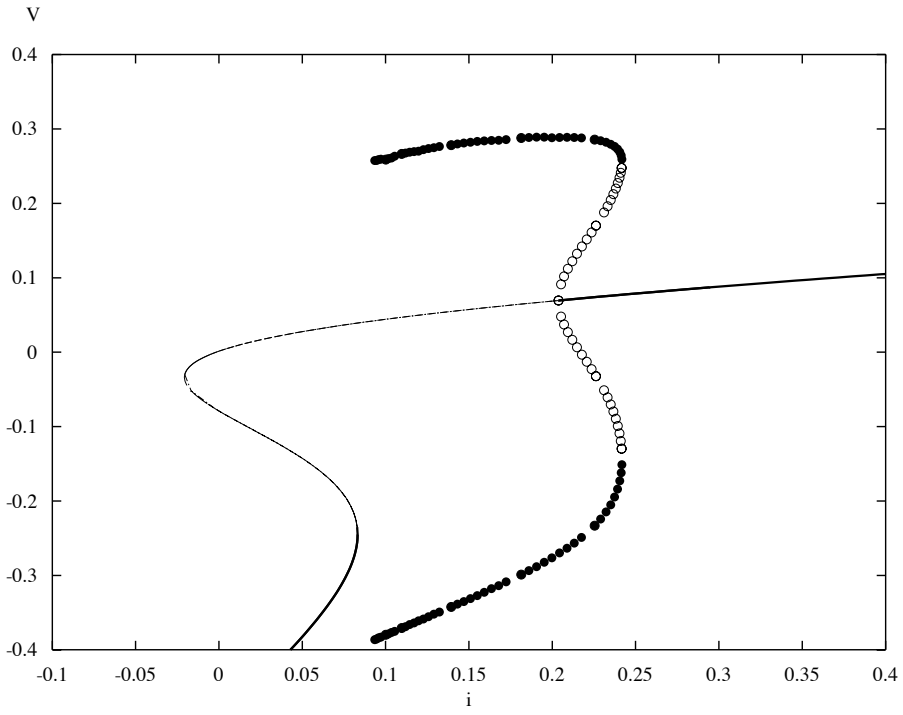

Figure 2.12: Bifurcation diagram for $g_{ca} = 1$

behavior. The non-dimensionalized form of the second-order system is given by (2.12). In this subsection we will examine the phase plane properties of (2.12) and study the different ways in which the system can enter an oscillatory state.

Let us begin with a short overview of the publications in this area. The properties of the reduced Morris-Lecar system were studied in [32] and [36]. [32] studies the behavior of (2.12) with respect to variation of the input i for several fixed sets of the other parameters, while [36] tracks the global bifurcation picture of the system with respect to variation of parameters i,v_3,g_{Ca},ϕ and v_4.

It is necessary to make a comment regarding the values of the physical parameters in (2.12) before proceeding further with the analysis. In the present subsection we will study the dynamics of (2.12) with respect to variation of the parameter i for two fixed sets of the other physical parameters of the system. One parameter set corresponds to the original physical parameter values used by Morris and Lecar in their their experiments in [29]. It is consistent with one of the sets of parameters used in [32]. For this parameter set the system (2.12) is a *type I* oscillator.

According to [36], variation of the single parameter g_{Ca} changes system (2.12) into a *type II* oscillator. Thus, the second parameter set that we are going to use corresponds to the *type II* oscillation and differs from the first set of parameters

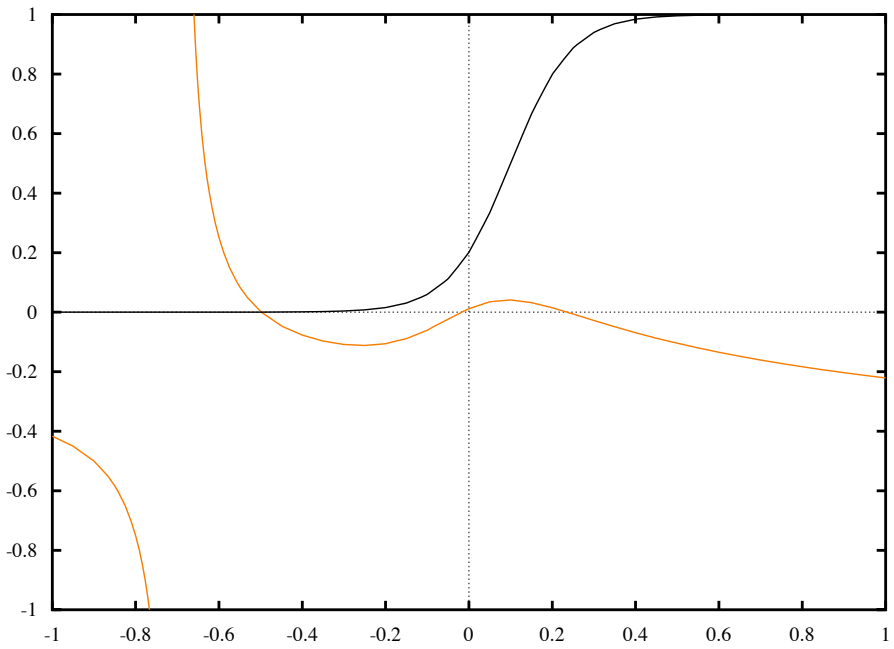

Figure 2.13: Nullclines of the Moris-Lecar system for $g_{ca} = 0.5$ and $i = 0$

only by the value of the parameter g_{Ca}. The numerical values of both parameter sets are given in table (2.1), and differ only by the value of g_{Ca}: $g_{Ca} = 1$ in case of the type I oscillation, and $g_{Ca} = 0.5$ in the case of type II oscillations (the values of applied current i for type I and type II parameter set in table (2.1) will be determined at the end of this subsection, since we will study the dynamics of (2.12) with respect to variation of i).

Now we are ready to analyze the behavior of (2.12) with respect to the variation of i. Consider the type I parameter set first. Let us examine the equilibrium points and their properties. The equilibrium points of (2.12) are determined by the intersections of its nullclines. [3] In our case nullclines have the following form:

$$\begin{cases} i - g_L(v - v_L) - g_{Ca} m_\infty(v)(v - 1) - g_K w_\infty(v - v_K) = 0 \\ w = w_\infty(v) \end{cases} \tag{2.13}$$

The w nullcline is given by $w = w_\infty(v)$ which is a hyperbolic tangent, while the v nullcline is N-shaped. Figure (2.10) shows nullclines for $i = 0$, i.e. in the absence of any input. In this case the system has 3 equilibrium points. However, as the

[3] Recall that the $i - th$ nullcline of an autonomous dynamical system $x' = f(x), \quad x \in \mathbb{R}^n$ is defined as a mathematical locus $x_i' = 0$, and is determined by an equation $f_i(x) = 0$.

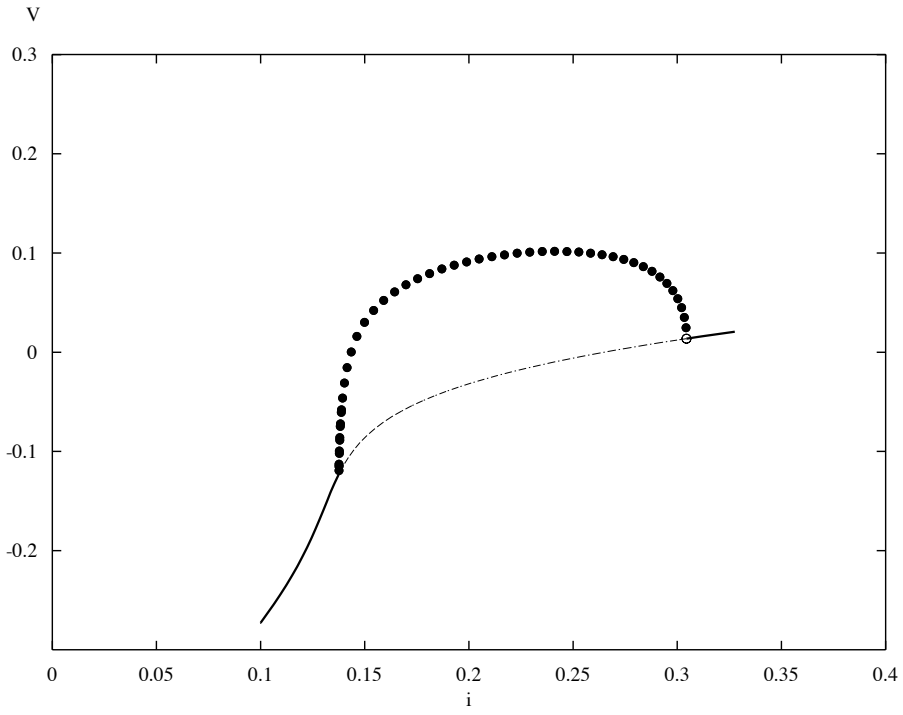

Figure 2.14: Bifurcation diagram for $g_{ca} = 0.5$

input, i, is increased through its critical value i_{lim}, two equilibrium points on the lower side of w nullcline disappear, since the v nullcline does not intersect the w nullcline at that side anymore, and only one equilibrium point is left (See figure (2.11)).

Let us consider the stability of the equilibria next. The leftmost equilibrium point on figure (2.10) is stable, while the two other equilibrium points are unstable. Thus, the system does not exhibit oscillations for $i < i_{lim}$. However, for $i > i_{lim}$ the system becomes oscillatory. This case corresponds to the oscillations of *type I*, since a limit cycle is created by coalescence of the equilibrium points. The critical value $i = i_{lim}$ thus corresponds to the oscillation of an infinite period. By setting the input current i arbitrarily close from above to the value i_{lim}, the frequency of oscillations can be made arbitrarily low. The oscillations continue for some range of i, until they are lost in a Hopf-bifurcation, in which the third equilibrium point becomes stable. Figure (2.12) provides a bifurcation diagram of system (2.12) with respect to i and illustrates the description above. A graph of the period vs i is given in figure (2.7) in subsection 2.1.2.

However, changing the single parameter g_{ca} dramatically changes the behavior of the system. Consider the nullclines of the system for parameter set corresponding

to the oscillation of type II, i.e. $g_{Ca} = 0.5$ instead of $g_{Ca} = 1$. The shape of the v nullcline is changed and there exists only one equilibrium point for all physical values of the parameter i. Figure (2.13) provides a plot of the nullclines for $i = 0$. As i increases, the v nullcline shifts up, but the number of equilibrium points remains unchanged. However, as i is increased, the stability of the equilibrium point is lost in a Hopf bifurcation, and the oscillatory solution is created. Since the periodic solution is created by a Hopf bifurcation, it has a finite period at $i = i_{Hopf}$, and thus the oscillations are of type II.

The bifurcation diagram corresponding to the latter parameter set is provided in figure (2.14), while a graph of the period vs i is provided in figure (2.8) in subsection 2.1.2.

2.4 Transmission of the information between neurons.

2.4.1 Overview of connection types.

The mechanism which is responsible for the transmission of a signal from one neuron to another is called a *synapse*. The components of the neuron which generates a signal are called *presynaptic*, while the components of the neuron which receives a signal are called *postsynaptic*. There are two qualitatively different types of the synapses, which are called *electrical* and *chemical* synapses respectively.

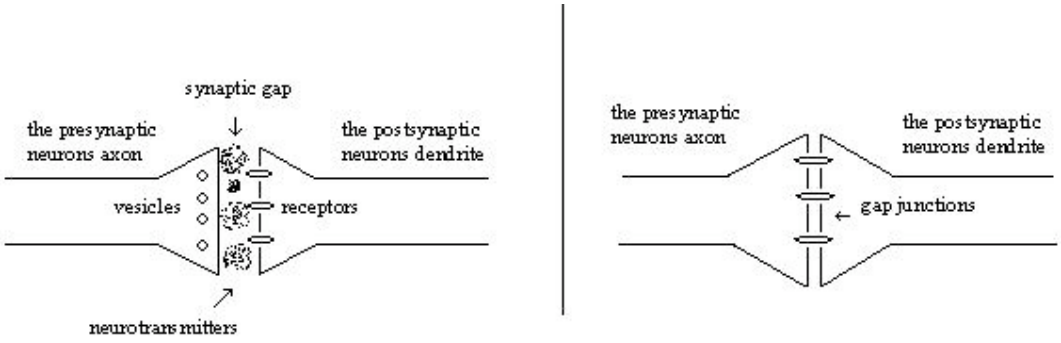

Figure 2.15: Schematic representation of the chemical (left) and electrical (right) synapses

Consider the structure of a typical chemical synapse first. Figure (2.15) provides a schematic representation of a *chemical* synapse. The *synaptic end* or *terminal* belongs to the axon of the presynaptic neuron. It contains special secretory organelles which are also called *synaptic vesicles*. The postsynaptic neuron is represented on the figure by the end of its dendrite. It contains the special proteins which are

called *receptors*. The axonal synaptic terminal is separated from the dendrite receptor with the narrow gap, which is typically 20 nanometers wide and is called a *synaptic gap*.

When an action potential reaches the *synaptic ending*, it excites *synaptic vesicles* and makes them release the special substances called *neurotransmitters* into synaptic gap. The neurotransmitters travel through the synaptic gap until they reach the dendrite receptors. As neurotransmitters reach the postsynaptic site, they bind with the receptors which make the dendrite membrane allow certain types of ions to pass through it.[4] Activation of the dendrite receptors changes its potential and thus gives rise to a *postsynaptic* output signal.

The structure of the *electrical synapse* is more straightforward (see right picture of figure (2.15)). The presynaptic and postsynaptic neurons are physically connected via special proteins which are called *gap junctions*. The gap junction is a channel which allows ions to pass through. Figure (2.15) schematically represents gap junctional connection between the axon of the presynaptic neuron and the dendrite of the postsynaptic one. However, gap junctions can be located in any part of the presynaptic and postsynaptic neurons - possible connection types are *axon-dendrite*, *axon-soma*, *soma-soma*, *soma-dendrite* or *dendrite-dendrite*.

The state of a gap junction generally can depend on some biophysical properties such as the concentrations of different ions on its presynaptic and postsynaptic sides, and is described by a synaptic conductance g_{syn}. The current travels both ways through a gap junction, and hence changes the voltages on the presynaptic and postsynaptic sides. Note that on the contrary with the chemical synapses, the electrical synapses affect both presynaptic and postsynaptic sides. An effect of the gap junction on the somas of presynaptic and postsynaptic neurons depends on the location of the synapse and will be discussed in subsection 2.4.2.

Both types of synapses are common in the neural systems of humans and different animals. Electrical synapses typically occur between neurons of the same type (see [3], [13], [15] and [28]). Recent studies have suggested that electrical synapses are important for the *synchronization* of signals from different neurons [27].

2.4.2 Modeling of the electrical synapses in single-compartment conductance-based models.

Let us denote the synaptic current received by a post-synaptic neuron by the term I_{syn}. Any kind of synapse between neurons could then be modeled by including the term I_{syn} in the equation describing the voltage of the post-synaptic cell membrane. In order to complete the model, one needs to define I_{syn} as an explicit function of the parameters of pre- and -postsynaptic cells and possibly some other biophysical quantities.

[4] One may define the receptors as ionic channels which are sensitive to the certain types of chemicals called neurotransmitters.

With chemical and electrical synapses I_{syn} is modeled differently. Since we are not going to consider chemical synapses in the present thesis, we will consider only the case of electrical synapses here. However, the information on modeling both electrical and chemical synapses can be found in [23].

Consider two neurons connected by the electrical synapse. Let us discuss the case of *soma-soma* connection first. The simplest model consists of replacing the synapse by the resistor connecting the electrical circuits representing pre- and post-synaptic neurons. According to Ohm's law, in this case synaptic current could be expressed as

$$I_{syn} = \bar{g}_{syn}(V_{pre} - V_{post})$$

The term $\bar{g}_{syn}$ represents conductance of the gap junction. In general g_{syn} could depend on some biophysical parameters, such as concentrations of some types of ions. The term $V_{pre} - V_{post}$ expresses the voltage difference between pre- and post-synaptic cells.

According to Kirchhoff's law the sum of the currents through any junction of the circuit is equal to zero. Thus, the pre-synaptic cell is affected by the same current as a postsynaptic one, but with a different sign:

$$I_{post} = -I_{pre} = \bar{g}_{syn}(V_{post} - V_{pre}).$$

It follows that electrical coupling is symmetric and there is no difference between pre- and post- synaptic cell. Thus two identical neurons coupled via a gap junction could be described by the following system:

$$\begin{cases} C\frac{dV_1}{dt} = f(V_1) + \bar{g}_{syn}(V_2 - V_1) \\ C\frac{dV_2}{dt} = f(V_2) + \bar{g}_{syn}(V_1 - V_2). \end{cases} \tag{2.14}$$

System (2.14) can be used in modeling *axon-dendrite*, *axon-soma*, *soma-dendrite* or *dendrite-dendrite* connections in the case when the time delay in transmission signal and losses of the signal in transmission from soma to soma are insignificant. In order to take into account these factors, model (2.14) has to be modified.

Consider the *axon-soma* connection. Due to the finite time for signal transmission along the axon, a voltage from the pre-synaptic neuron arrives to the gap junction with some time delay τ. Due to the specific structure of the axon, the signal does not propagate backwards along the axon without weakening, and hence it is possible to neglect a signal that goes backwards in the case when an axon is long enough. Thus, the system that describes an axon-soma coupled neurons has the following form:

$$\begin{cases} C\frac{dV_{Pre}(t)}{dt} &= f(V_{Pre}(t)) \\ C\frac{dV_{Post}(t)}{dt} &= f(V_{Post}(t)) + \bar{g}_{syn}(V_{Pre}(t-\tau) - V_{Post}(t)). \end{cases} \tag{2.15}$$

By analogy, it is possible to extend the model to the case of *axon-dendrite* and *dendrite-dendrite* connections. However, in the present thesis we will study only *soma-soma* and *axon-soma* connections.

Comments:

• Under non-dimensionalization procedure $\bar{g}_{syn}$ is scaled by the term $\bar{g}_{ref}$ (see subsection 2.3.5). We are going to refer dimensionless synaptic conductance as *coupling strength* γ: $\gamma = \bar{g}_{syn}/\bar{g}_{ref}$.

• Modeling of the electrical synapse by a single resistance does not include some possible effects the electrical synapses, such as the effect of the synaptic current being shunted by the extracellular cytoplasm. However, most of the gap junctions could be modeled by the single parameter γ.(See [23] pages 112-119 for a more detailed analysis).

2.5 Problem Formulation.

We consider two identical neurons coupled together with gap junctions by the scheme shown on figure (2.16). The type of connection between neurons is axon-soma, with gap junctions located at the end of the axon of each neuron. The applied current provided to each neuron is assumed to be equal for both neurons and to be at some constant value i for all time. Systems of this type are popular in

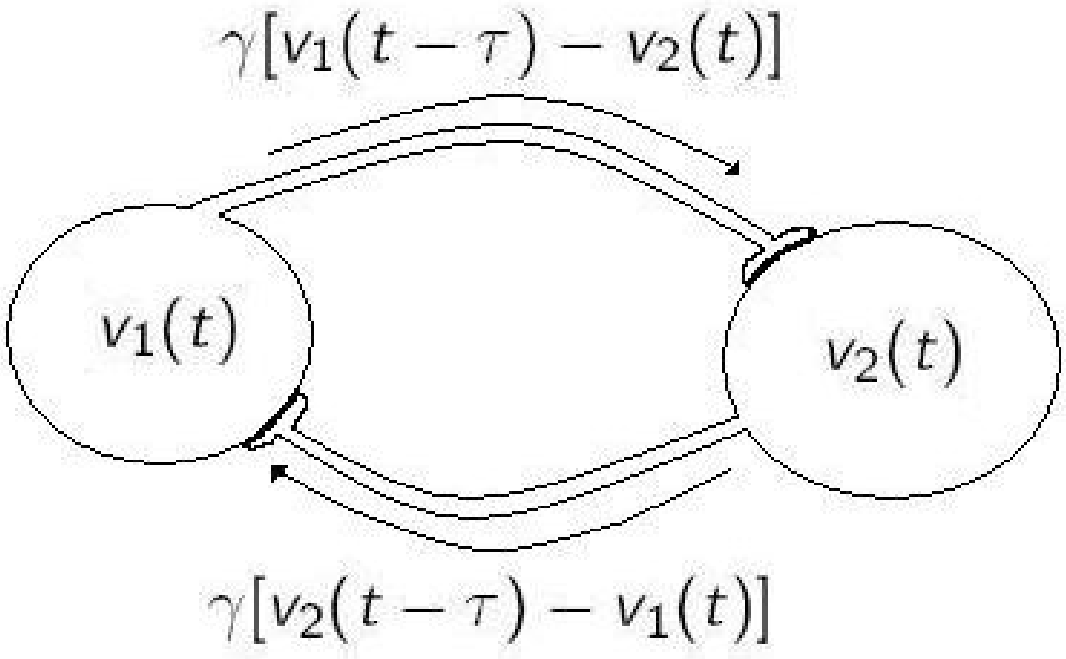

Figure 2.16: Scheme of two coupled neurons.

neuroscience, since such a setting of the model allows one to study and understand the effects of *synchronization* or *synchronous firing* in the neural networks, which are often observed in living organisms. The input i represents the influence from

the other elements of the network. We will focus our study in the effects of the *coupling strength* γ and the *time delay in transmission signal* τ on the behavior of the system. As was mentioned in chapter 1, both γ and τ could vary depending on the type of connection between neurons and type of the gap junction involved in the particular connection. In the present thesis we will try to answer the following questions:

• Under which conditions on γ and τ does the system admits stable synchronous solutions, and what is the type of these solutions(*inphase* or *antiphase*)?

• When are these synchronous solutions globally attractive?

We will model each neuron by the Morris-Lecar system (2.12). Such a choice is determined by several factors. First, the Morris-Lecar system is a simple two-dimensional model, which has a biophysical meaning and admits oscillations over a wide parameter range. This fact allows us to abstract from modeling the neuron itself, and concentrate our attention on the effects on the oscillations of the time delay and the coupling strength. Secondly, the Morris-Lecar system admits oscillations of both type I and type II. Transition between type I and type II is determined by a single parameter g_{Ca} (See subsection 2.3.6). We are going to study both *type I* and *type II* systems. This approach will allow us to understand which effects are common for both types of oscillations and are caused by variation of γ and τ, and which happen due to the difference in the oscillation type.

According to model (2.15) for the axon-soma connection, the complete system of equations describing our problem to be studied has the following form:

$$\begin{cases} v_1' &= -g_{Ca}m_\infty(v_1)(v_1-1) - g_K w_1(v_1-v_K) - g_L(v_1+v_L) \\ & \quad +i+\gamma(v_2(t-\tau)-v_1) \\ w_1' &= \phi\lambda(v_1)[w_\infty(v_1)-w_1] \\ v_2' &= -g_{Ca}m_\infty(v_2)(v_2-1) - g_K w_2(v_2-v_K) - g_L(v_2+v_L) \\ & \quad +i+\gamma(v_1(t-\tau)-v_2) \\ w_2' &= \phi\lambda(v_2)[w_\infty(v_2)-w_2], \end{cases} \tag{2.16}$$

Here index 1 or 2 represents the number of the neuron being modeled. Variables v_1, w_1, v_2 and w_2 are assumed to be computed at time t, unless otherwise is specified, in order to simplify notation.

The values of the parameters used in the model are given in table (2.1) in subsection 2.3.6. We consider two different cases: both neurons being of type I, and both neurons being of type II. In the case of both neurons being type I, the parameter values are consistent with the original physical parameters used by Morris and Lecar in [29] and by Rinzel and Ermentrout in [32]. The parameter set for type II differs from the type I set only by values of g_{Ca} and i.

Note that the input i is set close to a critical value i_{lim} at which oscillations are born both in cases of *type I* and of *type II* system. This have been done in order to magnify the difference between oscillations types, which is important in our study.

Note that for $\tau = 0$ asymmetry caused by delays in the signal propagation disappears, and system (2.16) takes form of the system for soma-soma coupled

neurons described by equations (2.14). However, due to neglecting of propagation of the signal backwards along the axons, coupling functions for system shown in figure (2.16) are $\gamma(v_i - v_j)$ instead of coupling functions $2\gamma(v_i - v_j)$ for *soma-soma* coupled neurons with two gap junctions of strength γ. In chapter 5 we will study two arbitrary neurons coupled by soma-soma connection.

In order to answer the questions stated in this subsection, we have to perform bifurcation analysis of (2.16) with respect to γ and τ. In the following chapter we are going to consider the case of γ being *small* which will allow us to reduce our system.

Chapter 3

Phase Model

In the present chapter we consider the case of *weakly coupled* neurons. The coupling strength γ will be considered as a small parameter. This assumption allows us to simplify the problem by considering a simpler set of *phase equations* corresponding to the model instead of the full set of equations (2.16).

The chapter has the following structure. First we provide the necessary general definitions and terms from the theory of the weakly coupled networks following [20]. Next we state the conditions under which the phase equations are valid and explicitly compute them in terms of the complete system (2.16). The theory is then applied to examine the behavior of both the non-delayed and delayed Morris-Lecar system. We determine the stable periodic solutions of the complete system by analysis of an equilibrium of the phase equations. The chapter is then concluded by deriving a theoretical estimate of the region of validity of the phase model.

3.1 Introduction to the theory of weakly connected networks.

Consider the following system:

$$\dot{X}_i = F_i(X_i) + \varepsilon G_i(X_1, .., X_n), \qquad i = 1...n \tag{3.1}$$

where each $X_i \in \mathbb{R}^m$, and ε is some small parameter (functions F_i and G_i are considered to be of the same order of magnitude).

Any system which has the form (3.1) is referred to as a *weakly connected network*. Such systems are special since it is possible to benefit from the fact that ε is small and reduce the number of dimensions of the system under certain conditions on ε, F_i and G_i. The theory of weakly connected networks is a powerful and well developed tool of mathematical analysis. The book of Hoppensteadt and Izhhikevich [20] provides good insight into the theory and gives further references.

Application of the theory to system (3.1) crucially depends on the properties of the *decoupled* system, i.e. system (3.1) with $\varepsilon = 0$. In case of $\varepsilon = 0$ system (3.1) breaks into n independent subsystems:

$$\begin{cases} \dot{X}_1 = F_1(X_1) \\ \dots \\ \dot{X}_n = F_n(X_n) \end{cases} \tag{3.2}$$

In present thesis we are interested in the case when each subsystem

$$\dot{X}_i = F_i(X_i), i = 1 \dots n \tag{3.3}$$

has an *exponentially orbitally stable limit cycle attractor* σ_i. Recall that a *limit cycle* is an isolated periodic solution of the dynamical system, or, equivalently, an isolated closed trajectory in the phase space of the dynamical system. Exponential orbital stability means that solutions starting close enough to the limit cycle approach it infinitely closely and exponentially fast as $t \to +\infty$. In explicit notation, there exists some open region D such that $\sigma_i \subset D$ and numbers $\alpha_0 > 0$ and $\beta_0 \geq 1$, such that $\inf_{y \in \sigma_i} |X_i(t) - y| \leq \beta_0 \inf_{y \in \sigma_i} |X_i(0) - y| e^{-\alpha_0 t}$ for any solution $X(t)$ with initial condition $X_i(0) \in D$ (from [21]). The region D is also called a basin of attraction of the limit cycle σ_i.

Let us study the limit cycle σ_i in more detail. The smallest positive number T_i such that $\sigma_i(t + T_i) = \sigma_i(t)\ \forall t \in \mathbb{R}$ is called the *minimal period* of the limit cycle σ_i, while the number $\Omega_i = 2\pi/T_i$ is called the *natural frequency* of the limit cycle σ_i.

Comment: The theory of weakly coupled networks is developed in the general case of σ_i having different periods, i.e. it is possible that $T_i \neq T_j$ for some i and j. However, for the sake of simplicity everywhere further in this thesis we will consider only the case when all subsystems X_i are identical, i.e. the case of $F_1 = \dots = F_n \equiv F$. In that case $\sigma_1 = \dots = \sigma_n \equiv \sigma$, $T_1 = \dots = T_n \equiv T$ and $\Omega_1 = \dots = \Omega_n \equiv \Omega$, while equation (3.3) takes form:

$$\dot{X}_i = F(X_i), \quad i = 1 \dots n. \tag{3.4}$$

This setup is sufficient for the goals of the present thesis, since we are studying two *identical* Morris-Lecar systems coupled together. The general case of differing σ_i with a different periods T_i is discussed in [20].

Let us continue to discuss properties of the limit cycle σ. Since the limit cycle is a closed curve in the phase space of the corresponding dynamical system, it could be parameterized by a single parameter. Note that any solution of the equation (3.4) with initial condition $X_i(0) \in \sigma$ defines a parametrization of σ by points of the interval $(0, T]$ through a mapping $X(t) = \sigma(t)$. However, the parametrization of σ provided above depends on a choice of the point $X_i(0)$ and on the period of the limit cycle T. Hence, it is convenient to get rid of these dependencies and

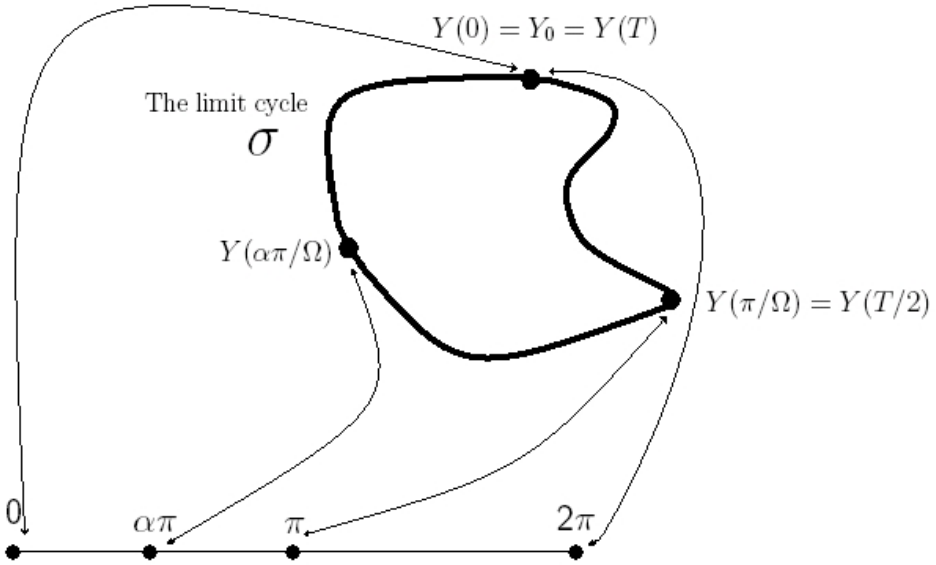

Figure 3.1: Parametrization of the limit cycle σ by the points of an interval $[0, 2\pi)$

define some special parametrization of σ with fixed starting point $X_i(0)$ and without dependency on the period T.

Consider the system $\dot{Y} = F(Y)$. Let us choose any arbitrary point $Y_0 \in \sigma$. Let $Y(t)$ be the solution of $\dot{Y} = F(Y)$ with initial condition $Y(0) = Y_0$. Since the limit cycle $\sigma(t)$ is a $T-$periodic solution of the system $\dot{Y} = F(Y)$, for each $t \in [0, T)$ there exists a unique point $z \in \sigma$, such that $z = Y(t)$. Let us define the mapping $\tilde{\theta} : [0, 2\pi) \to R^m$ as follows - each point $\tilde{\theta} \in [0, 2\pi)$ corresponds to the point with coordinate $Y(\tilde{\theta}/\Omega) = Y(\frac{T}{2\pi}\tilde{\theta})$ in $\mathbb{R}^m$. As $\tilde{\theta}$ changes between 0 and 2π, the point with coordinates $Y(\tilde{\theta}/\Omega) \subset \mathbb{R}^m$ makes one full trip along the limit cycle σ (see figure (3.1) for an illustration).

Comment: Note that the choice of the point $Y_0 \in \sigma$ in the parametrization above is arbitrary and serves only for consistency. In the case of differing limit cycles σ_i the question of parametrizing them all in a consistent way is more complicated. This is studied in some detail in the book [20]. One of the common approaches is to choose a point with the maximal norm, or with the maximal value with respect to some variable in each σ_i, as a starting point Y_0^i for the parametrization.

The parametrization of the limit cycle σ by $\tilde{\theta}$ defines the coordinate along the limit cycle σ. Thus, it is enough to define a scalar function $\theta(t) \in \mathbb{S}^1$ instead of a vector function $Z(t) \in \mathbb{R}^m$ in order to describe the dynamics of any system $Z \subset \mathbb{R}^m$

along the limit cycle σ. The symbol $\mathbb{S}^1$ in the notation above denotes the unit circle ($\mathbb{R} \mod 2\,\pi$).

Consider the decoupled system (3.2). Assume that at time $t = 0$ each of the subsystems X_i stays on its limit cycle σ, i.e. $X_i(0) \in \sigma$, $i = 1 \dots n$. Then the dynamics of (3.2) can be described by the system of n scalar equations:

$$\begin{cases} \theta_1(t) = \theta_1^0 + \Omega t \mod 2\pi \\ \dots \\ \theta_n(t) = \theta_n^0 + \Omega t \mod 2\pi \end{cases},$$

where variables $\theta_i(t)$ are defined by mapping $\tilde{\theta}$ applied to each of the solutions $X_i(t)$, and terms θ_i^0 correspond to the phase of the starting point $X_i(0)$. Note that each of the phase variables is restricted to the interval $[0, 2\pi)$ by the operator $\mod 2\pi$ due to the periodicity of the limit cycle σ and the definition of parametrization $\tilde{\theta}$. In the case when $X_i(0) = Y_0$ we have $\theta_i^0 = 0$, and the corresponding phase variable $\theta_i(t) = \Omega t \mod 2\pi$ is called the *natural phase* of the subsystem X_i.

Let us consider the full system (3.1) next. One may expect that for small ε the coupling between subsystems X_i does not change the amplitudes and shapes of the limit cycles σ for each subsystem X_i, but affects only relationship between phase variables θ_i. These assumptions are justified by the fact that limit cycle σ is an *exponentially orbitally stable limit cycle attractor* of each of the uncoupled systems (3.4). Since for $\varepsilon \neq 0$ the subsystems X_i start to affect each other, we may write the phase variables in the form

$$\begin{cases} \theta_1(t) = \Omega t + \phi_1(t) \\ \dots \\ \theta_n(t) = \Omega t + \phi_n(t) \end{cases} \tag{3.5}$$

where each function $\phi_i(t)$ represents *phase deviation* of the subsystem X_i from its natural phase due to the influence from the other parts of network. Sometimes it is more convenient to define phase variables $\theta_i(t)$ not as functions of time $\theta_i(t) = \Omega t + \phi_i(t)$, but through a system of differential equations.We shall show that the system may be written in the form

$$\begin{cases} \dot{\theta}_1 = \Omega + \varepsilon g_1(\theta_1, \dots, \theta_n) \\ \dots \\ \dot{\theta}_n = \Omega + \varepsilon g_n(\theta_1, \dots, \theta_n) \end{cases}, \tag{3.6}$$

where the *phase coupling functions* g_i depend only on the phase variables due to the fact that system (3.1) is autonomous. The latter system (3.6) expresses $\theta_i(t)$ in the form consistent with the notation of system (3.1).

The transition from system (3.1) to system (3.6) allows us to reduce the dimension of system (3.1), since each subsystem X_i is being restricted to the unit circle $\mathbb{S}^1$ instead of R^m. In order to complete the theory developed, we need to address the following 2 issues:

• We need to find out under which conditions on ε, F and G_i is it possible to map the solutions of system (3.1) to those of system (3.6).

• It is necessary to derive expressions for the phase coupling functions $g_i(\cdot)$ or phase deviations $\phi_i(t)$ in terms of the coefficients of the original system (3.1).

In the following section (3.2) we are going to provide theoretical foundations for the transition from (3.1) to the (3.6), and derive explicit formulas for the phase deviations $\phi_i(t)$ and phase coupling functions $g_i(\theta_1, \ldots, \theta_n)$.

3.2 Theoretical foundations

Consider the weakly coupled network of n *identical* subsystems with time delays in the coupling functions:

$$\dot{X}_i(t) = F(X_i(t)) + \varepsilon G_i(X_1(t-\tau_1), \ldots, X_n(t-\tau_n)), \qquad i = 1...n, \tag{3.7}$$

such that each subsystem $\dot{X}_i = F(X_i)$, $X_i \in \mathbb{R}^m$, $i = 1..n$ has an exponentially orbitally stable limit cycle σ with the nonzero natural frequency $\Omega = \frac{2\pi}{T}$. We will assume that functions $F(\cdot)$ and $G_i(\cdot)$, $i = 1 \ldots n$ are infinitely differentiable with respect to each of their variables.

Note that $G_i(\cdot)$ depend on $X_j(t-\tau_j)$ for $i \neq j$, but on $X_i(t)$, for $i = j$. This special type of dependance reflects the fact that each of the subsystems X_i needs time τ_i in order to affect the other subsystems, but it affects itself without any time delay. Such assumption on $G_i(\cdot)$ is satisfied in the case of the Morris Lecar system (2.16), as well as in many other applied problems. We will consider only that type of $G_i(\cdot)$ everywhere further in the present thesis in order to simplify the notation of the following theorems and proofs.

3.2.1 Invariant manifold reduction

As was mentioned in the previous section, under some conditions it is possible to map the solutions of system (3.7) to those of system (3.6). The mapping is based on the technique called *invariant manifold reduction*. In the present subsection we will shortly introduce the main definitions and concepts of the theory and provide references for the area. The description below closely follows [20].

First, let us introduce the notion of a *normally hyperbolic invariant manifold*.

Consider some dynamical system

$$\dot{Y} = F(Y), \qquad Y \in \mathbb{R}^k. \tag{3.8}$$

The set $M \subset \mathbb{R}^k$ is called an *invariant set* for the system (3.8), if $Y(0) \in M$ implies that $Y(t) \in M$ for all $t \in \mathbb{R}$. If, in addition, the set M is a manifold, it is called an *invariant manifold* of the system (3.8).

We will denote the tangent space of each point $Y \in M$ by $T_Y M$, while the normal space of each point $Y \in M$ will be denoted by $N_Y M$. Let $\Pi : T_Y M \to N_Y M$ be the orthogonal projection to the normal subspace $N_Y M$, and let $D\Phi_t(Y)$ denote the linear part of flow of the system (3.8) through the point $Y \in M$.

Let

$$\begin{aligned} v(t) &= D\Phi_t(Y)v(0), \qquad v(0) \in T_Y M \\ w(t) &= \Pi D\Phi_t(Y)w(0), \qquad w(0) \in N_Y M. \end{aligned}$$

The invariant manifold M is called *normally hyperbolic* if

$$\lim_{t\to\infty} \frac{|w(t)|}{|v(t)|} = 0,$$

for all $Y \in M$ and all nonzero vectors $w \in N_Y M$ and $v \in T_Y M$.

If the smooth compact invariant manifold is normally hyperbolic, it is persistent under small perturbations. In particular, this means that perturbed dynamical system (3.8) given by

$$\dot{Y} = F(Y) + \varepsilon G(Y, \varepsilon), \qquad Y \in \mathbb{R}^k$$

has an attractive normally hyperbolic compact invariant manifold M_ε which is an ε perturbation of M if ε is sufficiently small. (Follows from theorem 4.1 in [20]).

It can be shown that $M = \sigma \times \cdots \times \sigma$ is a normally hyperbolic invariant manifold of system (3.7). The proof of this fact is available in [20].

Hence, for the non-delayed case, i.e., $\tau_i \equiv 0$ for all $i \in 1...n$, persistence of M under ε perturbations is guaranteed by the normal hyperbolicity. When delay terms τ_i all are $O(1)$ with respect to ε, the persistence of the invariant manifold under ε perturbations was proved by Hirsch, Pugh and Shub in [17]. However, in the general case of τ_i of $O(1/\varepsilon)$ and higher, persistence has not been proved. In the present thesis we will consider delay only of $O(1)$ and less.

Knowledge of the normally hyperbolic invariant manifold of a system allows one to consider the dynamics only along the manifold, since the normal plane components are unimportant due to the normal hyperbolicity. In the case of an ε perturbed system one may find an ε perturbation of the invariant manifold, M_ε, and hence determine the behavior of the perturbed system.

3.2.2 Explicit formulas for the phase equations.

When the invariant manifold persists under ε perturbations, the phase deviations can be found explicitly. The following theorem 3.2.1 provides the equations for ϕ_i defined in terms of properties of the complete system (3.7). Theorem 3.2.1 and its proof are an adaptation of the main theorem and its proof stated in [22].

Theorem 3.2.1 *Assume that there exists $\varepsilon_0 > 0$, such that the normally hyperbolic invariant manifold $M = \sigma \times \cdots \times \sigma \subset \mathbb{R}^{mn}$ of system (3.7) persists for all ε such that $0 < |\varepsilon| < \varepsilon_0$. Let $\rho = \Omega t$ denote a scaled time variable, $\alpha = |\varepsilon|\rho = |\varepsilon|\Omega t$ denote the corresponding slow scaled time variable, and let functions $\phi_i(\alpha)$, $i = 1 \dots n$ denote the phase deviations of θ_i from its natural phase $\hat{\theta}_i = \Omega t \mod 2\pi$. Then*

$$\frac{d\phi_i}{d\alpha} = H_i(\phi_1(\alpha-\zeta_1)-\eta_1-\phi_i(\alpha), \dots, \phi_n(\alpha-\zeta_n)-\eta_n-\phi_i(\alpha)) + O(\varepsilon), \quad i = 1 \dots n, \tag{3.9}$$

where $\zeta_i = |\varepsilon|\Omega\tau_i$ and $\eta_i = \Omega\tau_i$. The functions $H_i(\cdot)$ have the following form:

$$\begin{aligned} &H_i(\phi_1(\alpha-\zeta_1)-\eta_1-\phi_i(\alpha), \dots, \phi_n(\alpha-\zeta_n)-\eta_n-\phi_i(\alpha)) = \\ &= \tfrac{1}{2\pi} \int_0^{2\pi} Q^T(s) G_i(\sigma[\phi_1(\alpha-\zeta_1)-\eta_1-\phi_i(\alpha)], \dots, \sigma[s], \\ &\dots, \sigma[s+\phi_n(\alpha-\zeta_n)-\eta_n-\phi_i(\alpha)])ds, \end{aligned} \tag{3.10}$$

where $\sigma[s]$ stands on the $i-$th position, and $Q(t) \in \mathbb{R}^m$ is the unique nontrivial 2π periodic solution to the linear system

$$\frac{dQ}{d\rho} = -\frac{1}{\Omega} DF(\sigma[\rho])^T Q,$$

satisfying the normalization condition

$$\frac{1}{2\pi} \int_0^{2\pi} Q_i^T(s) F(\sigma[s]) ds = 1.$$

Proof Let us introduce several preliminary steps before proceeding directly to the proof. First, it is convenient to re-scale the time t in order to make the period of the limit cycle σ equal to 2π. Let $\rho = \Omega t$. Then $\frac{d}{dt} = \frac{d\rho}{dt}\frac{d}{d\rho} = \Omega\frac{d}{d\rho}$, and system (3.7) takes the form:

$$\Omega\dot{X}_i(\rho) = F(X_i(\rho)) + \varepsilon G_i(X_1(\rho-\Omega\tau_1), .., X_n(\rho-\Omega\tau_n)), \qquad i = 1...n. \tag{3.11}$$

Note that the delay terms τ_i become scaled by Ω due to the re-scaling of the distances on the limit cycle σ. For simplicity, let us denote $\Omega\tau_i$ by η_i .

Without loss of generality we may consider only $\varepsilon > 0$, since the sign of ε is determined by the signs of the functions $G_i(\cdot)$, and there are no conditions set on the functions $G_i(\cdot)$. Thus, the case of $\varepsilon < 0$ is equivalent to the case of $\varepsilon > 0$ with $G_i(\cdot)$ replaced by $-G_i(\cdot)$. As we will see further, it is convenient to introduce the slow phase variable $\alpha = \varepsilon\rho$ and slow delay terms $\zeta_i = \varepsilon\eta_i$, where $i = 1 \dots n$.

Now we are ready to proceed to the proof. Due to the fact that a normally hyperbolic invariant manifold $M = \sigma \times \cdots \times \sigma$ of system (3.11) persists under ε perturbations, the solution of the i-th equation of (3.11) in an ε neighborhood of M can be written as

$$X_i(\rho) = \sigma(\rho + \phi_i(\alpha)) + \varepsilon P_i(\rho, \phi_1(\alpha), \dots, \phi_n(\alpha), \varepsilon), \tag{3.12}$$

where the term εP_i denotes the deviation from the manifold M in the normal plane, while the term $\phi_i(\alpha)$ denotes the deviation of the phase from its natural uncoupled phase $\hat{\theta}_i$. Terms X_i, $\sigma(\cdot)$ and P_i are considered to be of the same order of magnitude.

We assume that the phase deviations depend on the slow variable α. This assumption is justified by the fact that the coupling is of order ε in original system (3.7).

Differentiation of X_i with respect to ρ gives:

$$\frac{dX_i}{d\rho} = \sigma'(\rho+\phi_i(\alpha))\left(1+\varepsilon\frac{d\phi_i}{d\alpha}\right)+\varepsilon\frac{\partial P_i(\rho,\phi_1(\alpha),\ldots,\phi_n(\alpha),\varepsilon)}{\partial\rho}+O(\varepsilon^2). \quad (3.13)$$

The term $O(\varepsilon^2)$ is due to the $\varepsilon\sum\frac{\partial P_i(\rho,\phi_1,\ldots,\phi_n,\varepsilon)}{\partial\phi_j}\frac{d\phi_j(\alpha)}{d\rho}$. On the other hand, since X_i is a solution of (3.11), we may write that:

$$\frac{dX_i}{d\rho} = \frac{1}{\Omega}[F(X_i(\rho))+\varepsilon G_i(X_1(\rho-\eta_1),\ldots,X_n(\rho-\eta_n))].$$

Substitution of expression (3.12) in the equation above gives

$$\begin{aligned}\frac{dX_i}{d\rho} &= \frac{1}{\Omega}\{F(\sigma[\rho+\phi_i(\alpha)]+\varepsilon P_i(\rho,\phi_1(\alpha),\ldots,\phi_n(\alpha),\varepsilon))\\ &\quad+\varepsilon G_i[\sigma(\rho-\eta_1+\phi_1(\alpha-\zeta_1))+\varepsilon P_1(\rho,\phi_1(\alpha-\zeta_1),\ldots,\phi_n(\alpha-\zeta_n),\varepsilon),\\ &\quad\ldots,\sigma(\rho-\eta_n+\phi_n(\alpha-\zeta_n))+\varepsilon P_n(\rho,\phi_1(\alpha-\zeta_1),\ldots,\phi_n(\alpha-\zeta_n),\varepsilon)]\}.\end{aligned}$$

Using the fact that F and G_i are infinitely differentiable, we may expand them as power series in ε. Expansion to the first order with remainder in the form of $O(\varepsilon)$ gives

$$\begin{aligned}\frac{dX_i}{d\rho} &= \frac{1}{\Omega}\{F(\sigma[\rho+\phi_i(\alpha)])+\varepsilon DF(\sigma[\rho+\phi_i(\alpha)])P_i(\rho,\phi_1(\alpha),\ldots,\phi_n(\alpha),\varepsilon)\\ &\quad+\varepsilon G_i(\sigma(\rho+\phi_1(\alpha-\zeta_1)-\eta_1),\ldots,\sigma(\rho+\phi_n(\alpha-\zeta_n)-\eta_n))+O(\varepsilon^2)]\},\end{aligned} \quad (3.14)$$

where $DF(\sigma(\rho+\phi_i(\alpha)))$ is the Jacobian of $F(\cdot)$ evaluated at the point $\sigma(\rho+\phi_i(\alpha))$.

Equating the right hand sides of (3.13) and (3.14), and using the fact that $\sigma'(\rho+\phi_i(\alpha)) = \frac{1}{\Omega}F(\sigma[\rho+\phi_i(\alpha)])$ (since σ is a periodic solution of $\frac{dX_i}{dt} = F(X_i)$,

and hence it is a periodic solution of $\frac{dX_i}{d\rho} = \frac{1}{\Omega}F(X_i))$, we obtain the following:

$$F(\sigma[\rho+\phi_i(\alpha)])\frac{d\phi_i(\alpha)}{d\alpha} + \Omega\frac{\partial P_i(\rho,\phi_1(\alpha),\ldots,\phi_n(\alpha),\varepsilon)}{\partial\rho}$$

$$= DF(\sigma[\rho+\phi_i(\alpha)])P_i(\rho,\phi_1(\alpha),\ldots,\phi_n(\alpha),\varepsilon)$$

$$+G_i(\sigma(\rho+\phi_1(\alpha-\zeta_1)-\eta_1),\ldots,\sigma(\rho+\phi_n(\alpha-\zeta_n)-\eta_n)) + O(\varepsilon).$$

Assuming that $P_i(\rho,\phi_1(\alpha),\ldots,\phi_n(\alpha),\varepsilon)$ are smooth functions of ε, we may replace $P_i(\rho,\phi_1(\alpha),\ldots,\phi_n(\alpha),\varepsilon)$ by $P_i(\rho,\phi_1(\alpha),\ldots,\phi_n(\alpha),0)+O(\varepsilon)$. Since all P_i depend on the same argument, we will simplify notation and write P_i instead of $P_i(\rho,\phi_1(\alpha),\ldots,\phi_n(\alpha),0)$ everywhere further in the proof :

$$\begin{aligned} &F(\sigma[\rho+\phi_i(\alpha)])\tfrac{d\phi_i(\alpha)}{d\alpha} + \Omega\tfrac{\partial P_i}{\partial\rho} = DF(\sigma[\rho+\phi_i(\alpha)])P_i+ \\ &+G_i(\sigma(\rho+\phi_1(\alpha-\zeta_1)-\eta_1),\ldots,\sigma(\rho+\phi_n(\alpha-\zeta_n)-\eta_n)) + O(\varepsilon). \end{aligned} \tag{3.15}$$

At this point, we will take α and ρ as independent variables. Since α is a slow variable with respect to ρ, we will treat it as a constant on the scale of ρ. The partial derivative of P_i in (3.15) then could be replaced by a full derivative of P_i with respect to ρ, and (3.15) can be rewritten in a following form:

$$\frac{dP_i}{d\rho} = A(\rho,\phi_i)P_i + b_i(\rho,\phi_1,\ldots,\phi_n) + O(\varepsilon), \tag{3.16}$$

where

$$A(\rho,\phi_i) = \frac{1}{\Omega}DF(\sigma[\rho+\phi_i(\alpha)]),$$

$$b_i(\rho,\phi_1,\ldots,\phi_n) = \frac{1}{\Omega}\Big[G_i(\sigma(\rho+\phi_1(\alpha-\zeta_1)-\eta_1),\ldots,\sigma(\rho+\phi_n(\alpha-\zeta_n)-\eta_n))-$$

$$-F(\sigma[\rho+\phi_i(\alpha)])\frac{d\phi_i(\alpha)}{d\alpha}\Big].$$

The functions $\phi_i(\alpha)$ and $\phi_i(\alpha-\zeta_i)$ in the expression above are treated as parameters, since they do not depend directly on ρ. Thus, we have a linear non-homogeneous system for P_i, where both A and b_i are 2π periodic in ρ.

Let us consider the adjoint linear homogeneous system:

$$\frac{dQ_i}{d\rho} = -A(\rho,\phi_i)^T Q_i, \tag{3.17}$$

with the normalization condition:

$$\frac{1}{2\pi}\int_0^{2\pi} Q_i^T(\rho,\phi)F(\sigma[\rho+\phi_i(\alpha)])d\rho = 1. \tag{3.18}$$

Since the limit cycle σ is exponentially orbitally stable, the homogeneous system given by (3.16) with $b_i \equiv 0$, $i = 1 \dots n$ and the adjoint system (3.17) both have 1 as a simple Floquet multiplier, and all the other multipliers lie inside the unit circle. Thus, system (3.17),(3.18) has a unique nontrivial periodic solution $\hat{Q}_i(\rho,\phi_i)$.

Now, by the Fredholm alternative, the linear non-homogeneous system (3.16) has a unique periodic solution $\hat{P}_i$ if and only if the following orthogonality condition holds:

$$< \hat{Q}_i, b_i > +O(\varepsilon) = \frac{1}{2\pi}\int_0^{2\pi} \hat{Q}_i^T(\rho,\phi_i)b_i(\rho,\phi_1,\dots,\phi_n)d\rho + O(\varepsilon) = 0. \tag{3.19}$$

Next, assume that we have found $\hat{Q}(\rho,0)$. Since $A(\rho,\phi_i) = \frac{1}{\Omega}DF(\sigma[\rho+\phi_i(\alpha)]) = A(\rho+\phi_i(\alpha))$, it follows that $\hat{Q}(\rho,\phi_i) = \hat{Q}(\rho+\phi_i,0)$. Let us substitute the expression for $b_i(\rho,\phi_1,\dots,\phi_n)$ from (3.16) into the equation (3.19). The multiplier $\frac{1}{\Omega}$ in front of b_i cancels out, and we obtain the following:

$$\begin{aligned}&\tfrac{1}{2\pi}\int_0^{2\pi} \hat{Q}_i^T(\rho+\phi_i,0)G_i(\sigma(\rho+\phi_1(\alpha-\zeta_1)-\eta_1),\dots,\sigma(\rho+\phi_n(\alpha-\zeta_n)-\eta_n))d\rho + O(\varepsilon)\\ &= \tfrac{1}{2\pi}\int_0^{2\pi} \hat{Q}_i^T(\rho+\phi_i,0)F(\sigma[\rho+\phi_i(\alpha)])\tfrac{d\phi_i(\alpha)}{d\alpha}d\rho.\end{aligned}$$

Since $\frac{d\phi_i(\alpha)}{d\alpha}$ is treated as a parameter and is independent of ρ, it could be taken out of the second integral as a constant, and the remaining integral is equal to 1 due to normalization condition (3.18). Thus, we obtain the following equation for the phase deviations $\phi(\alpha)$:

$$\begin{aligned}\frac{d\phi_i(\alpha)}{d\alpha} &= \frac{1}{2\pi}\int_0^{2\pi} \hat{Q}_i^T(\rho+\phi_i,0)G_i(\sigma(\rho+\phi_1(\alpha-\zeta_1)-\eta_1),\\ &\qquad \dots,\sigma(\rho+\phi_n(\alpha-\zeta_n)-\eta_n))d\rho + O(\varepsilon).\end{aligned}$$

Finally, let us change the integration variable to $s = \rho + \phi_i$:

$$\begin{aligned}\tfrac{d\phi_i(\alpha)}{d\alpha} &= \tfrac{1}{2\pi}\int_0^{2\pi} \hat{Q}_i^T(s,0)G_i(\sigma(s+\phi_1(\alpha-\zeta_1)-\eta_1-\phi_i),\\ &\qquad \dots,\sigma(s+\phi_n(\alpha-\zeta_n)-\eta_n-\phi_i))ds + O(\varepsilon)\\ &= H_i(\phi_1(\alpha-\zeta_1)-\eta_1-\phi_i(\alpha),\dots,\phi_n(\alpha-\zeta_n)-\eta_n-\phi_i(\alpha)) + O(\varepsilon).\end{aligned}$$

(3.20)

Equation (3.20) gives precisely the statement of the theorem and hence completes the proof. Q. E. D.

Theorem 3.2.1 provides explicit formulas for the phase deviations. However, the equations for ϕ_i still have a delay in them. It turns out that under some assumptions, the form of the functions $H(\cdot)$ can be simplified. The following corollary of Theorem 3.2.1 is a restatement of the corresponding corollary from [22].

Corollary 3.2.1 (Short transmission delay) *There exists $\eta_0 > 0$, such that for $\eta_i < \eta_0$, $i \in 1...n$ the delay terms in system (3.9) can be neglected, and (3.9) takes form*

$$\frac{d\phi_i}{d\alpha} = H_i(\phi_1 - \eta_1 - \phi_i, \ldots, \phi_n - \eta_n - \phi_i) + O(\varepsilon), \tag{3.21}$$

where all phase deviations are computed at the point α, and the function H_i is defined by integral (3.10).

Proof Using the same argument as in the proof of Theorem 3.2.1, we may assume that $\varepsilon > 0$ without loss of generality. Recall that $\zeta_i = \varepsilon\eta_i$. Hence $\phi_i(\alpha - \zeta_i) = \phi_i(\alpha - \varepsilon\eta_i) = \phi_i(\alpha) + O(\varepsilon)$ provided that term η_i is of $O(1)$ with respect to ε. Substitution of the expansion for $\phi_i(\alpha - \zeta_i)$ in the formula for H_i and expansion of H_i in the Taylor series with respect to ε again gives us the following:

$$\begin{aligned} &H_i(\phi_1(\alpha - \zeta_1) - \eta_1 - \phi_i(\alpha), \ldots, \phi_n(\alpha - \zeta_n) - \eta_n - \phi_i(\alpha)) \\ &= H_i(\phi_1(\alpha) - \eta_1 - \phi_i(\alpha) + O(\varepsilon), \ldots, \phi_n(\alpha) - \eta_n - \phi_i(\alpha) + O(\varepsilon)) \\ &= H_i(\phi_1(\alpha) - \eta_1 - \phi_i(\alpha), \ldots, \phi_n(\alpha) - \eta_n - \phi_i(\alpha)) + O(\varepsilon). \end{aligned} \tag{3.22}$$

It follows that in the case when η_i are of $O(1)$ for all $i \in 1 \ldots n$ the delay term in equation (3.9) affects only $O(\varepsilon)$ remainder and hence could be neglected. More precisely, this means that there exists $\eta_0 > 0$, such that for $\eta_i < \eta_0$, $i \in 1...n$ equality (3.21) is valid.

Q.E.D.

Restatement in the form of the phase equations:

It is possible to rewrite the equations for the phase deviations as a system of equations for the phase variables θ_i. Note that $\theta_j(\rho - \eta_j) - \theta_i(\rho) = (\rho - \eta_j) + \phi_j(\alpha - \zeta_j) - \rho - \phi_i(\alpha) = \phi_j(\alpha - \zeta_j) - \eta_j - \phi_i(\alpha)$. We see that difference between phase variables depends only on the slow variable α and is precisely equal to the argument of the function $H_i(\cdot)$. Consider the phase variable $\theta_i(t)$. By its definition, $\theta_i(t) = \rho + \phi_i(\alpha)$, which implies

$$\frac{d\theta_i}{d\rho} = 1 + \frac{\phi_i(\alpha)}{d\rho} = 1 + \varepsilon\frac{\phi_i(\alpha)}{d\alpha}. \tag{3.23}$$

Applying the result of Theorem 3.2.1 to equation (3.23), we obtain the following system for the phase variables

$$\frac{d\theta_i}{d\rho} = 1 + \varepsilon H_i(\theta_1(\rho-\eta_1)-\theta_i(\rho),\ldots,\theta_n(\rho-\eta_n)-\theta_i(\rho)) + O(\varepsilon^2). \tag{3.24}$$

When the delay terms η_i satisfy the conditions of Corollary 3.2.1, equation (3.24) takes form

$$\frac{d\theta_i}{d\rho} = 1 + \varepsilon H_i(\theta_1-\eta_1-\theta_i,\ldots,\theta_n-\eta_n-\theta_i) + O(\varepsilon^2), \tag{3.25}$$

where all phase variables θ_i are computed at the point ρ.

3.3 Phase equations of the Morris-Lecar system.

Now we are ready to apply the theory developed to the our system of interest (2.16). Recall that in the general case it has form:

$$\left\{\begin{array}{rcl} v_1' &=& -g_{Ca}m_\infty(v_1)(v_1-1) - g_K w_1(v_1-v_K) - g_L(v_1+v_L) \\ && +i+\gamma(v_2(t-\tau)-v_1) \\ w_1' &=& \phi\lambda(v_1)[w_\infty(v_1)-w_1] \\ v_2' &=& -g_{Ca}m_\infty(v_2)(v_2-1) - g_K w_2(v_2-v_K) - g_L(v_2+v_L) \\ && +i+\gamma(v_1(t-\tau)-v_2) \\ w_2' &=& \phi\lambda(v_2)[w_\infty(v_2)-w_2]. \end{array}\right. \tag{3.26}$$

Subsystems X_1 and X_2 are given by the subsystems (v_1, w_1) and (v_2, w_2), while coupling strength γ plays the role of parameter ε. According to the problem setting provided in section 2.5 we choose the parameters so that each of the decoupled subsystems $\dot{X}_i = F(X_i)$ has an exponentially asymptotically stable limit cycle σ with the period T. According to section 3.2, there exists $\gamma_0 > 0$, such that for all $0 < |\gamma| < \gamma_0$ there exists an neighborhood W of $\sigma \times \sigma \subset \mathbb{R}^2$ and a continuous function $h : W \to \mathbb{T}^2$, which maps solutions of system (3.26) to those of the system:

$$\left\{\begin{array}{l} \frac{d\theta_1}{d\rho} = 1 + \gamma g_1(\theta_1,\theta_2) + O(\gamma^2) \\ \frac{d\theta_2}{d\rho} = 1 + \gamma g_2(\theta_1,\theta_2) + O(\gamma^2) \end{array}\right. , \tag{3.27}$$

where $\rho = \Omega t$ and $\Omega = 2\pi/T$. The explicit form of the functions g_1 and g_2 is determined by Theorem 3.2.1

$$g_1(\theta_1,\theta_2) = H_1(\theta_2(\rho-\eta)-\theta_1(\rho)) = \tfrac{1}{2\pi}\int_0^{2\pi} Q^T(s)G_1(\sigma[s],\sigma[s+\theta_2(\rho-\eta)-\theta_1(\rho)])ds,$$
$$g_2(\theta_1,\theta_2) = H_2(\theta_1(\rho-\eta)-\theta_2(\rho)) = \tfrac{1}{2\pi}\int_0^{2\pi} Q^T(s)G_2(\sigma[s+\theta_1(\rho-\eta)-\theta_2(\rho)],\sigma[s])ds.$$

(3.28)

Note that in case of system (3.26) $G_1(X_1, X_2) = v_2(t-\tau) - v_1(t)$ and $G_2(X_1, X_2) = v_1(t-\tau) - v_2(t)$, and thus we have that $G_1(X_1, X_2) = G_2(X_2, X_1)$. Thus, if we define a function H as

$$H(\cdot) = \frac{1}{2\pi} \int_0^{2\pi} Q_i^T(s) G_1(\sigma[s], \sigma[s+\cdot]) ds, \tag{3.29}$$

we will have that

$$\begin{aligned} H_1(\theta_2(\rho-\eta) - \theta_1(\rho)) &= \frac{1}{2\pi} \int_0^{2\pi} Q^T(s) G_1(\sigma[s], \sigma[s+\theta_2(\rho-\eta) - \theta_1(\rho)]) dt \\ &= H(\theta_2(\rho-\eta) - \theta_1(\rho)), \end{aligned}$$

while

$$H_2(\theta_1(\rho-\eta) - \theta_2(\rho)) = \frac{1}{2\pi} \int_0^{2\pi} Q^T(s) G_2(\sigma[s+\theta_1(\rho-\eta) - \theta_2(\rho)], \sigma[s]) ds$$

$$= \frac{1}{2\pi} \int_0^{2\pi} Q^T(s) G_1(\sigma[s], \sigma[s+\theta_1(\rho-\eta) - \theta_2(\rho)]) ds = H(\theta_1(\rho-\eta) - \theta_2(\rho)).$$

We have just shown that in the case when the subsystems X_1 and X_2 are identical and symmetrically coupled, functions H_1 and H_2 can be expressed in terms of a single function H, and dynamics of system (3.26) is thus given by a phase system:

$$\begin{cases} \frac{d\theta_1}{d\rho} = 1 + \gamma H(\theta_2(\rho-\eta) - \theta_1(\rho)) + O(\gamma^2) \\ \frac{d\theta_2}{d\rho} = 1 + \gamma H(\theta_1(\rho-\eta) - \theta_2(\rho)) + O(\gamma^2) \end{cases}. \tag{3.30}$$

The complete system for the phase variables (3.30) is hard to analyze since it is a system of delayed differential equations. Thus, at this point it is necessary to simplify the system by applying Corollary 3.2.1. It follows that there exists an $\eta_0 > 0$, such that for all $\eta < \eta_0$ the delay can be replaced by the phase shift without increasing the error more than by a term of $O(\gamma^2)$. System (3.31) then becomes a system of ordinary differential equations which has the form:

$$\begin{cases} \frac{d\theta_1}{d\rho} = 1 + \gamma H(\theta_2 - \theta_1 - \eta) + O(\gamma^2) \\ \frac{d\theta_2}{d\rho} = 1 + \gamma H(\theta_1 - \theta_2 - \eta) + O(\gamma^2) \end{cases}. \tag{3.31}$$

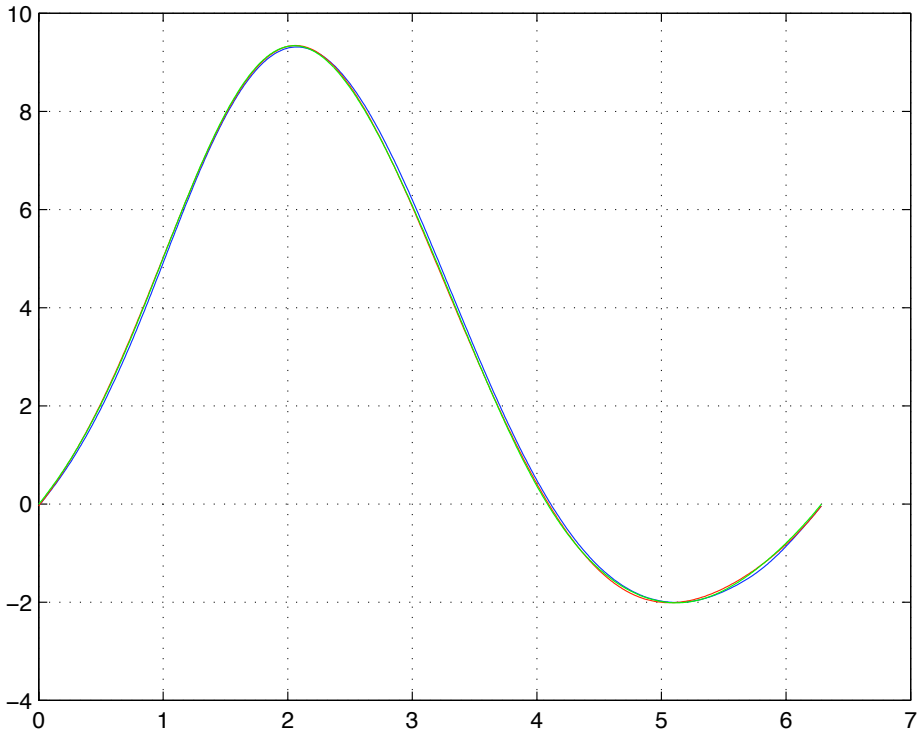

Figure 3.2: $H(\varphi)$ as the sum of first 3, first 5, and first 480 terms of its Fourier series expansion

Finally, let us introduce new variable $\varphi = \theta_2 - \theta_1$. The variable φ is called a *phase difference*, and describes the amount of synchronization between subsystems X_1 and X_2. $\varphi = 0$ corresponds to the case when X_1 and X_2 are completely synchronized. In terms of φ (3.31) reduces to the single equation:

$$\dot{\varphi} = \gamma(H(-\varphi - \eta) - H(\varphi - \eta)) + O(\gamma^2). \tag{3.32}$$

For γ small enough the impact of the term $O(\gamma^2)$ on the dynamics of equation (3.32) is negligible. Hence, at this point we will drop the term $O(\gamma^2)$, assuming that γ_0 stated in theorem 3.2.1 is sufficiently small. It is convenient to break the following analysis into the 2 branches - the case of $\eta = 0$ and the case of nonzero η satisfying condition $\eta < \eta_0$. Let us consider the simpler case of $\eta = 0$ first, and then generalize it for $\eta < \eta_0$.

3.3.1 Equation for the phase difference in the non-delayed case.

Consider $\eta = 0$. In this case equation (3.32) takes the form

$$\dot{\varphi} = \gamma(H(-\varphi) - H(\varphi)). \tag{3.33}$$

Recall that our general goal is to determine the stable periodic solutions of system (3.26) with respect to the values of parameter γ. Thus, we are interested in finding all equilibrium solutions of equation (3.33), and computing their stability.

Further analysis has to be done numerically or graphically, since there is no convenient way to compute function $H(\cdot)$ analytically. However, $H(\cdot)$ could be easily computed numerically. In the present thesis we used the XPPAUT software for the computation of $H(\cdot)$. The technical side of the calculations is provided in [10] on pages 223-226. Omitting unnecessary details, it worth mentioning that XPPAUT can compute $H(\varphi)$ in terms of its Fourier series expansion (recall that by its definition the function $H(\cdot)$ is 2π-periodic).

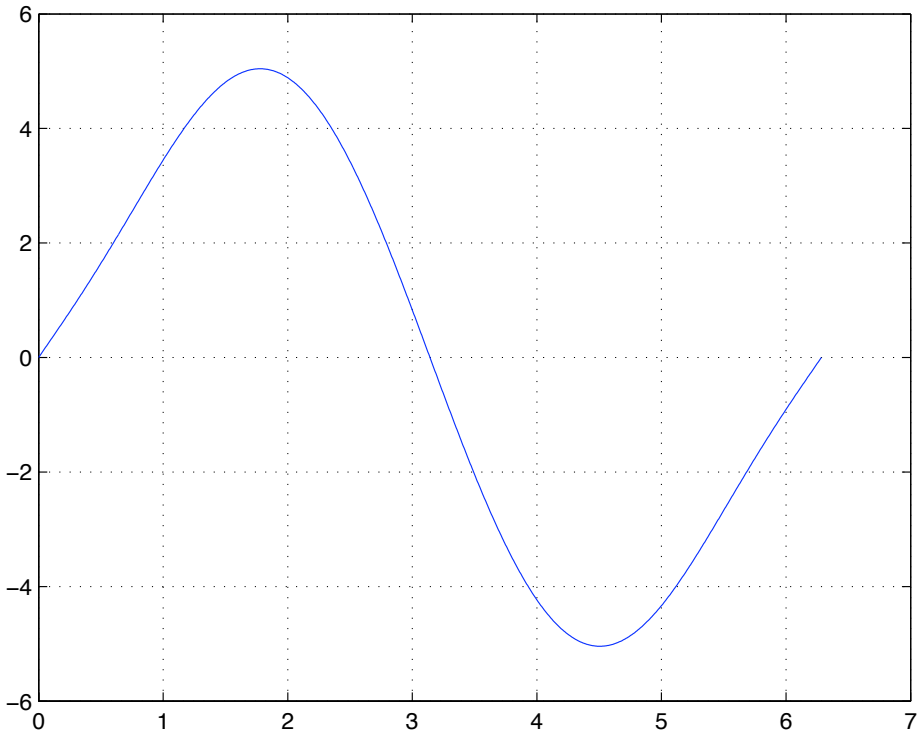

Figure 3.3: $H_{odd}(\varphi)$ vs φ for the type I parameter set

Let $H(\varphi) = \sum_{k=1}^{+\infty}(a_n \cos(k\varphi) + b_n \sin(k\varphi))$. Direct substitution in equation (3.33) shows that all the cosine terms cancel out, and only sine terms are left:

$$\dot{\varphi} = -2\gamma \sum_{k=1}^{+\infty} b_n \sin(k\varphi) = -2\gamma H_{odd}(\varphi). \tag{3.34}$$

This immediately implies that $\varphi = 0$ and $\varphi = \pi$ are the equilibrium solutions of the equation for any function H. Stability of the solutions $\varphi = 0$ and $\varphi = \pi$ as well as existence or nonexistence of the other equilibrium solutions has to be determined numerically by plotting the graph of $H(\varphi)$.

In order to proceed to direct analysis of the equilibrium, it is helpful to determine the number of terms so that the truncated series approximates the infinite series $\sum_{k=1}^{+\infty} b_n \sin(k\varphi)$ well. For our system it turns out that the Fourier coefficients of H decay very fast, and $N = 5$ provides a good agreement with the infinite series. Figure (3.2) shows the graphs of

$$H(\varphi) = \sum_{k=1}^{N} a_n \cos(k\varphi) + b_n \sin(k\varphi)$$

for $N = 3$, $N = 5$ and $N = 481$. Graph for $N = 3$ differs a little from the other graphs, while graphs for $N = 5$ and $N = 481$ are almost undistinguishable. Thus, we will use the truncated series with $N = 5$ as an approximation of the infinite series.

Let us study the stability of equilibria next. Figure (3.3) gives the graph $H_{odd}(\varphi) = \sum_{k=1}^{5} b_n \sin(k\varphi)$ with respect to φ over one period for the *Type I* oscillation. It follows that $\varphi = 0$ and $\varphi = \pi$ are the only possible equilibrium solutions in this case.

The stability of the equilibria is determined by the linearization of $H_{odd}(\varphi)$ at each equilibrium point $\varphi = \bar{\varphi}$, which is given by the equation

$$\dot{\varphi} = -2\gamma H'_{odd}(\bar{\varphi})\varphi.$$

It follows that the equilibrium point $\bar{\varphi}$ is stable when $\gamma H'_{odd}(\bar{\varphi}) > 0$, and unstable when $\gamma H'_{odd}(\bar{\varphi}) < 0$.

According to figure (3.3) $H'_{odd}(0) > 0$, while $H'_{odd}(\pi) < 0$. It follows, that for $\gamma > 0$ solution $\varphi = 0$ is stable, and $\varphi = \pi$ is unstable, while for $\gamma < 0$ $\varphi = 0$ is unstable, and $\varphi = \pi$ is stable.

Let us study the type II oscillations next. Figure (3.4) provides the graph of $H_{odd}(\varphi)$ vs φ in the case of type II parameter set. It follows, that $H'_{odd}(0) > 0$, while $H'_{odd}(\pi) < 0$. Thus, we may conclude that in the case of non-delayed coupling functions type I and type II Morris Lecar systems exhibit qualitatively the same behavior for small values of γ and $\eta = 0$.

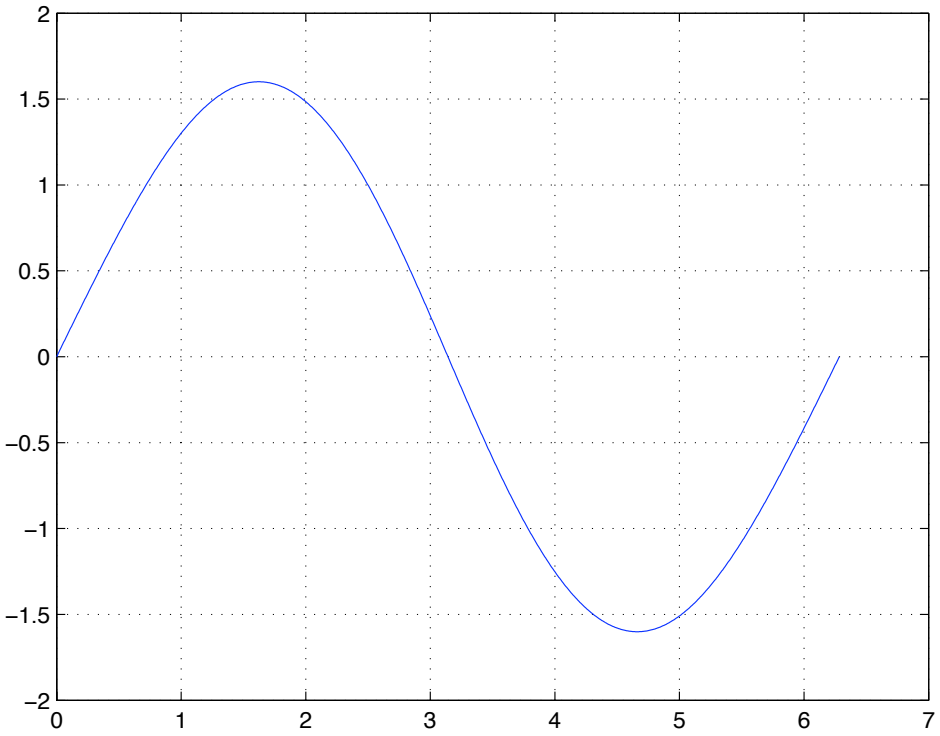

Figure 3.4: $H_{odd}(\varphi)$ vs φ for the type II parameter set

3.3.2 Equation for the phase difference in the delayed case.

Let us consider the case of nonzero η next. Substitution of the Fourier series expansion of $H(\cdot)$ into equation (3.32) leads to the equation

$$\begin{aligned}\dot{\varphi} &= \sum_{k=1}^{+\infty} a_k \cos(k[\varphi+\eta]) - b_k \sin(k[\varphi+\eta]) - \sum_{k=1}^{+\infty} a_k \cos(k[\varphi-\eta]) + b_k \sin(k[\varphi-\eta]) \\ &= \sum_{k=1}^{+\infty} a_k(\cos(k[\varphi+\eta]) - \cos(k[\varphi-\eta])) + b_k(-\sin(k[\varphi+\eta]) - \sin(k[\varphi-\eta])).\end{aligned} \tag{3.35}$$

Note that $\cos(x+y)-\cos(x-y) = -2\sin x \sin y$ and $-\sin(x+y)-\sin(x-y) = -2\sin x \cos y$. Substitution of these trigonometric identities to (3.35) leads to the following equation

$$\begin{aligned}&\dot{\varphi} = -2\gamma \sum_{k=1}^{+\infty} c_k \sin k\varphi \doteq -2\gamma H_{delay}(\varphi), \qquad \text{where} \\ &c_k = a_k \sin(k\eta) + b_k \cos(k\eta).\end{aligned} \tag{3.36}$$

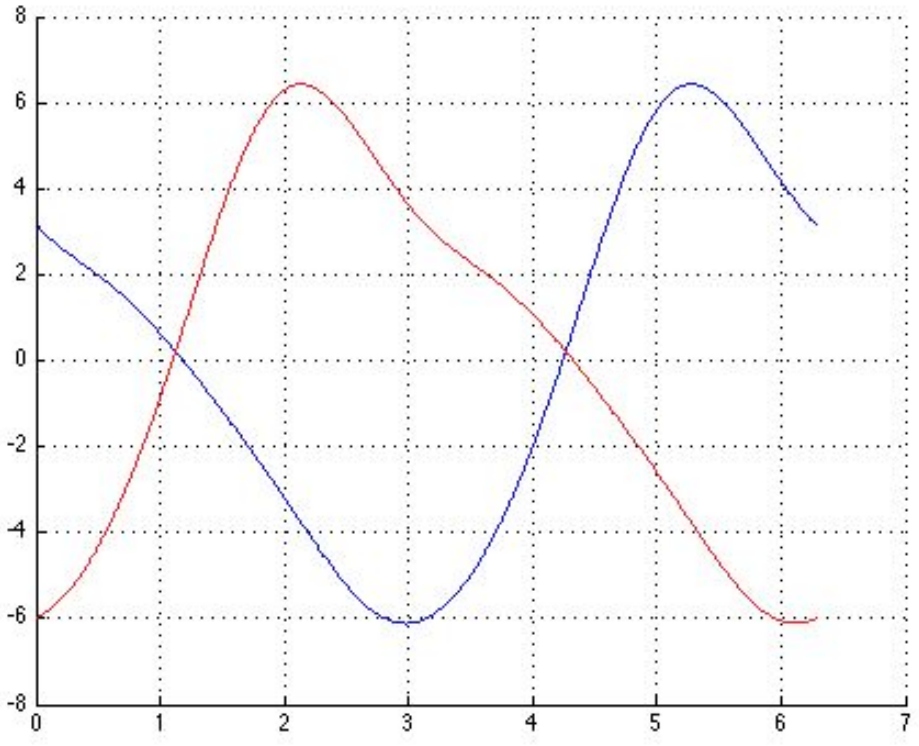

Figure 3.5: $H'_{delay}(\bar{\varphi})$ vs η for the type I parameter set

As in the case of $\eta = 0$, the form of equation (3.36) implies that values of $\varphi = 0$ and $\varphi = \pi$ are always the equilibrium solutions of (3.36). However, the stability of the given solutions is determined by the value of η as well as the values of a_k and b_k. By analogy with the case of $\eta = 0$, stability of the equilibrium point $\varphi = \bar{\varphi}$ is determined by the linearization of (3.36) at $\varphi = \bar{\varphi}$, which is given by

$$\dot{\varphi} = -2\gamma H'_{delay}(\bar{\varphi})\varphi, \tag{3.37}$$

where $H'_{delay}(\bar{\varphi}) = \sum_{k=1}^{+\infty} kc_k \cos k\bar{\varphi}$. The solution $\varphi = \bar{\varphi}$ is stable when $\gamma H'_{delay}(\bar{\varphi}) > 0$, and unstable when $\gamma H'_{delay}(\bar{\varphi}) < 0$.

Thus, it is possible to determine which of the equilibrium solutions is stable for each value of η by plotting the graphs of the approximations of $H'_{delay}(0) \approx \sum_{k=1}^{N} k[a_k \sin(k\eta) + b_k \cos(k\eta)]$ and $H'_{delay}(\pi) \approx \sum_{k=1}^{N} (-1)^k k[a_k \sin(k\eta) + b_k \cos(k\eta)]$. For the parameter set of type I the graphs are given by figure (3.5). The blue line represents $H'_{delay}(0)$, while the red line represents $H'_{delay}(\pi)$.

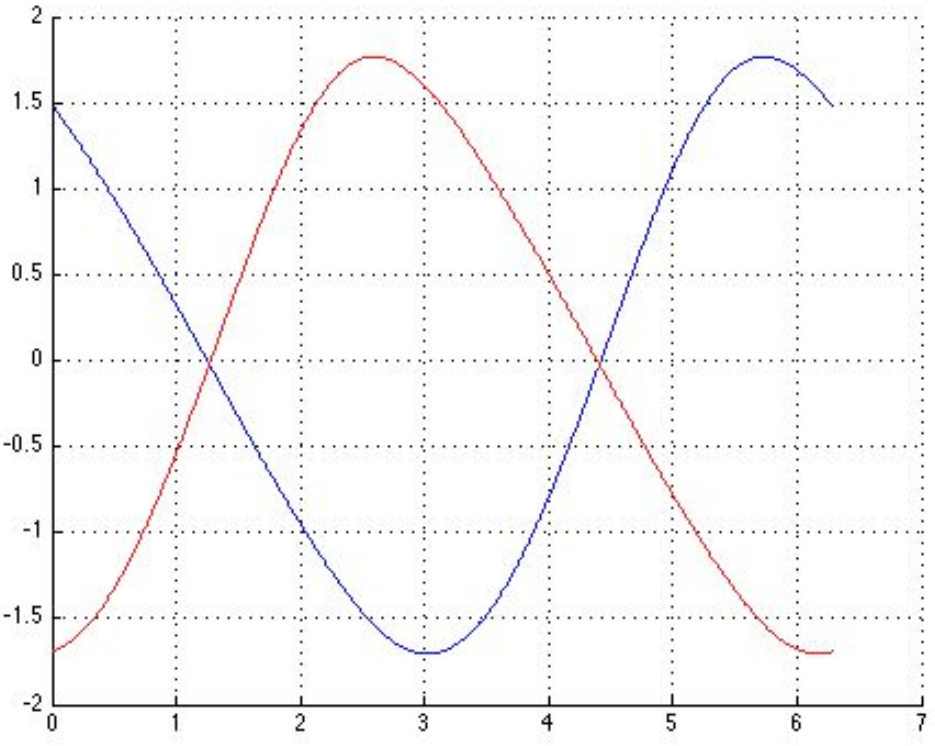

Figure 3.6: $H'_{delay}(\bar{\varphi})$ vs η for the type II parameter set

It follows that for $\gamma > 0$ the in-phase solution is stable for η between 0 and some critical value η_1, since $H'_{delay}(0)$ is positive in that range of η. The point $\eta = \eta_1$ is the point where the $H'_{delay}(\pi)$ becomes positive, and hence the anti-phase solution becomes stable. There is a small range of η in which the system exhibits multi-stability, until the in-phase solution becomes unstable at some value $\eta = \eta_2$. Then the anti-phase solution becomes the only stable solution, and remains in that state until the next period of multi-stability which is reached at $\eta = \eta_3$. At $\eta = \eta_4$ the anti-phase solution becomes unstable, and there is the only one stable in-phase solution up to $\eta = 2\pi$. Since $H'_{delay}(\cdot)$ is 2π periodic function of η, the picture described above repeats as η is increased beyond 2π.

For $\gamma < 0$ the stability picture is slightly different. The anti-phase solution is stable for $\eta \in (0, \eta_1)$, then in the region (η_1, η_2) neither in-phase, nor anti-phase solution is stable. For $\eta \in (\eta_2, \eta_3)$ the only stable solution is the in-phase solution. Then in the region (η_3, η_4) there is no known stable solution. Finally, the anti-phase solution becomes stable again at $\eta = \eta_4$ and remains stable up to $\eta = 2\pi$, after which the periods of stability and instability follow periodically.

Consider the stability diagram for the model of type II. The graphs of $H'_{delay}(0)$ and $H'_{delay}(\pi)$ are provided in figure (3.6). For the type II parameter set, the neurons exhibit multi-stability for $\gamma < 0$, while for positive values of γ there are

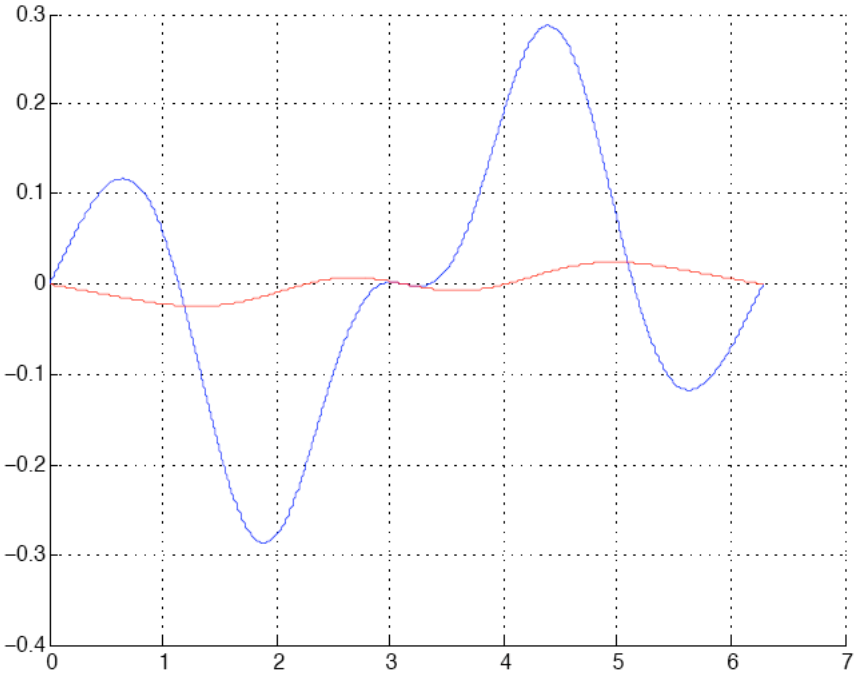

Figure 3.7: $H_{delay}(\varphi)$ vs φ for η in the transition interval for Type I (blue) and Type II (red) system

regions where neither anti-phase nor inphase solution is stable. In other aspects the behavior of type II model is qualitatively similar to that of the model of type I, the difference occurs only in small regions where the stability switch happens.

Let us study the behavior of type I and type II models in the region where stability switching occurs. Figure (3.7) provides graphs of $H_{delay}(\varphi)$ with respect to φ for $\eta \in (\eta_1, \eta_2)$ for both models. It follows that in both cases there exists a third equilibrium point $\bar{\varphi}$, which is neither in-phase nor anti-phase. However, the sign of $H'_{delay}(\varphi)$ is different for type I and type II system. For $\gamma > 0$ in the case of the system of type I the third equilibrium point is unstable but both in-phase and anti-phase solutions are stable, while for the system of type II the opposite statement holds.

To conclude the analysis it is worth mentioning that the values of the actual delay τ at which the stability switches are determined from the expression $\tau_i = \eta_i/\Omega$. It follows that the smaller the value of Ω, the larger the intervals between stability switches in τ. This determines an important difference between type I and type II models of neuron, since in neurons of type I the value of Ω could be made arbitrarily small by appropriate choice of the input signal i (see section 2.3.6).

3.4 Region of validity of the phase model

Theorem 3.2.1 and Corollary 3.2.1 imply that analysis of the phase model for the Morris-Lecar equation is valid only for $|\gamma| < \gamma_0$ and $0 \geq \eta < \eta_0$ for some γ_0 and η_0 in $\mathbb{R}$.

The value of γ_0 defines the region in which the coupling can be considered as small, and hence is determined by the properties of the original Morris-Lecar system (3.26). The value of γ_0 can be estimated numerically (see chapter 4).

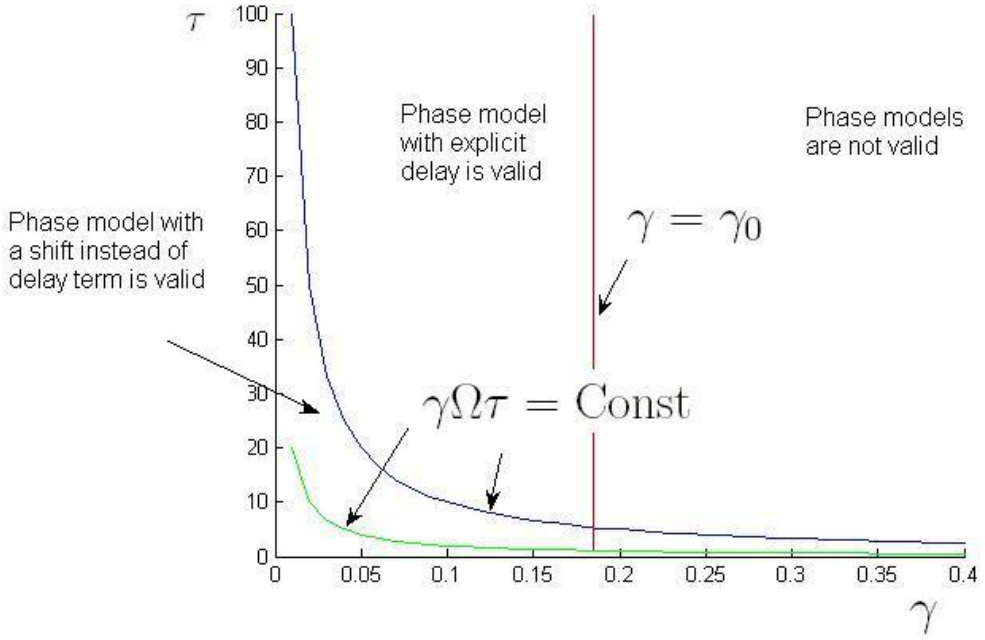

Figure 3.8: Scheme of the phase model validity

The situation with η_0 is more interesting. Recall that $\eta = \Omega\tau$, while the actual value of delay is given by the parameter τ. Corollary (3.2.1) states that η has to be of $O(1)$ on the γ scale in order to validate replacement of the delay term by the phase shift. Thus, the smaller values of γ we will consider, the larger values of τ would allow replacement of the delay term by the phase shift. Small values of Ω should increase region of validity of the phase model with shift with respect to τ as well. This may play an important role in the difference between Type I and Type II models, since for the model of Type II frequency has a minimal value Ω_0, while in the case of Type I model the frequency $\Omega \to 0$ as input approaches a critical value where the oscillations are set.

The analysis done in the present chapter suggests the scheme of validity of the phase model shown on figure (3.8). Although the region of validity has to be determined in $O(\cdot)$ notation and hence may not have precise border, straight lines

are drawn to schematically visualize the form of the region. For $\gamma > \gamma_0$ the phase model is not valid, since the coupling cannot be considered small anymore, and the normally hyperbolic manifold is not guaranteed to persist. In the region of validity of the phase model, small values of the delay allow a phase model with a shift instead of delay, while for large values of the delay the delayed differential equations (3.24) have to be considered. According to the form of η, the line where predictions of phase model with a phase shift (3.25) break should have form $\gamma\Omega\tau = const$. Note that the smaller Ω is, the larger the region of validity of the phase model, which can be seen by comparison of the green and blue lines ($\Omega_{green} = 5\Omega_{blue}$) in figure (3.8).

3.5 Conclusion

When the physical parameters of system (3.26) are fixed either to the type I or the type II parameter set (see table (2.1)) the non-delayed system (3.26) has only one stable periodic solution in the region of the validity of the phase model, i.e. for $|\gamma| < \gamma_0$. For $\gamma > 0$ the stable solution is given by the *synchronous* periodic solution, while for $\gamma < 0$ the *antiphase* solution is the only stable periodic solution of system (3.26).

In the case of the delayed system (3.26) the type I and type II neurons switch between in-phase and anti-phase solution being stable as η is increased to η_0 (see section 3.3.2). The switches in stability occur for nearly the same values of η for both types of neurons.

It follows that the value of the time delay η is an important factor affecting the stability of the solutions of (3.26). For most values of η in-phase or anti-phase solution is the only stable solution, while switches between stability occur over the small intervals of η. Over the interval of η where stability change occurs either there is multi-stability or there exists a third stable periodic solution (see section 3.3.2). The systems of type I and type II demonstrate qualitatively the same behavior except for how the changes of stability occur.

The dynamics of the delayed Morris Lecar system doesn't depend on the absolute value of the time delay τ, but is determined by the relative size of delay τ with respect to the natural frequency of oscillations Ω, since $\eta = \Omega\tau$. The estimate of the region of validity of phase model done in section 3.4 and Theorem 3.2.1 produce this conclusion.

It follows that the smaller the value of Ω, the bigger the intervals before the stability switches in τ, and the larger the region of validity of the phase model (3.32) with respect to τ. This factor is especially important for the neurons of type I and might seriously affect the behavior of the network, since the period of oscillation of the neuron of type I vary in a wide range with respect to the value of applied input i. The neurons of type II are not as sensitive to the relationship between τ and Ω.

The difference in behavior over the intervals where stability is changed can be caused by the difference in parameters of type I and type II neuron. We will study this question in more detail in the next chapter.

Chapter 4

Bifurcation analysis

In the present thesis we study the dynamics of system (2.16) with respect to the variation of parameters τ and γ. So far, we have determined the nature of the stable periodic solutions of the system (2.16) for small values of γ and τ by studying the corresponding phase equations (see chapter 3). However, it is not yet clear how small the parameters γ and τ should be in order to apply the phase model, and what happens when γ and τ are beyond the region of validity of the phase model.

In the present chapter we will try to answer this question by numerical analysis of system (2.16). In order to obtain a starting point for our analysis, we will first analyze the equilibrium points of system (2.16). In particular, we will answer the following question: how do the equilibrium points of the system change with respect to the variation of the parameter γ? We will address this question by analyzing the algebraic equations corresponding to system (2.16) using Matlab. The structure of the equilibrium points with respect to γ will allow us to determine an upper bound for the region of validity of the phase model, γ_0 (defined in section 3.4), and will provide a foundation for the bifurcation analysis of system (2.16) with respect to variation of γ and τ.

The second part of the present chapter is devoted to numerical analysis of system (2.16) in the special case of $\tau = 0$. In that case, (2.16) is a system of ordinary differential equations. We will do the bifurcation analysis of the system with respect to parameter γ using the software programs XPPAUT and AUTO.

Finally, the last part of the chapter covers the numerical analysis of system (2.16) for the arbitrary values of γ and τ. Using the information gathered in the previous parts of the chapter as a starting point, we will do a two-parameter bifurcation analysis of system (2.16) with respect to variation of γ and τ by using a special software package for delay differential equations called DDE-BIFTOOL.

4.1 The equilibrium points

One of the important characteristics of any dynamical system is the number and the stability of its equilibrium points. Since we are studying the behavior of system (2.16) with respect to variation of the parameters γ and τ, it is important to determine the number of equilibrium points of (2.16) for each value of the parameter γ and to understand how each equilibrium point evolves as γ is varied. The answer to this question will allow us to find all the equilibrium points numerically and to perform the further bifurcation analysis of system (2.16). Moreover, the structure of the equilibrium points is independent of the value of the parameter τ. Hence, the results of the present section will be applicable for any value of τ.

4.1.1 Theoretical foundation

Consider system (2.16). For the type I parameter set it has the following explicit form:

$$\begin{cases} v_1' = -m_\infty(v_1)(v_1-1) - 2w_1(v_1+0.7) - 0.5(v_1+0.5) + 0.09 + \gamma(v_2(t-\tau) - v_1) \\ w_1' = \frac{1}{3}\lambda(v_1)[w_\infty(v_1) - w_1] \\ v_2' = -m_\infty(v_2)(v_2-1) - 2w_2(v_2+0.7) - 0.5(v_2+0.5) + 0.09 + \gamma(v_1(t-\tau) - v_2) \\ w_2' = \frac{1}{3}\lambda(v_2)[w_\infty(v_2) - w_2], \end{cases} \tag{4.1}$$

where $v_\infty(\cdot), w_\infty(\cdot)$ and $\lambda(\cdot)$ are the functions defined in subsection 2.3.5.

By definition, the equilibrium points of system (4.1) are the solutions where v_1,v_2,w_1 and w_2 are constant in time. These are the solutions of the following system of equations:

$$\begin{cases} -m_\infty(v_1)(v_1-1) - 2w_1(v_1+0.7) - 0.5(v_1+0.5) + 0.09 + \gamma(v_2 - v_1) = 0 \\ \frac{1}{3}\lambda(v_1)[w_\infty(v_1) - w_1] = 0 \\ -m_\infty(v_2)(v_2-1) - 2w_2(v_2+0.7) - 0.5(v_2+0.5) + 0.09 + \gamma(v_1 - v_2) = 0 \\ \frac{1}{3}\lambda(v_2)[w_\infty(v_2) - w_2] = 0. \end{cases} \tag{4.2}$$

Hence, the equilibrium points are the same for all values of τ in $\mathbb{R}$.

System (4.2) is nonlinear, its explicit solution is impossible. Nevertheless it could be reduced to a two-dimensional system. The second and the fourth equations of (4.2) allow us to express the variables w_1 and w_2 in terms of v_1 and v_2: $w_1 = w_\infty(v_1)$ and $w_2 = w_\infty(v_2)$. After elimination of the variables w_i we obtain two equations that completely determine all possible equilibrium solutions of (4.1) :

$$\begin{cases} f(v_1) + \gamma(v_2 - v_1) = 0 \\ f(v_2) + \gamma(v_1 - v_2) = 0 \end{cases}, \tag{4.3}$$

where $f(v) = -m_\infty(v)(v-1) - 2w_\infty(v)(v+0.7) - 0.5(v+0.5) + 0.09.$

To determine how many different solutions (4.3) has for each value of $\gamma \in \mathbb{R}$ it is convenient to introduce new variable: $x = v_2 - v_1$, i.e., $v_2 = x + v_1$. After replacing v_2 by x (4.3) has the following form:

$$\begin{cases} f(v_1) + \gamma x = 0, \\ f(v_1 + x) - \gamma x = 0. \end{cases} \tag{4.4}$$

This form is more useful since it has just one variable x multiplying the parameter γ, instead of a combination of two variables v_1 and v_2. By taking the sum and difference of equations in the latter system we may rewrite it in the form:

$$\begin{cases} f(v_1) + f(v_1 + x) = 0, & (*) \\ f(v_1 + x) - f(v_1) - 2\gamma x = 0. & (**) \end{cases}$$

Let us consider only equation $(*)$ first. This equation is independent of the parameter γ. It gives us the relationship between variables x and v_1 that has to be satisfied for all values of $\gamma \in \mathbb{R}$. Numerical simulations suggested that equation $(*)$ defines v_1 implicitly as a function of x for all $x \in \mathbb{R}$.

Next we consider equation $(**)$. Since we have found $v_1(x)$ from the equation $(*)$, it depends only on the variable x. We may rewrite $(**)$ as

$$f(v_1(x) + x) - f(v_1(x)) = 2\gamma x.$$

The left part of this equation is a function of the variable x only and is *independent* of γ. The right part is just a straight line passing through the origin with slope 2γ. The number of solutions of the system (4.4), and thus the number of different equilibrium points of the system (4.1), could be computed by plotting curves

$$y_1 = f(v_1(x) + x) - f(v_1), \qquad \text{and} \qquad y_2 = 2\gamma x$$

together and computing the number of intersections for each value of γ.

4.1.2 Analysis of the graph

It is possible to construct the graph of $y_1(x)$ numerically using Matlab. The graph of $y_1(x)$ is given by the red curve on the figure (4.1), while the blue, green and cyan lines correspond to graphs of $y_2(x) = 2\gamma x$ for several special values of the parameter γ which will be discussed later.

Note that both $y_1(x)$ and $y_2(x)$ are odd functions of the variable x. Oddness of $y_2(x) = 2\gamma x$ is obvious, while the function $y_1(x)$ is odd due to the symmetry of the coupled Morris-Lecar equations. To see this, note that changing the sign of the variable x is equivalent to interchanging v_1 and v_2 since $x = v_2 - v_1$. However, interchanging of v_1 and v_2 leaves the equations (4.3) unchanged since the first and the second neurons are identical.

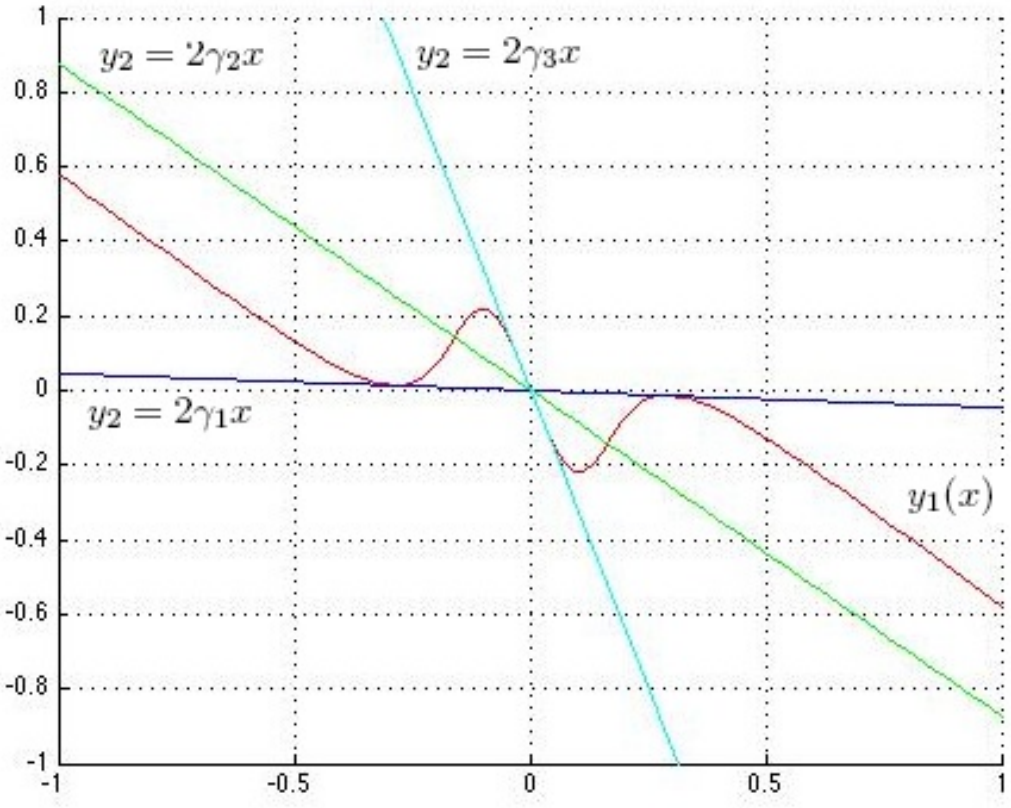

Figure 4.1: Graphs of $y_1(x)$ and $y_2(x)$ with respect to x for important values of γ. The number of intersection points is the number of equilibrium points of (4.1) for the type I parameter set

Recall that we are considering two *identical symmetrically coupled* Morris Lecar neurons. The symmetry implies that if $(\bar{\alpha}_1, \bar{\beta}_1, \bar{\alpha}_2, \bar{\beta}_2)$ is an equilibrium point of the system (2.16), then the point $(\bar{\alpha}_2, \bar{\beta}_2, \bar{\alpha}_1, \bar{\beta}_1)$ is an equilibrium point as well, which is consistent with the oddness of $y_1(x)$ and $y_2(x)$.

Let us continue our analysis of figure (4.1). The blue line corresponds to $\gamma = \gamma_1 = -0.023$ for which the graph of $y_2(x)$ is tangent to the graph of $y_1(x)$ at the rightmost maximum, the green line corresponds to $\gamma = \gamma_2 = -0.4375$ for which the slope of $y_1(x)$ as $x \to \pm\infty$ is equal to $2\gamma_2$, and the cyan line corresponds to $\gamma = \gamma_3 = -1.644$ for which the graph of $y_1(x)$ is tangent to the graph of $y_1(x)$ at the point $x = 0$.

It follows from the graph that $y_1(x)$ and $y_2(x)$ intersect at $x = 0$ for all $\gamma \in \mathbb{R}$. Thus, the system (4.1) has the symmetric equilibrium point $(\bar{v}, \bar{w}, \bar{v}, \bar{w})$ for all values of $\gamma \in \mathbb{R}$. This fact is easy to explain. Note that for $v_1 \equiv v_2 = v$ and $w_1 \equiv w_2 = w$ the coupling terms in the system (4.1) are equal to zero, and (4.1) is equivalent to

two identical, decoupled Morris Lecar neurons:

$$\begin{cases} v' = -m_\infty(v)(v-1) - 2w(v+0.7) - 0.5(v+0.5) + 0.09 \\ w' = \frac{1}{3}\lambda(v)[w_\infty(v) - w], \\ v' = -m_\infty(v)(v-1) - 2w(v+0.7) - 0.5(v+0.5) + 0.09 \\ w' = \frac{1}{3}\lambda(v)[w_\infty(v) - w]. \end{cases}$$

As was shown in section 2.3.6, the system

$$\begin{cases} v' = -m_\infty(v)(v-1) - 2w(v+0.7) - 0.5(v+0.5) + 0.09 \\ w' = \frac{1}{3}\lambda(v)[w_\infty(v) - w] \end{cases}$$

has a unique equilibrium point $(\bar{v}, \bar{w})$. Thus, the system (4.1) has a symmetric equilibrium point $(\bar{v}, \bar{w}, \bar{v}, \bar{w})$ for all $\gamma \in \mathbb{R}$, which completely agrees with figure (4.1).

Let us analyze the non-symmetric equilibrium points next. Recall that γ determines the slope of line $y_2(x) = 2\gamma x$. According to figure (4.1), there is no intersection between $y_1(x)$ and $y_2(x)$ for $\gamma \in (\gamma_1, +\infty)$. Thus, the system (4.1) has no non-symmetric equilibrium points for $\gamma \in (\gamma_1, +\infty)$. There are exactly 2 non-symmetric equilibrium points for $\gamma = \gamma_1$ by the definition of γ_1, since at $\gamma = \gamma_1$ $y_1(x)$ and $y_2(x)$ intersect twice. By similar reasoning, there are 4 non-symmetric equilibrium points for $\gamma \in (\gamma_2, \gamma_1)$. At $\gamma = \gamma_2$ two of the intersections between $y_1(x)$ and $y_2(x)$ are lost, and hence there are only 2 non-symmetric equilibrium points for $\gamma \in (\gamma_3, \gamma_2)$. Finally, there are no non-symmetric equilibrium points for $\gamma \in (-\infty, \gamma_3]$.

Note that the number of non-symmetric equilibrium points is always even due to the oddness of the functions $y_1(x)$ and $y_2(x)$, which is due to the symmetry of the coupled Morris Lecar equations.

4.1.3 Analysis of the type II parameter set

In the preceding subsections 4.1.1-4.1.2 we have studied the structure of the equilibrium points for the type I parameter set. Exactly the same procedure is applicable to the type II parameter set. As for the type I parameter set, equation $(*)$ defines v_1 as a function of x for all x in $\mathbb{R}$. The number and the behavior of equilibrium points is determined following the same graphical procedure. Figure (4.2) provides a graph of $y_1(x) = v_1(x)$ together with graphs of $y_2(x) = 2\gamma x$ for three critical values of γ for the type II parameter set. The figure (4.2) is harder to visualize than the corresponding figure for the type I parameter set, but it is still possible to determine the critical values of γ by magnifying the figure.

The values of γ_1, γ_2 and γ_3 are:

$\gamma_1 = -0.1873$
$\gamma_2 = -0.4286$
$\gamma_3 = -0.2415,$

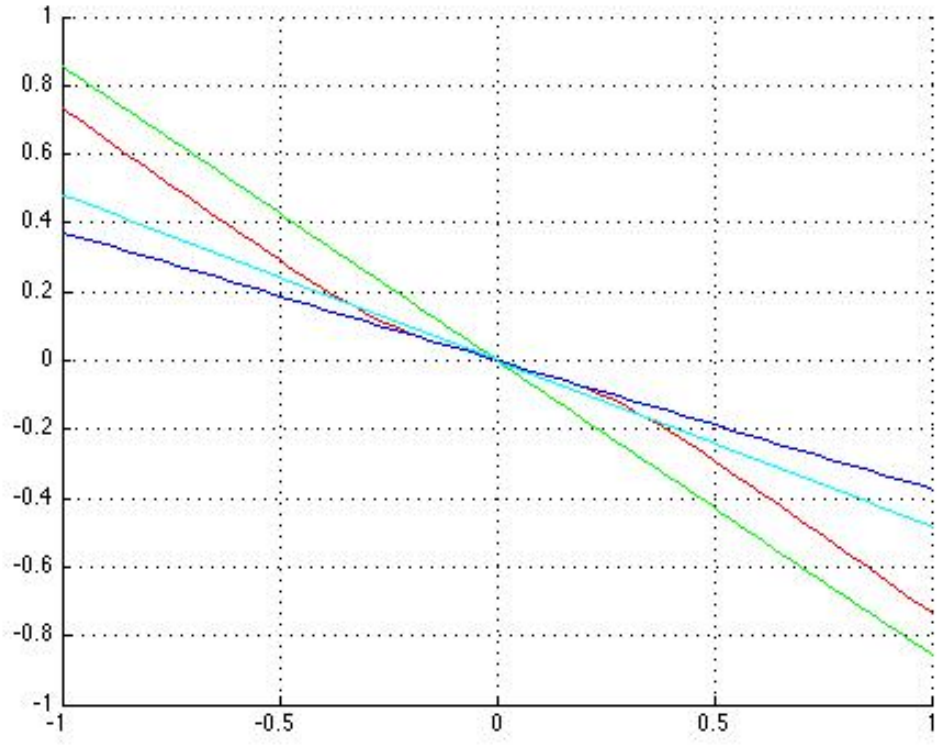

Figure 4.2: Graphs of $y_1(x)$ and $y_2(x)$ with respect to x for important values of γ. The number points of intersection is the number of equilibrium points of (2.16) for type II parameter set. The red line corresponds to $y_1(x)$, the blue line - to $y_2(x) = 2\gamma_1 x$, the green line - to $y_2(x) = 2\gamma_2 x$ and the cyan line - to $y_2(x) = 2\gamma_3 x$.

where γ_i are defined as in the the subsection (4.1.2) - γ_1 corresponds to the point where $y_2(x) = 2\gamma x$ is tangent to the graph of $y_1(x)$ at the rightmost maximum, γ_2 is the value of γ at which y_2 and y_1 become parallel, while for $\gamma = \gamma_3$ graph of $y_2(x)$ is tangent to $y_1(x)$ at the point $x = 0$. Note that the value γ_2 is relatively unchanged in comparison with type I parameter set, while the values of γ_1 and γ_3 become bigger. Note that the order of these values has changed with $\gamma_2 < \gamma_3$ for this parameter set.

It follows that for the type II parameter set, we have the following structure of equilibrium points: there is no non-symmetric equilibrium points for $\gamma \in (\gamma_1, +\infty)$, there are exactly two non-symmetric equilibrium points for $\gamma = \gamma_1$, there are 4 non-symmetric equilibrium points for $\gamma \in (\gamma_3, \gamma_1)$ and there are only 2 non-symmetric equilibrium points for $\gamma \in [\gamma_3, \gamma_2)$. Finally, there are no non-symmetric equilibrium points for $\gamma \in (-\infty, \gamma_2)$.

4.1.4 Conclusion

Knowledge of the number and behavior of the equilibrium points allows us to find them numerically, and to build the bifurcation diagram of system (2.16), which is discussed in section 4.2. The existence of the symmetric equilibrium for all $\gamma \in \mathbb{R}$ and the symmetry of the Morris Lecar equations with respect to interchanging of (v_1, w_1) and (v_2, w_2) is not surprising and can be easily derived without analysis of the equilibrium point structure. However, the fact that graphical analysis allows us to predict these facts verifies its correctness.

The significant part of the present section is the analysis of the non-symmetric equilibrium points, and is quite important for further analysis of the Morris-Lecar system. The following aspects of the non-symmetric equilibrium point behavior are particularly interesting:

• It follows that the symmetric equilibrium point $(\bar{v}, \bar{w}, \bar{v}, \bar{w})$ is the only equilibrium point of (2.16) for all $\gamma \in (\gamma_1, +\infty)$, and is independent of γ. In particular, there are no non-symmetric equilibrium points in the *physical range* of $\gamma > 0$ for all $\tau > 0$. That fact simplifies further numerical analysis of (4.1), since it shows that for all $\gamma > 0$ there is no unstable equilibrium point, which can be missed by bifurcation analysis and then become stable in some range of delay τ.

• The pair of non-symmetric equilibrium points that is lost at $\gamma = \gamma_2$ has a norm that diverges to infinity, since $x = (v_1 - v_2) \to \infty$ as $\gamma \to \gamma_2$ from the left (see figure (4.1)). As we will see in section 4.2, this behavior leads to the global instability of system (4.1) and hence puts an upper bound on the value of γ_0, which cannot be bigger than $\gamma_2 = -0.4375$ in the case of type I oscillator and $\gamma_2 = -0.4286$ in the case of oscillator of type II. That fact that γ_2 can be taken as an upper bound of γ_0 will be precisely explained in section 4.2, which is devoted to the bifurcation analysis of (2.16) with respect to γ in the case of $\tau = 0$.

• Both type I and type II parameter sets lead to nearly the same values of γ_2, while the values of γ_1 and γ_3 are slightly different. This observation suggests that γ_2 characterizes a global property of system (2.16), and hence γ_2 is robust with respect to the variation of parameters of system (2.16). We will study this question in the next chapter.

4.2 Bifurcation analysis in the non-delayed case

In the present section we will analyze the behavior of the non-delayed Morris Lecar system with respect to the variation of the parameter γ. In the case of $\tau = 0$, the

Morris Lecar system (2.16) takes the following form:

$$\begin{cases} v_1' = -g_{Ca} m_\infty(v_1)(v_1 - 1) - g_K w_1(v_1 - v_K) - g_L(v_1 + v_L) + i + \gamma(v_2 - v_1) \\ w_1' = \phi\lambda(v_1)[w_\infty(v_1) - w_1] \\ v_2' = -g_{Ca} m_\infty(v_2)(v_2 - 1) - g_K w_2(v_2 - v_K) - g_L(v_2 + v_L) + i + \gamma(v_1 - v_2) \\ w_2' = \phi\lambda(v_2)[w_\infty(v_2) - w_2]. \end{cases} \tag{4.5}$$

It follows that system (4.5) consists of two *identical* subsystems which are coupled together. It can be rewritten as

$$\begin{cases} X_1' = F(X_1) + \gamma G(X_1, X_2) \\ X_2' = F(X_2) + \gamma G(X_2, X_1) \end{cases}, \quad \text{where} \tag{4.6}$$

$$X_1 = \begin{pmatrix} v_1 \\ w_1 \end{pmatrix}, X_2 = \begin{pmatrix} v_2 \\ w_2 \end{pmatrix}, \quad G(X_k, X_j) = v_j - v_k,$$

$$F(X_j) = \begin{pmatrix} -g_{Ca} m_\infty(v_j)(v_j - 1) - g_K w_j(v_j - v_K) - g_L(v_j + v_L) + i \\ \phi\lambda(v_j)[w_\infty(v_j) - w_j] \end{pmatrix}.$$

Due to its specific structure, system (4.6) exhibits certain symmetries. Consider any solution of (4.6), $\hat{X}(t) = (v_1(t), w_1(t), v_2(t), w_2(t))$, with the property:

$$v_1(t) \equiv v_2(t) = \hat{v}(t) \quad \text{and} \quad w_1(t) \equiv w_2(t) = \hat{w}(t) \quad \text{for all} \quad t \in \mathbb{R}.$$

We will call such solutions $\hat{X}(t)$ *symmetric* or *in-phase*. Since $v_1(t) \equiv v_2(t)$ for all $t \in \mathbb{R}$, we have that $G(\hat{X}_1, \hat{X}_2)$ and $G(\hat{X}_2, \hat{X}_1)$ are identically equal to zero, and the subsystems X_1 and X_2 become decoupled. Thus, any symmetric solution $(\hat{v}(t), \hat{w}(t), \hat{v}(t), \hat{w}(t))$ is independent of γ and will exist for all $\gamma \in \mathbb{R}$. The stability of such a symmetric solution may, however, depend on γ.

It follows that the pair $(\hat{v}(t), \hat{w}(t))$ has to satisfy the equations for a single Morris-Lecar neuron, $X' = F(X)$. As we have determined in section 2.3.6, the single Morris-Lecar system $X' = F(X)$ has one stable periodic solution and one unstable equilibrium point for both the type II and type I parameter sets. It follows that coupled Morris-Lecar system (4.6) will have a symmetric equilibrium point and a symmetric in-phase periodic solution for all values of γ in $\mathbb{R}$, for both the type I and type II parameter sets.

Let us consider the non-symmetric solutions of system (4.6) next. System (4.5) is invariant with respect to interchanging of subsystems X_1 and X_2. More specifically, if $(v_1(t), w_1(t), v_2(t), w_2(t)$ is a solution of system (4.6), then $(v_2(t), w_2(t), v_1(t), w_1(t))$ will be a solution of system (4.6) as well. We have already encountered this property in section 4.2, where all the non-symmetric equilibrium points appeared in pairs. We see that this property can be extended to periodic orbits as well.

Let us summarize what we have determined so far. System (4.5) has a branch of in-phase periodic solutions and a branch of symmetric equilibrium points for all $\gamma \in \mathbb{R}$. The profiles of these symmetric solutions are independent of the value of γ. All the non-symmetric equilibrium points and periodic solutions have to enter the system in pairs due to the fact that the neurons are identical. The structure of the non-symmetric equilibrium points of the system is determined and described in subsection 4.1.4.

4.2.1 Software and algorithms.

We used the program called **XPPAUT** in order to numerically integrate the ODE's and study some properties of ODE's for the fixed values of parameters. We used the **Auto** software package which is included in XPPAUT in order to analyze the bifurcation diagram of system (4.5) with respect to the variation of the parameter γ. XPPAUT was used in order to find the equilibrium points and some stable limit cycles of system (4.5) for a few fixed values of γ, and to plot the solution profiles. The information obtained by XPPAUT was used as a starting point to create general bifurcation diagrams using Auto.

Without getting too much into the details of the numerical procedures employed in the **Auto** program, it is however necessary to make a short comment about the numerical algorithms used.

Assume that we are interested in tracking the limit cycle of the system

$$\dot{X} = F(X, \alpha) \tag{4.7}$$

with respect to the variation of parameter α. Suppose that we know the T periodic limit cycle solution $\sigma_0(t)$ corresponding to $\alpha = \alpha_0$. The general idea of the algorithm implemented in the Auto software is the following:

1. The bifurcation parameter α is given a new value $\alpha_1 = \alpha_0 + \varepsilon$, where ε is the step size which can be varied by user.

2. Assuming that (4.7) has periodic solution for $\alpha = \alpha_1$ as well, the program tries to find that periodic solution $\sigma_1(t)$ by solving the following boundary value problem:
$$\begin{cases} \dot{X} = F(X, \alpha_1) \\ X(0) = \sigma_0(0) \\ X(T) = \sigma_0(0), \end{cases}$$
which is easy to solve numerically. The values of $X(0)$ and $X(t+T)$ are initially set equal to $\sigma_0(0)$ assuming that the limit cycle does not change a lot with small variation of α, and the corrections corresponding to the variation of T and $\sigma_0(0)$ are computed later.

Thus, the algorithm described above allows us to track any type of limit cycle including ones of saddle type, since it does not try to converge to the limit cycle by integration forward or backward in time, but rather solves a boundary value problem. A more detailed overview of the algorithms used in the bifurcation analysis is available in [24], while the description of the Auto and XPPAUT programs is available in [10].

4.2.2 Analysis

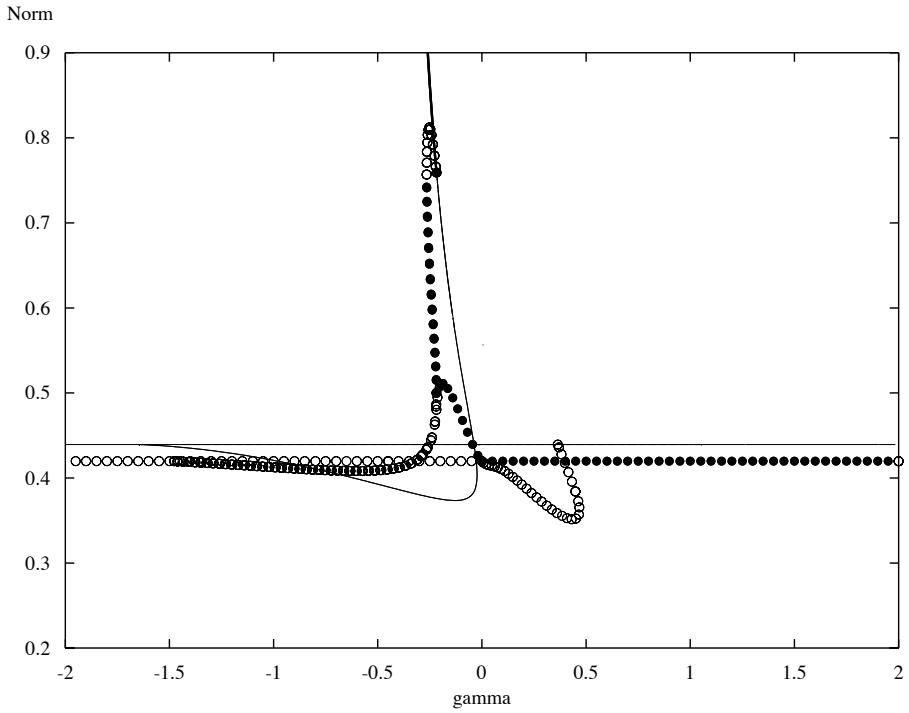

Figure 4.3: Bifurcation diagram of system (4.5) with respect to γ for the type I parameter set. The y axis provides the L_2 norm of each solution, while the x axis corresponds to the value of γ.

Let us consider the general bifurcation diagram of system (4.5) first. Figures (4.3) and (4.4) provide a bifurcation diagram for equation (4.5) with respect to variation of γ for the type I parameter set. The thick lines represent stable equilibrium points and the solid circles represent stable limit cycles, while the thin lines and the empty circles represent unstable equilibrium points and limit cycles respectively.

The horizontal line of limit cycles represents the in-phase periodic solutions of the system discussed above, while the horizontal line of equilibrium points repre-

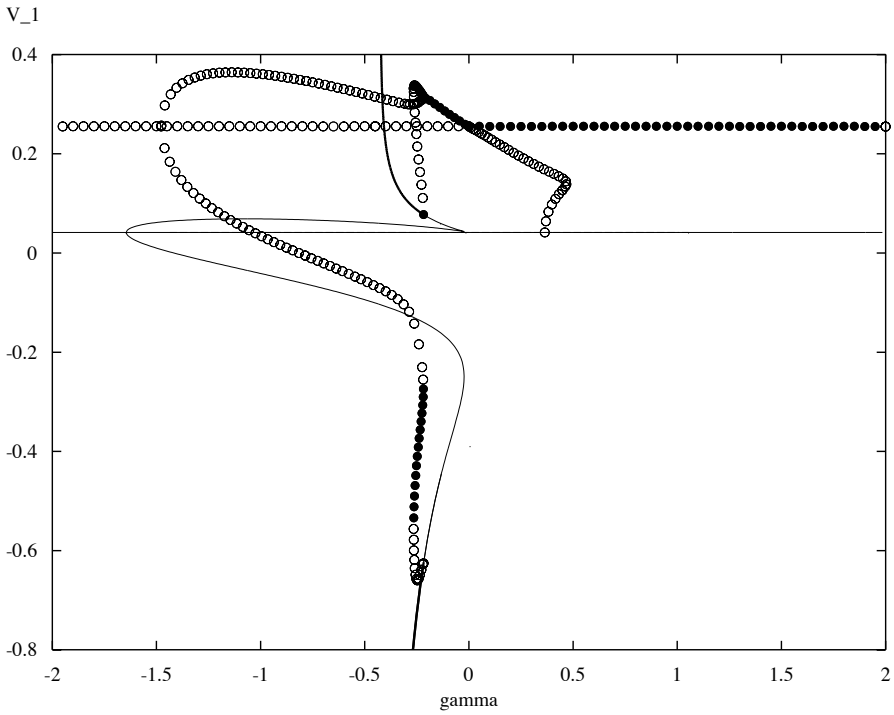

Figure 4.4: Bifurcation diagram of system (4.5) with respect to γ for the type I parameter set. The y axis provides the maximum of $v_1(t)$ along each solution profile, while the x axis corresponds to the value of γ.

sents the symmetric equilibrium point $(\bar{v}, \bar{w}, \bar{v}, \bar{w})$ discussed in the previous section. We see that the profiles of solutions both along the branch of in-phase limit cycles and along the branch of symmetric equilibrium points are independent of γ, since in the case of complete synchrony subsystems X_1 and X_2 are decoupled. The symmetric equilibrium point is unstable for all $\gamma \in \mathbb{R}$, while the in-phase periodic solution is stable for all $\gamma > 0$, and unstable for all $\gamma < 0$.

Let us consider the non-symmetric equilibrium points and limit cycles next. Note that since figure (4.3) gives *the L_2 norm* of solution $(v_1(t), w_1(t), v_2(t), w_2(t))$, the points corresponding to the solutions (u, v, x, y) and (x, y, u, v) are indistinguishable on figure (4.3), since the L_2 norms of the solutions (u, v, x, y) and (x, y, u, v) are equal. Hence, each non-symmetric branch of solutions on figure (4.3) in fact corresponds to the two branches - (u, v, x, y) and (x, y, u, v).

Figure (4.4) allows us to distinguish non-symmetric equilibrium points and limit cycles, since it plots only the maximum along the variable $v_1(t)$. For the equilibrium points it is simply $\bar{v}_1$, while for the limit cycle $\max_{t\in[0,T]} v_1(t)$ is plotted.

The branch of symmetric equilibrium points gives birth to the branch of the

anti-phase limit cycles through a Hopf bifurcation, which occurs at $\gamma = 0.3645$, and to the two branches of non-symmetric equilibrium points through a bifurcation at $\gamma = -1.644$. Each branch of non-symmetric equilibrium points separates into two branches in a limit point bifurcation at $\gamma = -0.2321$. Finally, the two non-symmetric branches become stable through a Hopf bifurcation and give birth to two more branches of limit cycles, which are neither in-phase nor anti-phase. In these limit cycles one neuron suppresses another, i.e. prevents it from firing. See figure (4.5) for an example of the solution from one of the branches mentioned above.

The anti-phase periodic solution is unstable for $\gamma > 0$ and stable for small negative values of γ. However, the stability of the anti-phase solution is lost as the magnitude of the negative γ is increased. Let us consider the region where the anti-phase solution becomes unstable in more detail. The magnified bifurcation diagram is provided in figure (4.6). In the very narrow region of γ first the anti-phase solution is lost in the limit point bifurcation at $\gamma_{ant} = -0.213$. Next, the pair of non-symmetric equilibrium points becomes stable via the Hopf bifurcation at $\gamma_H = -0.2179$, which also creates the pair of unstable "suppressed" limit cycles. The "suppressed" limit cycles become stable in the limit point bifurcation at $\gamma_{lps} = -0.2182$, and the system exhibits multi-stability for the short range of γ, until the stable "suppressed" limit cycles are lost in the limit point bifurcation at $\gamma_{lp} = -0.2655$. For more negative values of γ only the pair of equilibrium points is stable.

These results agree with the analysis done in the previous section. As we know from the analysis of the equilibrium point structure, the norm of the stable pair of non-symmetric equilibrium points diverges to infinity, and these equilibrium points become non-existent at $\gamma = -0.4375$. Numerical simulations suggested that all solutions of (4.5) diverge to infinity for $\gamma < -0.4375$. Summing up the results of section 4.2 with the analysis of figure (4.3), we may conclude that solutions "blow up" via the stable equilibrium point, the norm of which grows unboundedly with a vertical asymptote at a point $\gamma_{inf} = -0.4375$. For $\gamma < \gamma_{inf}$ there are no more stable solutions and all solutions diverge. We will theoretically validate this behavior in the following chapter.

It follows that for small negative γ the normally hyperbolic stable limit cycle "overcomes" the effect of the destabilizing part $-\gamma v_i$ and there exists a stable anti-phase solution. Hence we may estimate the value of γ_0 from theorem 3.2.1. The best estimate is given by γ_{ant} - the point at which the stability of the anti-phase solution is lost, while the point $\gamma_2 = -0.4375$, corresponding to the asymptote for the pair of stable equilibrium points, provides an upper bound on γ_0. Although the upper bound on γ_0 is worse than the estimate of γ_0 by γ_{ant}, it is easier to compute and analyze. Hence, it may be used in order to study the robustness of the system with respect to the variation of its physical parameters.

Note: The case of the type II parameter set is provided in figure (4.7). In spite of the fact that the type of Hopf bifurcation of anti-phase limit cycles and solution norms are different, the system demonstrates qualitatively the same behavior as

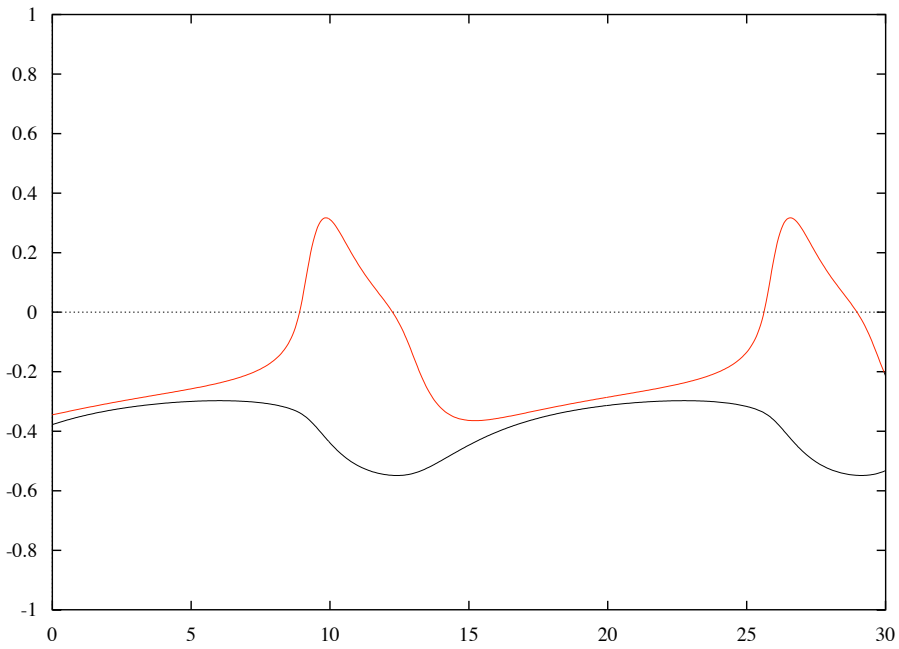

Figure 4.5: Suppressed periodic solution for $\gamma = -0.22$. The x axis denotes time t, while the y axes shows voltages $v_1(t)$ and $v_2(t)$

for the type I parameter set. This observation suggests that electrical coupling causes the same effects on the neurons independently of their type. For the sake of simplicity we have estimated the region of validity of the phase model for the type I neuron. However, the whole procedure is equally applicable to the type II neuron, and gives the same qualitative result.

4.2.3 Conclusion

1. The numerical study of the system (4.5) fully agrees with the predictions of non-delayed phase model (3.33) - for $|\gamma|$ small enough the branch of in-phase limit cycles is stable for $\gamma > 0$, while for $\gamma < 0$ the branch of anti-phase limit cycles is stable.

2. In the physically reasonable parameter range (i.e. $\gamma > 0$) the branch of in-phase solutions is the only stable branch. This result agrees with the supposition often found in biological literature, that electrical coupling tends to synchronize neuronal behavior, and motivates us to prove this in the case of strong coupling (see the chapter 5).

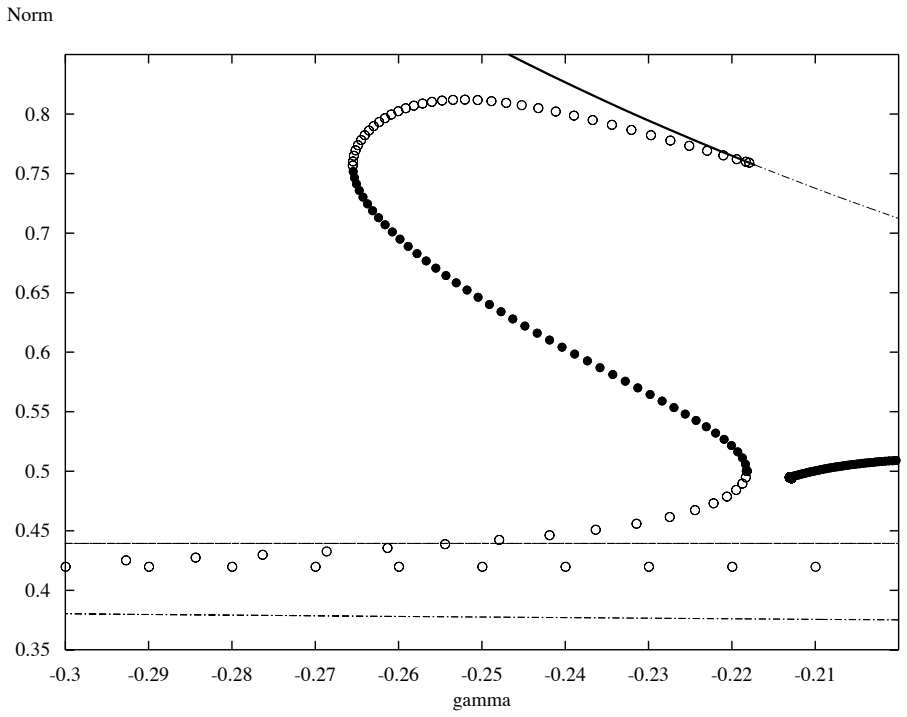

Figure 4.6: Bifurcation diagram of system (4.5) in Norm-γ axes with greater resolution.

3. In the case of negative γ, stability of the anti-phase solution branch is lost at $\gamma = -0.213$. Predictions of the phase model are no longer valid and for $\gamma < -0.213$ anti-phase solutions do not exist. Although consideration of the negative γ values has no physical meaning, it allows us to estimate the region of validity of the phase model, i.e. to estimate γ_0.

4. The point γ_2 from section 4.2 gives an upper bound on γ_0. For $\gamma < \gamma_2$ all solutions of (4.5) diverge to infinity, except for unstable equilibrium points and unstable limit cycle solutions. (This will be proven in chapter 5).

Finally, we may postulate that electrical coupling should always cause the unbounded growth of solutions for large enough negative values of γ. That fact could be used in an estimate of the region of validity of the phase model for any conductance-based model of electrically coupled neurons. The fact that the in-phase limit cycle is stable both for small $\gamma > 0$ by predictions of the phase model and for all $\gamma > 0$ by the numerical studies verifies the assumption that, in the physical case of positive γ, electrical coupling tends to synchronize oscillations.

We will analytically prove that subsystems X_1 and X_2 synchronize as $\gamma \to +\infty$,

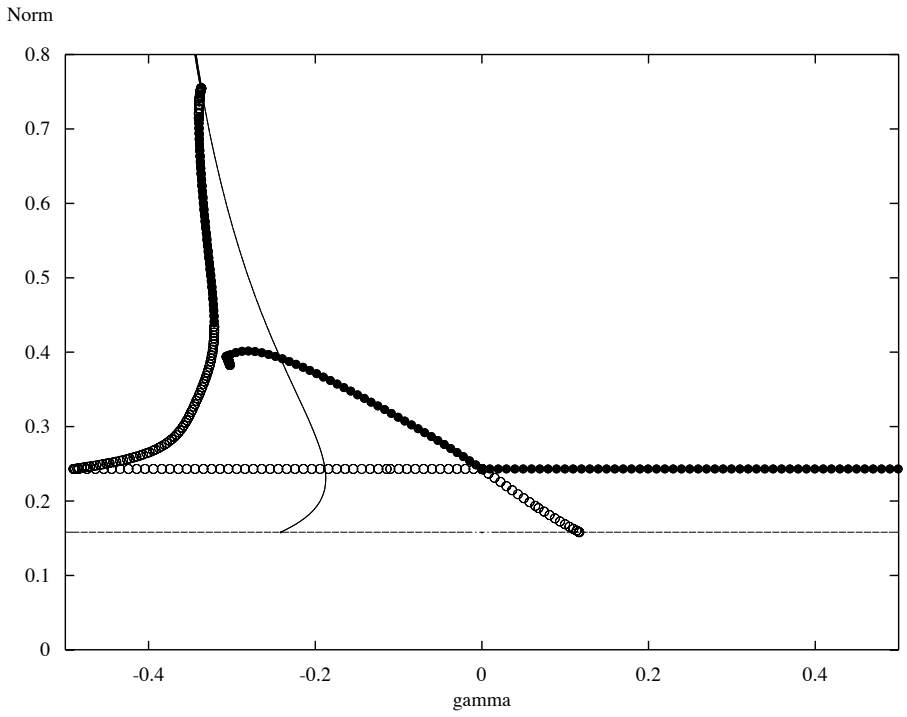

Figure 4.7: Bifurcation diagram of the system (4.5) for the type II parameter set

and that solutions diverge to infinity as $\gamma \to -\infty$ for an arbitrary single-compartment conductance-based model in chapter 5. To conclude, it is worth mentioning that both type I and type II oscillators qualitatively demonstrate the same behavior, which suggests that electrical coupling acts similarly on the neurons of both type I and type II.

4.3 Bifurcation analysis in the delayed case

In this section we will consider the bifurcation analysis of the Morris-Lecar system (2.16) with respect to arbitrary values of γ and τ. The analysis will be done numerically by the software and algorithms which will be described further in subsection

4.3.1. System (2.16) is repeated below for the reader's convenience:

$$\begin{cases} v_1' &= -g_{Ca}m_\infty(v_1)(v_1-1) - g_K w_1(v_1-v_K) - g_L(v_1+v_L) \\ & \quad +i+\gamma(v_2(t-\tau)-v_1) \\ w_1' &= \phi\lambda(v_1)[w_\infty(v_1)-w_1] \\ v_2' &= -g_{Ca}m_\infty(v_2)(v_2-1) - g_K w_2(v_2-v_K) - g_L(v_2+v_L) \\ & \quad +i+\gamma(v_1(t-\tau)-v_2) \\ w_2' &= \phi\lambda(v_2)[w_\infty(v_2)-w_2]. \end{cases} \tag{4.8}$$

The goal of the present section is twofold. First, we will analyze the general behavior of system (4.8) with respect to variation of γ and τ both for type I and type II parameter sets in subsection 4.3.2. Next, we will numerically validate the results for small values of $|\gamma|$ obtained in chapter 3. We will estimate the values of $\gamma_0(\tau)$ and η_0 for the type I and the type II parameter sets and we will analyze the agreement between experimental and theoretical results. This part of the analysis is done in subsection 4.3.3.

4.3.1 Software and algorithms

For the numerical bifurcation analysis of the delay differential equations we will use the program called DDE-BIFTOOL. DDE-BIFTOOL is a set of Matlab routines for bifurcation analysis of systems of delay differential equations. DDE-BIFTOOL allows one to continue periodic solutions or equilibrium points of the delay differential equation with respect to selected parameters, and to determine the stability of a given equilibrium point or periodic solution. DDE-BIFTOOL is capable of finding the bifurcation points of a system of delay differential equations and can switch between different solution branches at the bifurcation points. A detailed description of the routines and numerical algorithms used in DDE-BIFTOOL is available in [9].

4.3.2 Global bifurcation analysis of the delayed Morris-Lecar system

Let us briefly summarize our knowledge of the delayed Morris-Lecar system. System (4.8) is invariant with respect to interchanging of the subsystems X_1 and X_2, as for the non-delayed system (4.5). Hence, all the non-symmetric equilibrium points and periodic solutions will appear in pairs $(x(t), y(t), u(t), v(t))$ and $(u(t), v(t), x(t), y(t))$. The in-phase periodic solution, however, is not independent of γ for $\tau \neq 0$, since the delayed coupling functions $G(X_k, X_j) = v_j(t-\tau) - v_k(t)$ are non-zero for $v_j(t) \equiv v_k(t)$, and existence of the in-phase solution depends on the values of τ and γ.

As has been shown in section 4.2, the structure of the equilibrium points is *independent* of τ. Hence, we start the analysis of the delayed system (4.8) by studying how the variation of τ changes the stability along each branch of equilibrium points.

In order to determine the effect of non-zero delay on the system, it is convenient to first consider the bifurcation diagrams of system (4.8) with respect to γ for several fixed values of τ. We may construct a bifurcation diagram with respect to γ for any fixed value of τ by taking the previously computed for $\tau = 0$ branches of equilibrium points and computing the stability along each branch. Computation of stability allows us to determine the points of Hopf bifurcations and hence find the periodic solutions of the system and study their behavior with respect to the variation of γ.

At this point it is necessary to provide a little background from the theory of delay differential equations. Stability of the zero equilibrium of the linear delay differential equation

$$\dot{X} = AX(t) + BX(t-\tau), \quad A, B \in \mathbb{R}^{n\times n}$$

is determined by the roots of its characteristic equation, which has the form

$$\det(A - \lambda I + Be^{-\lambda\tau}) = 0. \tag{4.9}$$

Due to the summand $Be^{-\lambda\tau}$, equation (4.9) has infinitely many roots in the complex plane $\mathbb{C}$. However, there always exists a root with the maximal real part (see [5] for the proof), and the stability can hence be determined by computing a finite number of roots. As in the case of ordinary differential equations, the zero equilibrium solution is asymptotically stable if all roots of its characteristic equation have negative real parts.

The stability of an equilibrium point of a nonlinear delay differential equation may be found by linearising the system in the neighborhood of the equilibrium point and computing the roots of the characteristic equation of the resulting linear system.

Now we are ready to proceed with further analysis of system (4.8). It is convenient to analyze the stability along the branch of equilibrium points by plotting the real parts of the roots of the characteristic equation versus the parameter along the branch.

Consider the branch of the symmetric equilibrium points first. Figures (4.8) and (4.9) show the stability along the branch of symmetric equilibrium points of the type II parameter set for $\tau = 0.01$ and $\tau = 2.7$ respectively. The value of $\tau = 2.7$ was chosen arbitrarily in order to illustrate the effects of the delay on the branch of equilibrium points. For $\tau = 0.01$, the stability information is relatively unchanged with respect to the system with no delay. There are two points where the roots of characteristic equations cross zero, which are located at $\gamma = -0.2415$ and $\gamma \approx 0.117$. $\gamma = -0.2415$ corresponds to the pitchfork bifurcation creating the branch of non-symmetric equilibrium points, while $\gamma \approx 0.117$ corresponds to the

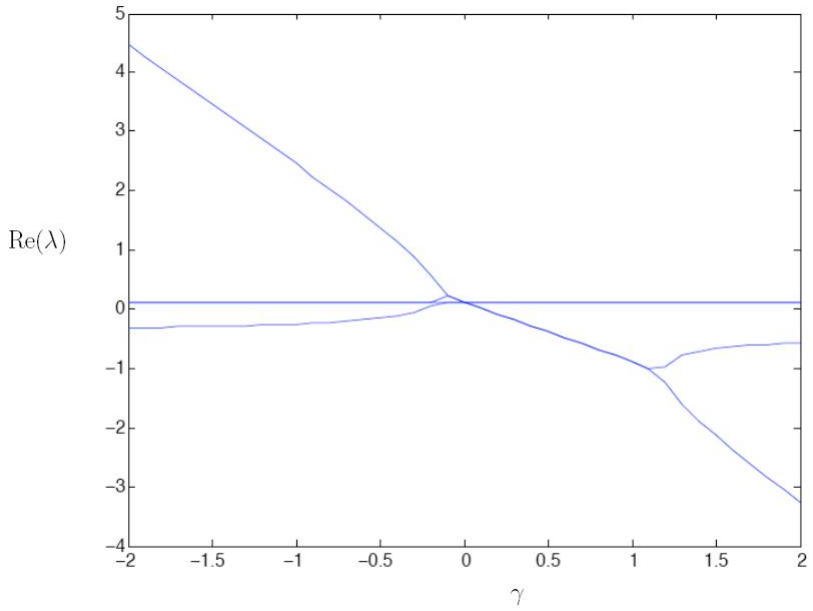

Figure 4.8: Stability diagram of the symmetric branch of equilibrium points for type II parameter set and $\tau = 0.01$

Hopf bifurcation creating the anti-phase solution. The dynamics is qualitatively the same as in the case of zero delay, as the roots of the characteristic equation introduced by the delay have very large negative real parts and don't affect the dynamics.

The situation changes as τ is increased to 2.7, as we can see in figure (4.9). The roots of the characteristic equation introduced by the delay have real parts of order 1, and hence start affecting the dynamics. Note that the root of the characteristic equation corresponding to the pitchfork bifurcation creating the branch of non-symmetric equilibrium points remains at its place, while the curve that corresponds to the anti-phase Hopf bifurcation has moved up. The anti-phase Hopf no longer exists, while its place was taken by another root at $\gamma \approx 0.164$. Numerical simulations have shown that $\gamma \approx 0.164$ corresponds to the *in-phase* Hopf bifurcation.

Let us generalize our observations. Although dependance of the roots of characteristic equations on τ is nonlinear, as a general rule, the real parts of the infinite set of roots created by the presence of τ increase and start to cross the zero axis as τ is being increased. Each zero crossing corresponds to a bifurcation point. Note that all the bifurcation points created as τ is being increased are Hopf due to the fact that the structure of equilibrium points is independent of τ, and the roots of the characteristic equations hence can cross zero only as a pair of imaginary roots, not as a zero root. New Hopf points appear at $\gamma \to \pm\infty$ and travel towards $\gamma = 0$, where they vanish as τ gets large enough. The larger the value of the delay, the more Hopf bifurcations are created and the more complicated the dynamics of the

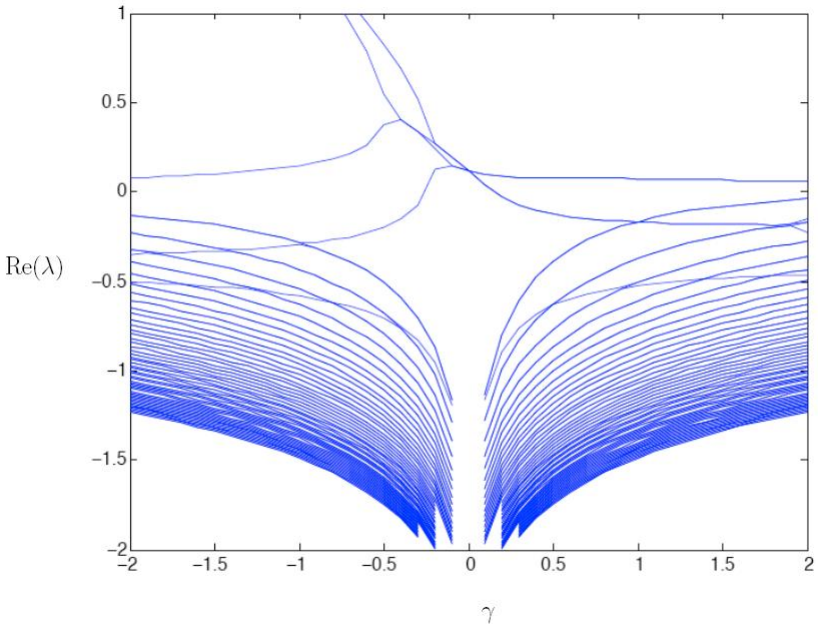

Figure 4.9: Stability diagram of the symmetric branch of equilibrium points for type II parameter set and $\tau = 2.7$

system becomes. Numerical simulations suggested that Hopf bifurcations created out of the branch of symmetrical equilibrium points lead to in-phase or anti-phase solutions, which exchange with each other.

It is possible to find the Hopf points and to track their behavior in the γ-τ plane. The corresponding graph is provided in figure (4.11). We see that the Hopf points come from infinity and approach some vertical asymptote close to $\gamma = 0$, as was expected from the analysis of the stability of the equilibrium points.

The stability along the branch of non-symmetric equilibrium points for type II parameter set and $\tau = 2.7$ is provided in figure (4.10). We see two zero crossings that correspond to the limit points of equilibrium points, and two zero crossings that correspond to the Hopf bifurcations creating the suppressed limit cycles. The stability of the branch of non-symmetric equilibrium points at $\tau = 2.7$ is still unaffected by the roots of characteristic equations corresponding to the delay, but we can see that these roots are already close to the zero axes. As τ gets bigger, these roots will give rise to a new limit cycles through a Hopf bifurcations, leading to the complicated dynamics in the region where the predictions of the phase model fail.

Figure (4.12) provides the bifurcation diagrams with respect to γ for $\tau = 0.01$. We see that for small values of τ, the behavior of the system is qualitatively the same as in the case of $\tau = 0$ (see figure (4.4)), as was expected by the analysis of the stability of the branches of equilibrium points. It is possible to create the bifurcation diagrams with respect to γ for large non-zero values of τ, but this analysis is computationally expensive. Thus, we will proceed to the analysis of the

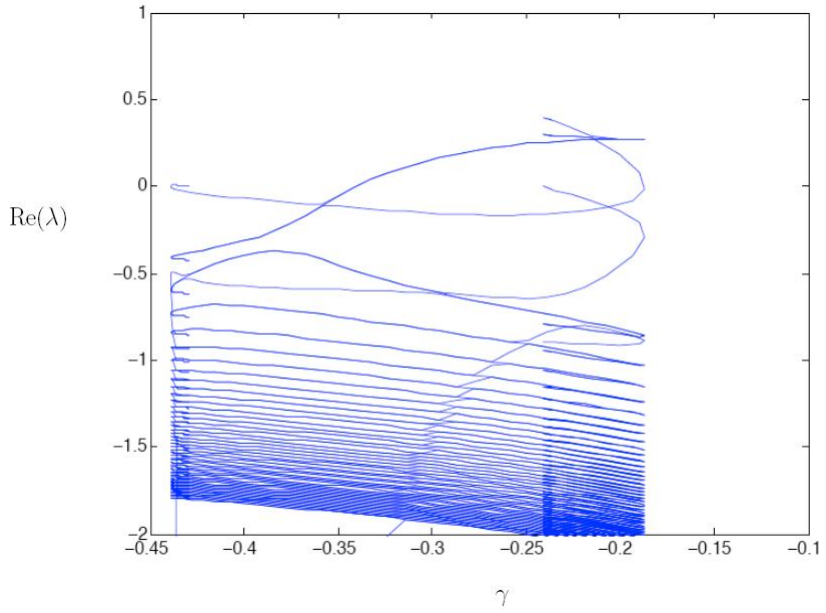

Figure 4.10: Stability diagram of the non-symmetric branch of equilibrium points for type II parameter set and $\tau = 2.7$

results of the phase model which was studied in chapter 3.

4.3.3 Numerical analysis of the results of the phase model

The analysis of the phase model done in chapter 3 determines the stable periodic solutions for τ and γ small enough for both type I and type II parameter sets. The region of validity of phase model (3.36) with respect to τ and γ, however, is yet undetermined.

In the present subsection we will compare the results of the phase model with numerical data. The numerical data was obtained by picking up the in-phase and anti-phase periodic solutions from the bifurcation diagrams provided in figure (4.12) for three different values of γ: $\gamma = 0.001$, $\gamma = 0.01$ and $\gamma = 0.1$ for both type I and type II parameter sets. Next we continued these solutions with respect to τ and hence we obtained twelve branches of in-phase and anti-phase solutions with respect to τ. Finally, we determined the regions of stability and instability of the in-phase and anti-phase solutions with respect to τ by computing the stability along each branch.

The graphs of the resulting branches with respect to τ are available in figures (4.13)-(4.16). The red solid circles denote the stable solutions while the green + signs correspond to the unstable ones. The x axes of each diagram corresponds to the value of τ, while the y axis shows the $\max_{t\in[0,T]} v_1(t)$ for each periodic solution. We see that for $\gamma = 0.001$ and $\gamma = 0.01$ the profiles of the solutions are relatively

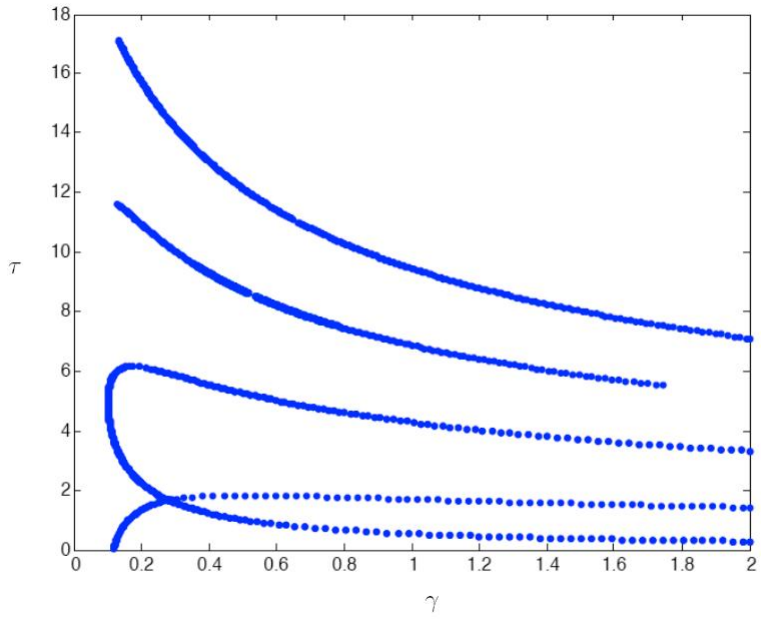

Figure 4.11: Hopf points in the γ-τ plane for the type II parameter set

unaffected by τ, while for $\gamma = 0.1$ the profiles of the solutions depend on the value of delay. The type I and type II systems behave nearly the same for each γ. Note that stability switching for the type II parameter sets occurs more often due to the fact that the period of oscillation of the type system II is much smaller than that of the type I system.

Information about the stability switching points allows us to compare the results of the experiment with the theoretical expectations based on the phase model. The theoretical and experimental data is provided in tables (4.1) and (4.2). Note that the values of η_i from chapter 3 are converted to τ by multiplying them by $1/\Omega = T/2\pi$ for each parameter set.

Let us discuss the agreement between the theoretical and numerical data. First of all, it is necessary to make a comment about the accuracy of the numerical data. The step-length in the continuation of the limit cycles with respect to τ was 0.05 for all the limit cycles with the type I parameter set and 0.1 for all the limit cycles with the type II parameter set. The stability switching values of τ were computed by taking the midpoint of the interval joining the values of τ corresponding to the neighboring stable and unstable limit cycles. The margin of error in the determination of the experimental values of τ hence is equal to 0.025 for type I and 0.05 for type II parameter sets. This error does not include possible errors in the computation of stability close to the stability switching points.

Recall that a limit cycle is stable when $\max(\|\mu\|) > 1$, where μ denotes a set of Floquet multipliers. In our numerical simulations we used the condition $\max(\|\mu\|) > 1.001$ in order to avoid numerical error in computation of the Floquet exponent which is identically equal to 1. However, this error is negligible since

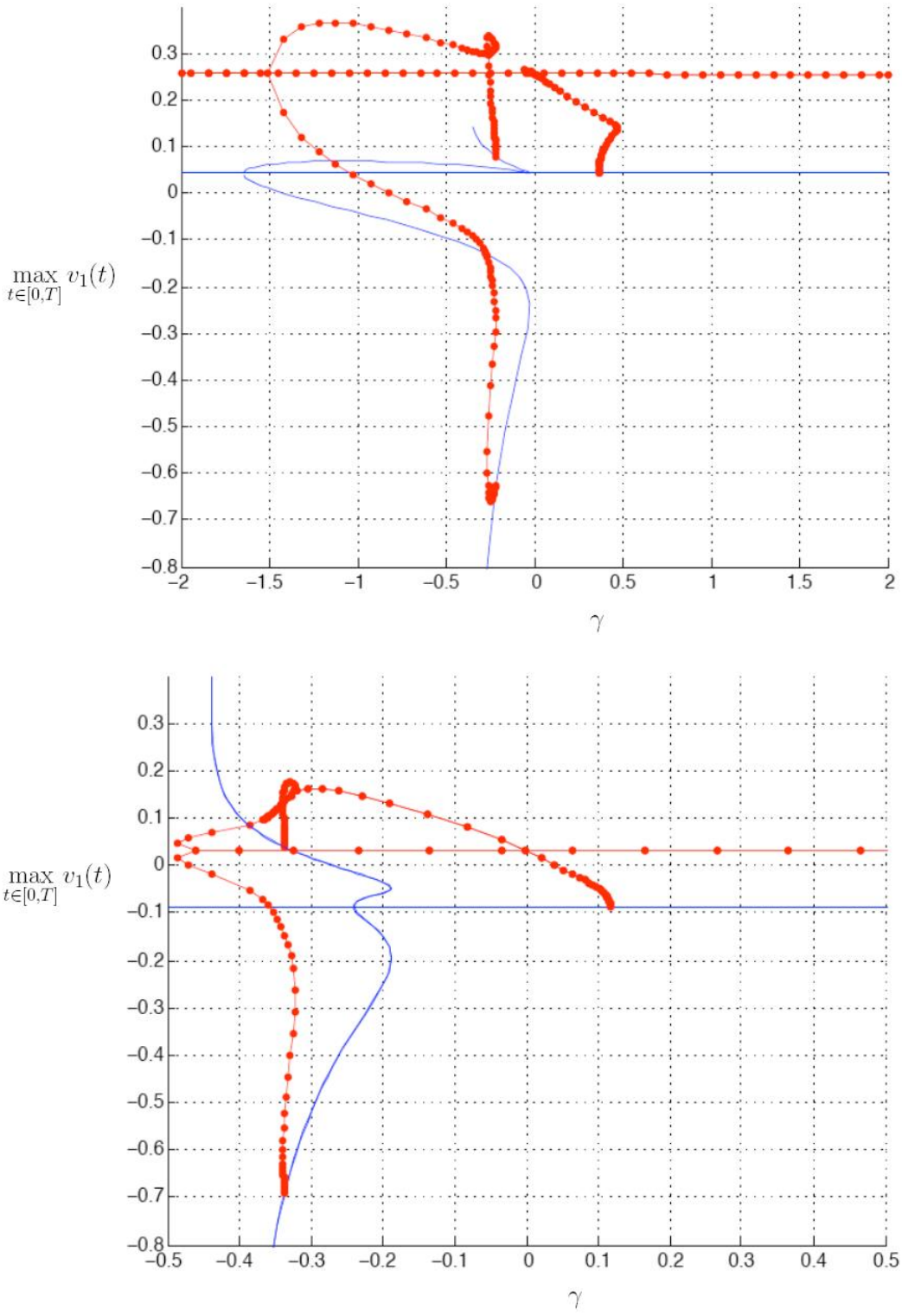

Figure 4.12: Bifurcation picture with respect to γ for type I (top) and type II (bottom) parameter sets

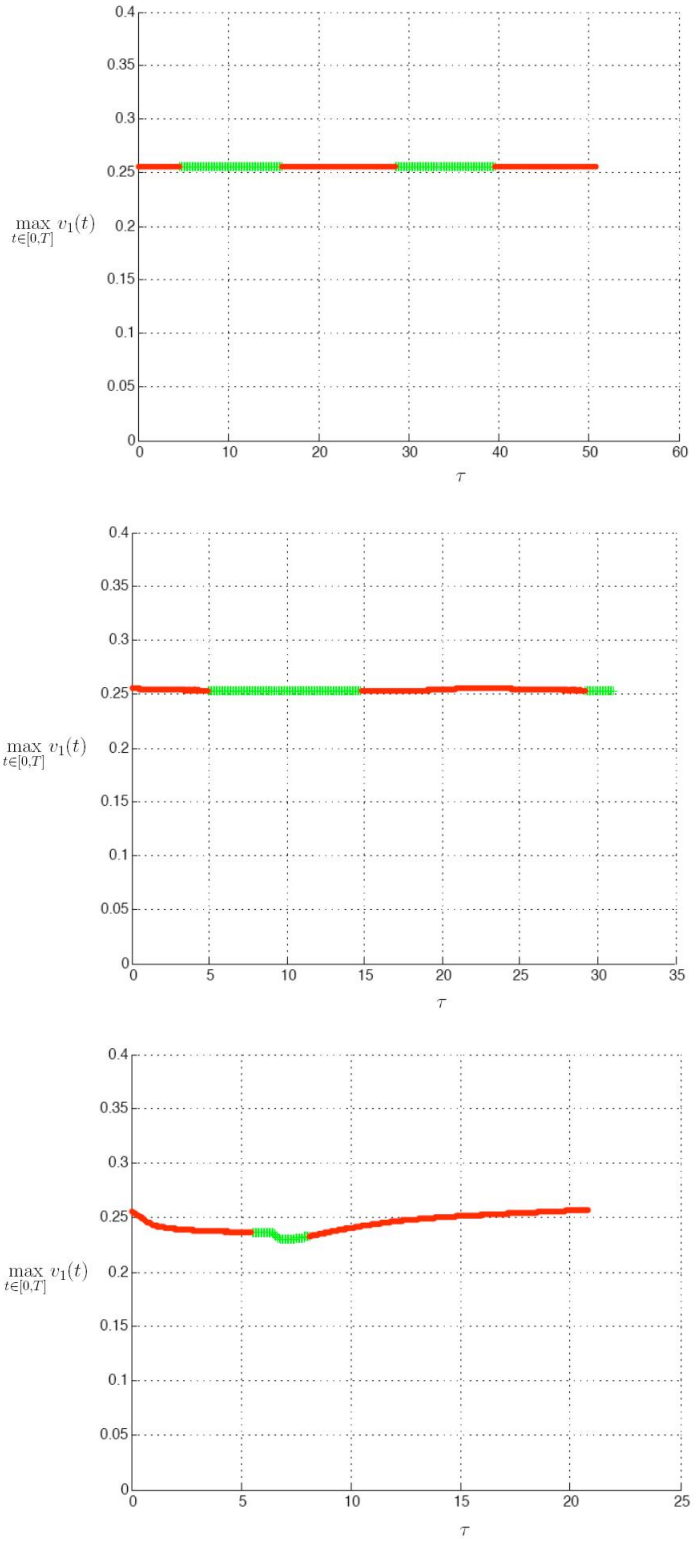

Figure 4.13: Branches of in-phase periodic solutions with respect to τ for $\gamma = 0.001$ (top), $\gamma = 0.01$ (middle) and $\gamma = 0.1$ (bottom) for the type I parameter set. Red circles correspond to the stable solutions, and green "+" signs correspond to the unstable solutions.

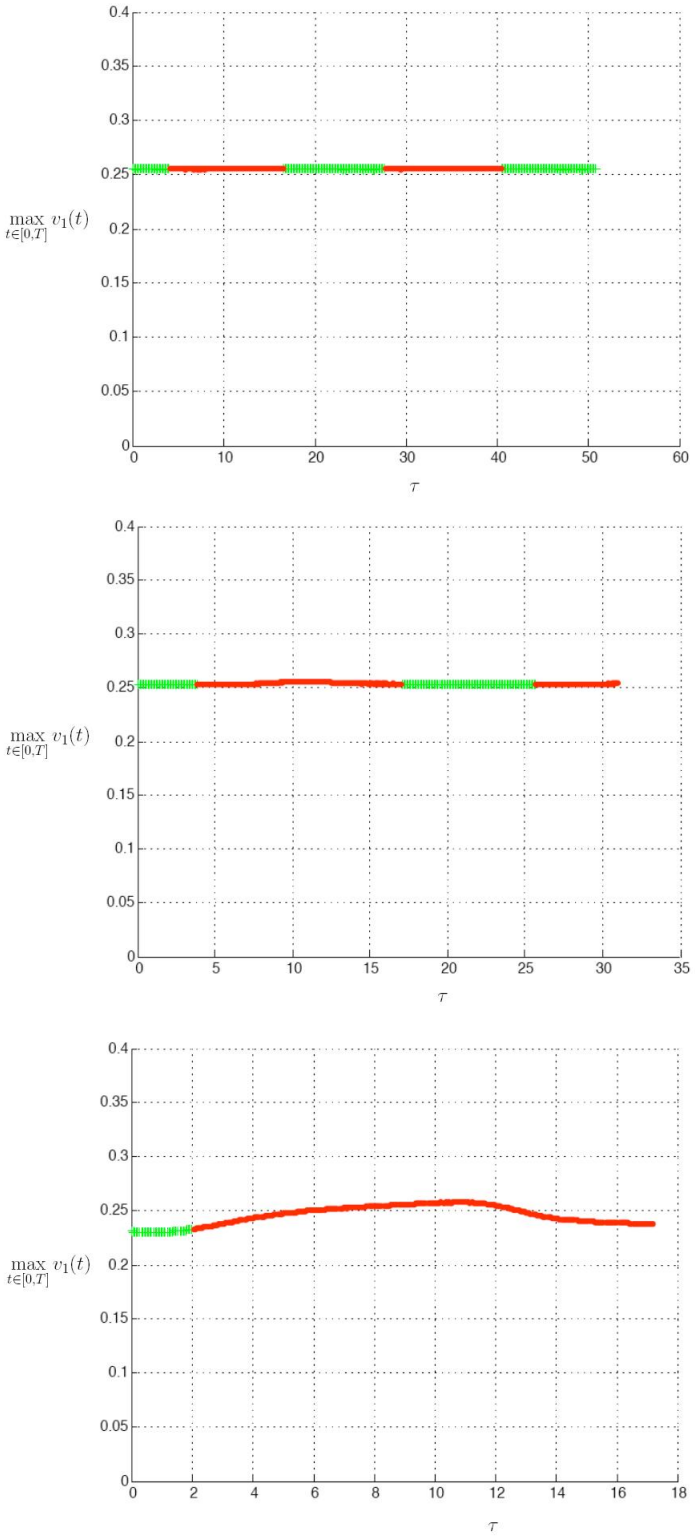

Figure 4.14: Branches of anti-phase periodic solutions with respect to τ for $\gamma = 0.001$ (top), $\gamma = 0.01$ (middle) and $\gamma = 0.1$ (bottom) for the type I parameter set. Red circles correspond to the stable solutions, and green "+" signs correspond to the unstable solutions.

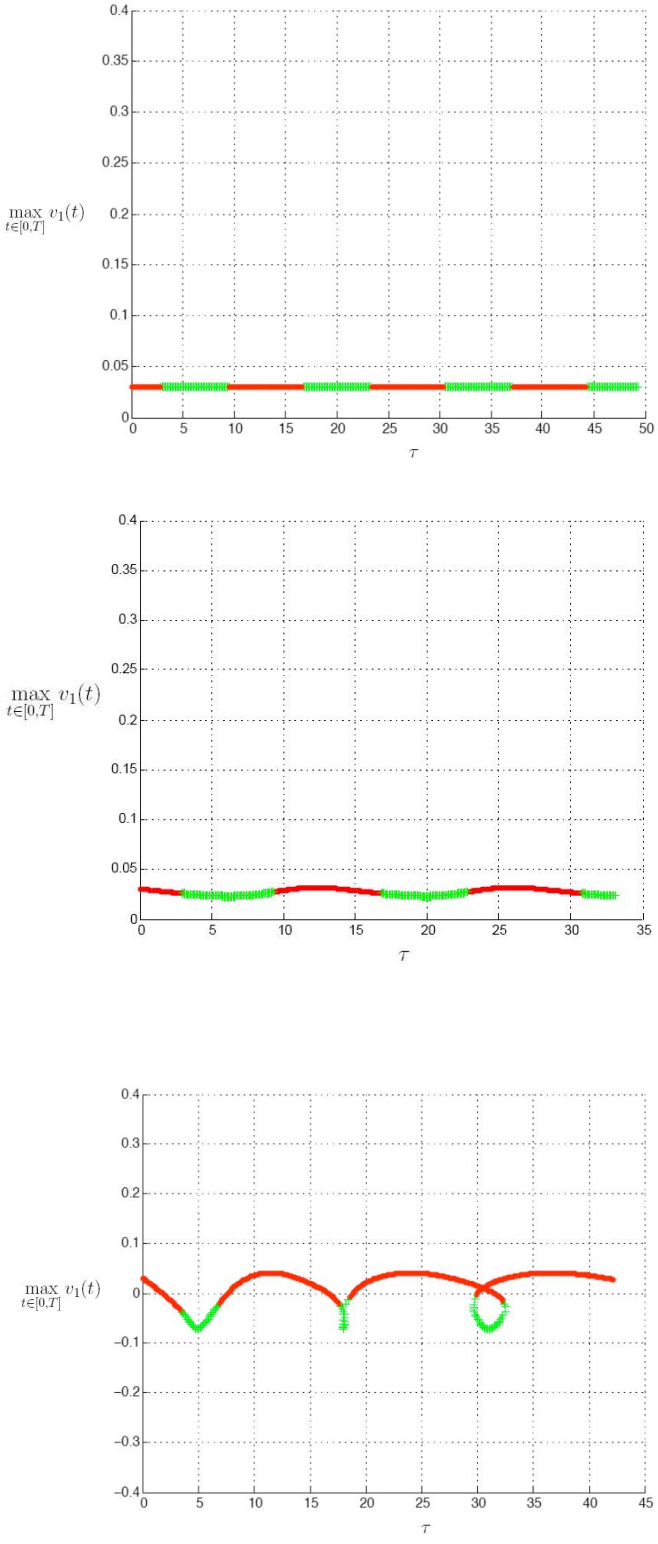

Figure 4.15: Branches of in-phase periodic solutions with respect to τ for $\gamma = 0.001$ (top), $\gamma = 0.01$ (middle) and $\gamma = 0.1$ (bottom) for the type II parameter set. Red circles correspond to the stable solutions, and green "+" signs correspond to the unstable solutions.

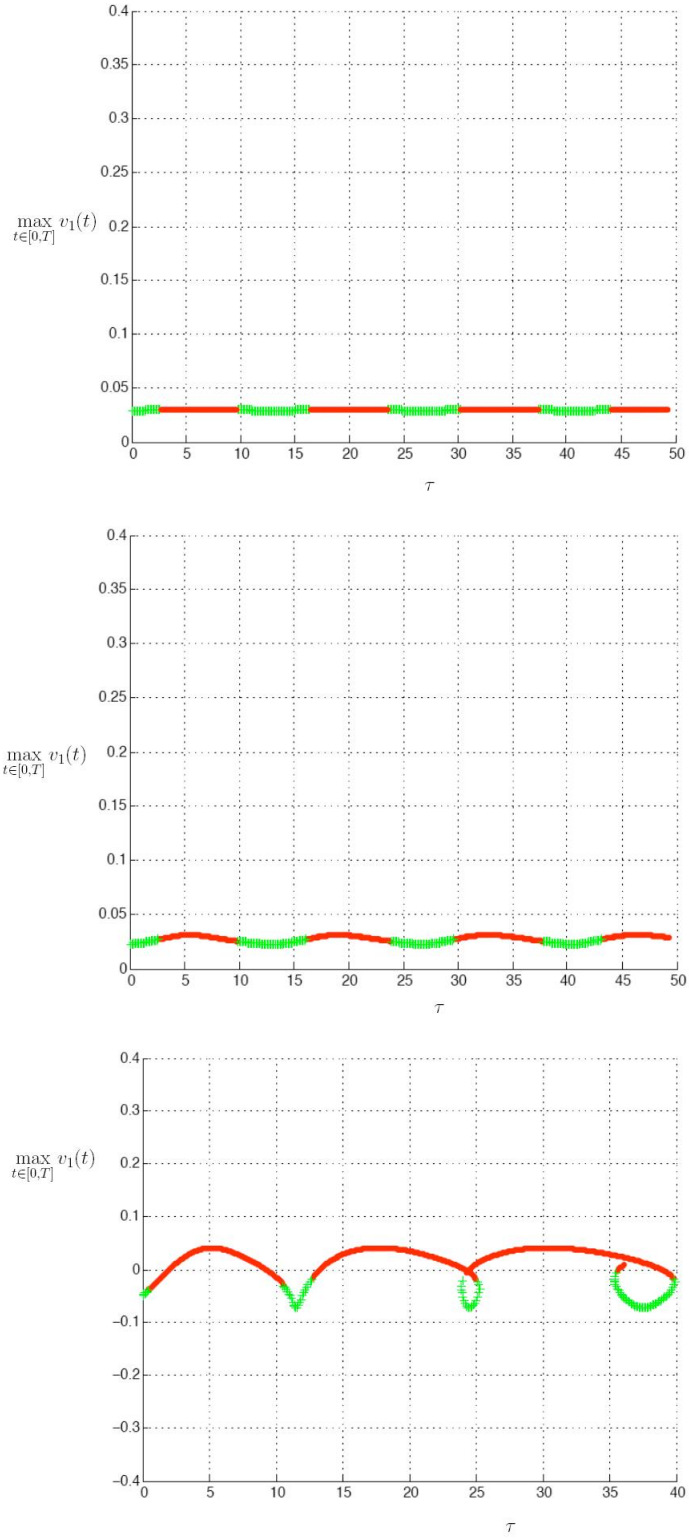

Figure 4.16: Branches of anti-phase periodic solutions with respect to τ for $\gamma = 0.001$ (top), $\gamma = 0.01$ (middle) and $\gamma = 0.1$ (bottom) for the type II parameter set. Red circles correspond to the stable solutions, and green "+" signs correspond to the unstable solutions.

Floquet exponents grow exponentially fast as the limit cycles becomes unstable.

Let us discuss the tables next. For $\gamma = 0.001$, the experimental values for the type II parameter sets agree with the theoretical results within the margin of error, while the results for the type I parameter set show a little discrepancy with the margin of error for τ greater than one period, or for $\eta > 2\pi$. For $\gamma = 0.01$, both type I and type II oscillators deviate from the theoretical expectations as τ gets large enough. The type II parameter set shows better agreement with the model than the type I parameter set, however, for both of them the error increases as τ is increased. Finally, for $\gamma = 0.1$ both type I and type II oscillators highly deviate from the expected behavior. For large values of τ behavior is completely different from the expectations. However, both type I and type II parameter sets agree with the expectations for the small values of τ.

Thus, experimental observations verify the conjecture that η_0 lies on the curve $\tau\gamma = Const$, but contradict the prediction that η_0 lies on the curve $\tau\gamma\Omega = Const$. The latter contradiction might be caused by the differences in behavior of system (4.8) for type I and type II parameter sets, that overcome the theoretical estimate on the η_0 which was derived in section 3.4.

4.3.4 Conclusion

As τ is increased, more and more limit cycles are created out of the Hopf bifurcations and the dynamics of the system gets more and more complicated. However we may predict the dynamics for γ small enough by using the phase model with a phase shift instead of delay, which was developed in chapter 3. As it was expected, the region of validity of the phase model is bounded by the curves $\gamma\tau = Const$ and $\gamma = \gamma_0(\tau)$, where the curve $\gamma_0(\tau)$ corresponds to the region of validity of the phase model in γ. Note that $\gamma_0(0)$ is the region of validity of the phase model with no delay found in the section 4.2. No matter how large the value of τ, we can still correctly predict the behavior of the system in the neighborhood of $\gamma = 0$ small enough.

The assumption that the region of validity lies on the curve $\Omega\tau\gamma = Const$ has been contradicted by the simulation. Differences between type I and type II models overcome the expected behavior.

Table 4.1: Comparison of theoretical and experimental values of τ for the type I parameter set

Description of a point	Theoretical	$\gamma = 0.001$		$\gamma = 0.01$		$\gamma = 0.1$	
		value	error	value	error	value	error
Anti-phase becomes stable	4.1566	4.0939	-0.0627	3.8433	-0.3133	2.0207	-2.1359
In-phase loses stability	4.4911	4.6431	0.1520	4.8948	0.4037	4.3688	-0.1223
In-phase becomes stable	16.1010	15.9432	-0.1578	14.7558	-1.3452	5.2380	-10.8630
Anti-phase loses stability	16.4116	16.5939	0.1824	17.0651	0.6536	17.1110	0.6995
Anti-phase becomes stable	28.0215	27.7439	-0.2776	25.6654	-2.3561	-	-
In-phase loses stability	28.3559	28.5432	0.1873	29.2058	0.8499	5.4799	-22.8760
In-phase becomes stable	39.9658	39.5932	-0.3726	-	-	8.1087	-31.8572
Anti-phase loses stability	40.2764	40.5439	0.2675	-	-	-	-

Table 4.2: Comparison of theoretical and experimental values of τ for the type II parameter set

Description of a point	Theoretical	$\gamma = 0.001$		$\gamma = 0.01$		$\gamma = 0.1$	
		value	error	value	error	value	error
In-phase loses stability	2.7377	2.8450	0.1073	2.9426	0.2049	2.6011	-0.1366
Anti-phase becomes stable	2.8068	2.6450	-0.1619	2.6456	-0.1612	1.4613	-1.3455
Anti-phase loses stability	9.6373	9.7450	0.1077	9.8456	0.2084	9.4669	-0.1703
In-phase becomes stable	9.7064	9.5450	-0.1614	9.3926	-0.3138	7.4038	-2.3026
In-phase loses stability	16.5506	16.6450	0.0944	16.8427	0.2921	16.4042	-0.1464
Anti-phase becomes stable	16.6198	16.4450	-0.1748	16.1457	-0.4741	13.1981	-3.4216
Anti-phase loses stability	23.4502	23.5450	0.0948	23.8457	0.3955	23.4965	0.0463
In-phase becomes stable	23.5193	23.3450	-0.1743	22.8927	-0.6266	19.0247	-4.4946
In-phase loses stability	30.3636	30.4450	0.0814	30.7927	0.4291	30.4513	0.0877
Anti-phase becomes stable	30.4327	30.2450	-0.1877	29.6458	-0.7869	24.7260	-5.7067
Anti-phase loses stability	37.2631	37.4450	0.1818	37.7458	0.4827	37.7238	0.4607
In-phase becomes stable	37.3323	37.1450	-0.1873	-	-	30.4513	-6.7100
In-phase loses stability	44.1765	44.3450	0.1685	-	-	-	-
Anti-phase becomes stable	44.2457	44.0450	-0.2007	43.1459	-1.0998	36.0583	-8.1873

Chapter 5

Asymptotic analysis for large values of γ

Numerical analysis of the electrically coupled Morris-Lecar neurons done in chapter 4 suggested that electrically coupled Morris-Lecar neurons synchronize their voltages for large positive values of γ , and that solutions of the coupled Morris-Lecar system diverge for large enough negative values of γ. In the present chapter we will generalize and prove these properties.

We consider a network of two arbitrary electrically coupled neurons. Each neuron is represented by a single compartment conductance-based model with an arbitrary number of ionic conductances and corresponding gating variables. We set only general assumptions on the smoothness of the functions used in the model for each neuron.

We study the asymptotic behavior of the neuron voltages in the extreme cases of $\gamma \to +\infty$ and $\gamma \to -\infty$. Our analysis closely follows the general perturbation framework for initial value problems of nearly linear systems, which was developed in [30]. We will prove that for $\gamma > 0$ large enough, the voltages of the neurons synchronize, while for large $\gamma < 0$ the voltage of each neuron grows unboundedly with time.

The method developed for analysis of the case $\gamma \to +\infty$ contributes to the general theory of nearly linear systems. In particular, the analysis of nearly linear systems done in [30] by Murdock has been extended to the special case of nearly linear systems with non-positive eigenvalues.

5.1 Problem setting

The concept of a single compartment conductance-based model was introduced in section 2.2. Recall that a single compartment conductance based model of a neuron is a system of ordinary differential equations. One equation describes the change

of the neurons voltage with respect to time, while the other equations describe dynamics of activation and inactivation variables corresponding to the voltage-dependent ionic channels of the neuron.

Now, consider two neurons described by different conductance based models. The first neuron is represented by a system of $m+1$ ordinary differential equations, while the second neuron is represented by a system of $k+1$ ordinary differential equations. v_1 and v_2 are the voltages of each neuron, while a_1 ... a_m are activation and inactivation variables corresponding to ionic channels of the first neuron, and b_1 ... b_k are activation and inactivation variables corresponding to the second neuron. Then the system of two electrically coupled neurons has the following form, which is the general form of a network of two electrically coupled single-compartment conductance based neuronal models:

$$\begin{cases} \dot{v}_1 = f_1(v_1, a_1, \ldots, a_m) + \gamma(v_2 - v_1) \\ \dot{v}_2 = f_2(v_2, b_1, \ldots, b_k) + \gamma(v_1 - v_2) \\ \dot{a}_i = g_i(v_1, a_i), \qquad i = 1 \ldots m \\ \dot{b}_j = h_j(v_2, b_j) \qquad j = 1 \ldots k \end{cases} . \tag{5.1}$$

Note that the dimension of the coupled system is $m + k + 2$. For simplicity of notation we will denote $m + k + 2$ by n everywhere further in the present chapter. The functions $f_1(\cdot)$,$f_2(\cdot)$, $g_i(\cdot)$ for $i = 1 \ldots m$ and $h_j(\cdot)$ for $j = 1 \ldots k$ are assumed to be continuous everywhere in their domain $\Sigma \subset \mathbb{R}^n$ (it can be $\Sigma = \mathbb{R}^n$) and to be Lipschitz in any compact convex set $D \subset \Sigma$ throughout this chapter. These conditions are set in order to verify that solutions of (5.1) exist and are unique for any initial condition in Σ, and should hold for any well-defined conductance based model. We will set some additional conditions for these functions in section 5.5.

We will study asymptotic behavior of the solutions of (5.1) for $\gamma \to +\infty$ and $\gamma \to -\infty$. It will be shown that $v_1(t)$ and $v_2(t)$ synchronize for $\gamma > 0$ large enough, and that $|v_1(t) - v_2(t)|$ grows unboundedly with time for $\gamma < 0$ large enough. Precise mathematical definitions of "synchronization" and "unbounded growth" will be given when we develop an appropriate mathematical description of the model.

5.2 Problem in perturbations.

We will rewrite system (5.1) in the general framework known as a "nearly linear system". The theory of nearly linear systems is well-developed (see [30]), and they can be analyzed by the methods of perturbation theory.

Let us re-scale time by introducing a new "fast time" variable $T = |\gamma|t$. Then $\frac{d}{dt} = \frac{d}{dT}\frac{dT}{dt} = |\gamma|\frac{d}{dT}$. Since (5.1) is autonomous system, this change would affect only the derivatives of all variables with respect to time ($\dot{s}$ corresponds to $\frac{ds}{dt}$, while

s' corresponds to $\frac{ds}{dT}$). Substitution of the scaled time in system (5.1) yields the following system:

$$\begin{cases} |\gamma| v_1' = f_1(v_1, a_1, \ldots, a_m) + \gamma(v_2 - v_1) \\ |\gamma| v_2' = f_2(v_2, b_1, \ldots, b_k) + \gamma(v_1 - v_2) \\ |\gamma| a_i' = g_i(v_1, a_i), \qquad i = 1 \ldots m \\ |\gamma| b_j' = h_j(v_2, b_j) \qquad j = 1 \ldots k \end{cases} \tag{5.2}$$

Let us introduce a small parameter $\varepsilon = 1/|\gamma|$. After dividing each equation of system (5.2) by $|\gamma|$ we obtain the following:

$$\begin{cases} v_1' = & \text{sgn}(\gamma)(v_2 - v_1) + & \varepsilon f_1(v_1, a_1, \ldots, a_m) \\ v_2' = & \text{sgn}(\gamma)(v_1 - v_2) + & \varepsilon f_2(v_2, b_1, \ldots, b_k) \\ a_i' = & & \varepsilon g_i(v_1, a_i), \qquad i = 1 \ldots m \\ b_j' = & & \varepsilon h_j(v_2, b_j), \qquad j = 1 \ldots k \end{cases} \tag{5.3}$$

It is convenient to perform a change of variables in order to group together linear terms independent of ε. Let

$$x = \frac{1}{2}(v_1 - v_2) \qquad \text{and} \qquad y = \frac{1}{2}(v_1 + v_2),$$

then $v_1 = x + y$, $v_2 = y - x$, and system (5.3) takes form

$$\begin{cases} x' = & -2\text{sgn}(\gamma)x + & \varepsilon \frac{1}{2}(f_1(x + y, a_1, \ldots, a_m) - f_2(y - x, b_1, \ldots, b_k)) \\ y' = & & \varepsilon \frac{1}{2}(f_1(x + y, a_1, \ldots, a_m) + f_2(y - x, b_1, \ldots, b_k)) \\ a_i' = & & \varepsilon g_i(x + y, a_i), \qquad i = 1 \ldots m \\ b_j' = & & \varepsilon h_j(y - x, b_j), \qquad j = 1 \ldots k \end{cases} \tag{5.4}$$

For simplicity of notation we will denote the function $1/2(f_1(v_1, a_1, \ldots, a_m) - f_2(v_2, b_1, \ldots, b_k))$ by $p(x, y, a_i, b_j)$, and the function $1/2(f_1(v_1, a_1, \ldots, a_m) + f_2(v_2, b_1, \ldots, b_k))$ by $q(x, y, a_i, b_j)$.

Let us consider an initial value problem for system (5.4) next. In vector form it can be rewritten as

$$\begin{cases} z' = Az + \varepsilon F(z) \\ z(0) = C \end{cases}, \qquad \text{where} \tag{5.5}$$

$$z = \begin{pmatrix} x \\ y \\ a_1 \\ \dots \\ a_m \\ b_1 \\ \dots \\ b_k \end{pmatrix}, A = \begin{pmatrix} -2\mathrm{sgn}(\gamma) & 0 & \dots & 0 \\ 0 & 0 & \dots & 0 \\ \vdots & & & \\ 0 & 0 & \dots & 0 \end{pmatrix}, F = \begin{pmatrix} p(x, y, a_1, \dots, b_k) \\ q(x, y, a_1, \dots, b_k) \\ g_1(x + y, a_1) \\ \dots \\ g_m(x + y, a_m) \\ h_1(y - x, b_1) \\ \dots \\ h_k(y - x, b_k) \end{pmatrix},$$

$$C = \begin{pmatrix} C_1 \\ \vdots \\ C_n \end{pmatrix}.$$

5.3 Solution in perturbations

Any system of the form (5.5) where ε is a small parameter can be referred to as an initial value problem for a nearly linear system. Since (5.5) satisfies the conditions of the theorem of existence and uniqueness, the solution of the IVP (5.5) exists for any $T \geq 0$. Let us write the exact solution of (5.5) in the form

$$z(T) = z_0(T) + \varepsilon z_1(T) + R(T, \varepsilon),$$

where $z_0(T)$ and $z_1(T)$ are solutions of the following $O(1)$ and $O(\varepsilon)$ initial value problems:

$$\begin{cases} z_0' = Az_0 \\ z_0(0) = C \end{cases}, \qquad \text{and} \tag{5.6}$$

$$\begin{cases} z_1' = Az_1 + F(z_0) \\ z_1(0) = 0 \end{cases}. \tag{5.7}$$

The term $R(T, \varepsilon)$ represents the difference between the exact solution and the approximation $z_0(T) + \varepsilon z_1(T)$. Thus, $R(T, \varepsilon)$ has to satisfy the following initial value problem:

$$\begin{cases} R' = AR + \varepsilon[F(z_0 + \varepsilon z_1 + R) - F(z_0)] \\ R(0, \varepsilon) = 0 \end{cases}, \tag{5.8}$$

since $R' = z' - z_0' - \varepsilon z_1' = Az + \varepsilon F(z) - Az_0 - \varepsilon Az_1 - \varepsilon F(z_0) = A(z_0 + \varepsilon z_1 + R) - A(z_0 + \varepsilon z_1) + \varepsilon[F(z_0 + \varepsilon z_1 + R) - F(z_0)]$.

This construction of the approximate solution is convenient since functions $z_0(T)$ and $z_1(T)$ can be found explicitly in terms of A and $F(\cdot)$, while the term $R(T, \varepsilon)$ can be estimated from above. Let us consider the properties of $z_0(T)$ and $z_1(T)$ next.

5.4 Explicit form of $z_0(T)$ and $z_1(T)$.

Consider $z_0(T)$ first. The initial value problem (5.6) is linear and homogeneous, and hence $z_0(T) = e^{AT}C$. It follows that

$$z_0(T) = \begin{pmatrix} C_1 e^{-2\mathrm{sgn}(\gamma)T} \\ C_2 \\ \vdots \\ C_n \end{pmatrix}.$$

We see that at first order all variables except $x(T)$ remain constant, while variable $x_0(T) = C_1 e^{-\mathrm{sgn}(\gamma)T}$ changes exponentially fast. For $\gamma > 0$ $x_0(T)$ exponentially approaches zero, while for negative values of γ $x_0(T)$ grows exponentially fast for $C_1 \neq 0$.

Let us consider $z_1(T)$ next. System (5.7) is linear but non-homogeneous. The solution can be found by variation of constants and has form $z_1(T) = \int_0^T e^{A(T-s)} F(e^{As}C)ds$. In explicit form

$$z_1(T) = \begin{pmatrix} e^{-2\mathrm{sgn}(\gamma)T} \int_0^T p(C_1 e^{-2\mathrm{sgn}(\gamma)s}, C_2, \ldots, C_n) e^{2\mathrm{sgn}(\gamma)s} ds \\ \int_0^T q(C_1 e^{-2\mathrm{sgn}(\gamma)s}, C_2, \ldots, C_n) ds \\ \vdots \\ \int_0^T b_k(C_2 - C_1 e^{-2\mathrm{sgn}(\gamma)s}, C_n) ds \end{pmatrix}.$$

5.5 Synchronization in the case of $\gamma > 0$

In the present section we will consider the solution of system (5.5) for $\gamma > 0$. We will estimate terms $z_1(T)$ and $R(T, \varepsilon)$, and hence prove that $x(T) = x_0(T) + O(\varepsilon)$ uniformly on the time intervals $[0, 1/\varepsilon]$. Throughout this section we will assume that $F(\cdot)$ is globally Lipschitz in its domain Σ, i.e. that there exist $L \in \mathbb{R}$, such that

$$\|F(u) - F(v)\| \leq L\|u - v\|, \qquad \text{for all} \quad x, y \in \Sigma,$$

where $\|\cdot\|$ denotes a Euclidean norm in $\mathbb{R}^n$.

5.5.1 Properties of $z_1(T)$.

Due to the specific form of the integrals for $z_1(T)$ it is possible to estimate each of them in the case $\gamma > 0$. Consider term $x_1(T)$ first. For $\gamma > 0$

$$x_1(T) = e^{-2T} \int_0^T p(C_1 e^{-2s}, C_2, \ldots, C_n) e^{2s} ds.$$

Let us change the variable of integration by introducing $u = e^{-2s}$.Then

$$ds = -\frac{du}{2u}, \qquad \text{and the limits of integration change by the rule} \qquad \begin{cases} T \to e^{-2T} \\ 0 \to 1 \end{cases}.$$

It follows that

$$x_1(T) = e^{-2T} \int_{e^{-2T}}^1 \frac{p(C_1 u, C_2, \ldots, C_n)}{2u^2} du.$$

Note that new variable u changes only between 1 and 0 as T changes between 0 and $+\infty$. Since $[0, 1]$ is a compact interval, and $p(\cdot)$ is a continuous function, $|p(C_1 u, C_2, \ldots, C_n)|$ is bounded by a constant for $u \in [0, 1]$.

$$\text{Let} \qquad D_x = \max_{u \in [0,1]} |p(C_1 u, C_2, \ldots, C_n)|.$$

$$\begin{aligned} \text{Then} \qquad |x_1(T)| &= e^{-2T} \left| \int_{e^{-2T}}^1 \frac{p(C_1 u, C_2, \ldots, C_n)}{2u^2} du \right| \\ &\le e^{-2T} \int_{e^{-2T}}^1 \frac{|p(C_1 u, C_2, \ldots, C_n)|}{2u^2} du \le e^{-2T} \int_{e^{-2T}}^1 \frac{D_x}{2u^2} du \\ &= e^{-2T} \left[-\frac{D_x}{2u} \right]_{e^{-2T}}^1 = \frac{D_x}{2} \left(1 - e^{-2T}\right) \le \frac{D_x}{2}. \end{aligned}$$

It follows that $x_1(T)$ is bounded by a constant for all $T \ge 0$. The constant D_x is independent of T and ε and depends only on the initial conditions C.

The same idea is applicable to the terms $y_1(T), \ldots, b_{k,1}(T)$. For example, consider $y_1(T)$.

$$y_1(T) = \int_0^T q(C_1 e^{-2s}, C_2, \ldots, C_n) ds = \int_{e^{-2T}}^1 \frac{q(C_1 u, C_2, \ldots, C_n)}{2u} du.$$

$$\text{Let} \qquad D_y = \max_{u \in [0,1]} |q(C_1 u, C_2, \ldots, C_n)|.$$

$$\text{Then} \qquad |y_1(T)| = \left| \int_{e^{-2T}}^{1} \frac{q(C_1 u, C_2, \ldots, C_n)}{2u} du \right| \leq \int_{e^{-2T}}^{1} \frac{|q(C_1 u, C_2, \ldots, C_n)|}{2u} du$$

$$\leq \int_{e^{-2T}}^{1} \frac{D_y}{2u} du = \left[-\frac{D_y}{2} \ln u \right]_{e^{-2T}}^{1} = D_y T.$$

Exactly the same technique leads to similar estimates for the functions $a_{1,1}, \ldots, b_{k,1}$. We see that the undamped $O(\varepsilon)$ terms grow at linear speed. This is explained by the fact that these terms are constant at $O(1)$, and hence their $O(\varepsilon)$ approximations have secular terms. The perturbation problem is badly defined for functions $y_1, ..., b_{k,1}$. However, our goal is to prove the synchronization of voltages, which is described by the $x(T)$ component of solution. We will need components $y_1, ..., b_{k,1}$ only to estimate the error term.

To conclude, we note that the norm of the whole vector-function $z_1(T)$ grows at linear speed for all T as well, since

$$||z_1(T)|| = \sqrt{x_1(T)^2 + y_1(T)^2 + \cdots + b_{k,1}(T)^2}$$

$$\leq \sqrt{\left(\frac{D_x}{2}\right)^2 + D_y^2 T^2 + \cdots + D_{b,k}^2 T^2} \leq DT + \bar{D}$$

for some constants $D, \bar{D} \in \mathbb{R}$ depending only on the initial conditions C.

5.5.2 Estimate of the norm of $R(T, \varepsilon)$

The estimation procedure for $R(T, \varepsilon)$ in the case of a general nearly linear system is developed in [30] on pages 140-153. Here we utilize the procedure introduced by [30] for the special case when the matrix A has non-positive eigenvalues.

Consider the initial value problem (5.8). We may rewrite the equation for $R(T, \varepsilon)$ as an integral equation using an integrating factor technique. Recall

$$R' = AR + \varepsilon[F(z_0 + \varepsilon z_1 + R) - F(z_0)].$$

Multiplication by matrix e^{-AT} from the right leads to the equation

$$(e^{-AT} R)' = \varepsilon e^{-AT}[F(z_0 + \varepsilon z_1 + R) - F(z_0)].$$

Finally, integrating the latter equation from 0 to T with the initial condition $R(0, \varepsilon) = 0$, we obtain the following integral equation for $R(T, \varepsilon)$

$$R(T, \varepsilon) = \varepsilon \int_0^T e^{A(T-s)}[F(z_0 + \varepsilon z_1 + R) - F(z_0)] ds \tag{5.9}$$

Consider the matrix $e^{A(T-s)}$. In explicit notation it can be written as

$$\begin{pmatrix} e^{-2(T-s)} & 0 & \dots & 0 \\ 0 & 1 & \dots & 0 \\ \vdots & & & \\ 0 & 0 & \dots & 1 \end{pmatrix}.$$

It follows that $e^{A(T-s)}$ is bounded in the region $\Omega : T \geq 0, s \in [0,T]$, and $||e^{A(T-s)}|| \leq 1$ for all $(T,s) \in \Omega$. Using this property of $e^{A(T-s)}$ and the fact that $F(\cdot)$ is globally Lipschitz, we may estimate $\|R(T,\varepsilon)\|$ as follows

$$\begin{aligned} \|R(T,\varepsilon)\| &= \varepsilon \left| \int_0^T e^{A(T-s)}[F(z_0 + \varepsilon z_1 + R) - F(z_0)]ds \right| \\ &\leq \varepsilon \int_0^T \|F(z_0 + \varepsilon z_1 + R) - F(z_0)\| \, ds. \end{aligned} \tag{5.10}$$

At this point it is necessary to use the property that $F(\cdot)$ is globally Lipschitz. Applying the Lipschitz inequality, we obtain

$$\|R(T,\varepsilon)\| \leq \varepsilon \int_0^T L \, \|\varepsilon z_1 + R\| \, ds \leq \varepsilon L \int_0^T [\varepsilon \, \|z_1(s)\| + \|R(s,\varepsilon)\|]ds.$$

Finally, we may use the estimate $\|z_1(T)\| \leq DT + \bar{D}$ from the previous subsection, which holds for all T and is independent of ε. Substitution of the estimate for $\|z_1(T)\|$ leads to the following integral inequality for $\|R\|$:

$$\|R(T,\varepsilon)\| \leq \varepsilon L \int_0^T (\varepsilon D s + \varepsilon \bar{D} + \|R\|)ds. \tag{5.11}$$

An inequality of the form (5.11) is called *Gronwall's inequality* and can be resolved by using the following argument. Let

$$S(T,\varepsilon) = \varepsilon L \int_0^T (\varepsilon D s + \varepsilon \bar{D} + \|R(s,\varepsilon)\|)ds. \tag{5.12}$$

Inequality (5.11) implies that $\|R(T,\varepsilon)\| \leq S(T,\varepsilon)$. Differentiation of (5.12) and application of the Fundamental Theorem of Calculus leads to the following differential equation

$$\frac{dS}{dT} = \varepsilon^2 L(DT + \bar{D}) + \varepsilon L \|R(T,\varepsilon)\|.$$

Since $\|R(T,\varepsilon)\| \leq S(T,\varepsilon)$, we may replace R by S and obtain the differential inequality:

$$\frac{dS}{dT} \leq \varepsilon^2 L(DT + \bar{D}) + \varepsilon L S(T,\varepsilon),$$

which can be resolved using an integrating factor. Multiplication by $e^{-\varepsilon LT}$ and subsequent integration from 0 to T with initial condition $S(0) = 0$ preserve the inequality and lead to the following result:

$$\begin{aligned} Se^{-\varepsilon LT} &\leq \varepsilon^2 L \int_0^T (D\rho + \bar{D}) e^{-\varepsilon L\rho} d\rho \varepsilon^2 L \left[-\frac{D}{\varepsilon L} \rho e^{-\varepsilon L\rho} - \frac{D+\bar{D}}{(\varepsilon L)^2} e^{-\varepsilon L\rho} \right]_0^T \\ &= \varepsilon^2 L \left[-\frac{D}{\varepsilon L} T e^{-\varepsilon LT} - \frac{D+\bar{D}}{(\varepsilon L)^2} e^{-\varepsilon LT} + \frac{D+\bar{D}}{(\varepsilon L)^2} \right] \\ &= \frac{D+\bar{D}}{L} \left(1 - e^{-\varepsilon LT}\right) - \varepsilon DT e^{-\varepsilon LT}. \end{aligned}$$

Finally, multiplying the inequality by $e^{\varepsilon LT}$ and using the fact that $\|R(T,\varepsilon)\| \leq S(T,\varepsilon)$, we obtain the following estimate for the norm of $R(\varepsilon, T)$:

$$\|R(T,\varepsilon)\| \leq S(T,\varepsilon) \leq \frac{D+\bar{D}}{L} \left(e^{\varepsilon LT} - 1\right) - \varepsilon DT.$$

It follows that the error is of order 1 on the *expanding intervals* $[0, 1/\varepsilon]$. Precisely, there exists $K > 0$ independent of ε, such that

$$\|R(T,\varepsilon)\| \leq K, \qquad \forall T \in [0, 1/\varepsilon]. \tag{5.13}$$

The time intervals $[0, 1/\varepsilon]$ are called expanding, since they increase as ε is decreasing. Note that time intervals of length $(0, k/\varepsilon)$ on the fast time scale T correspond to the regular time intervals of length $(0, k)$ on the normal time scale.

The estimate of the error norm established by (5.13) is of $O(1)$ and hence is not very useful in obtaining a good approximation of complete solution. However, we may expect that such an estimate on the error norm is caused by the secular terms in the non-damped components of the solution, and that the damped component of the solution $x(T)$ is approximated with better accuracy even on expanding time intervals of length $1/\varepsilon$. It turns out that this prediction is true, and it is possible to obtain a better estimate on the error of the approximation to $x(T)$. Note that the error in the approximation of $x(T)$ is given by the first component of vector $R(T,\varepsilon)$, which we will denote by $R_x(T,\varepsilon)$.

5.5.3 The estimate of $R_x(T,\varepsilon)$

As has been shown in equation (5.9) in the previous subsection, $R_x(T,\varepsilon)$ has to satisfy the following integral equation

$$R_x(T,\varepsilon) = \varepsilon e^{-2T} \int_0^T e^{2s} \left[p(z_0 + \varepsilon z_1 + R) - p(z_0)\right] ds.$$

Using the results of previous subsections, we obtain the following estimate of $R_x(T,\varepsilon)$:

$$\begin{aligned}
|R_x(T,\varepsilon)| &= \varepsilon e^{-2T}\left|\int_0^T e^{2s}\left[p(z_0+\varepsilon z_1+R)-p(z_0)\right]ds\right| \\
&\leq \varepsilon e^{-2T}\int_0^T e^{2s}|p(z_0+\varepsilon z_1+R)-p(z_0)|ds \\
&\leq \varepsilon e^{-2T}\int_0^T e^{2s}\|F(z_0+\varepsilon z_1+R)-F(z_0)\|ds \\
&\leq \varepsilon e^{-2T}\int_0^T e^{2s}L(\varepsilon\|z_1(T)\|+\|R\|)ds.
\end{aligned}$$

Now it is necessary to use the previously computed estimates of $\|R(T)\|$ and $\|z_1(T)\|$. As we have shown, $\|z_1(T)\| \leq DT+\bar{D}$ for all $T \geq 0$, and hence $\|z_1(T)\| \leq D/\varepsilon+\bar{D}$ on the time interval $[0,1/\varepsilon]$.On the other hand, $\|R(T)\| \leq K$ for $T \in [0,1/\varepsilon]$. It follows that

$$\begin{aligned}
|R_x(T,\varepsilon)| &\leq \varepsilon L e^{-2T}\int_0^T e^{2s}\varepsilon D/\varepsilon+\bar{D}+Ke^{2s}ds \\
&= \varepsilon L e^{-2T}\int_0^T (D+\bar{D}\varepsilon+K)e^{2s}ds \\
&= \varepsilon e^{-2T}\frac{LD+LK+\varepsilon L\bar{D}}{2}\left(e^{2T}-1\right) \\
&= \varepsilon\frac{LD+LK+\varepsilon L\bar{D}}{2}\left(1-e^{-2T}\right) \leq \varepsilon M,
\end{aligned}$$

where $M=(LD+LK+L\bar{D})/2$ and depends only on the initial conditions C and the Lipschitz constant. We have just shown that $R_x(T,\varepsilon)$ is of $O(\varepsilon)$ uniformly on the expanding time intervals $[0,1/\varepsilon]$.

5.5.4 Approximation of $x(t)$

Let us fix some $t_0 \geq 0$. Consider an initial value problem for system (5.1) on the interval $[0,t_0)$. Applying the changes of variables introduced in section 5.2, we see that the initial value problem for system (5.1) considered on the interval $[0,t_0)$ is equivalent to an initial value problem for the system (5.5) defined on the interval $[0,t_0/\varepsilon)$ on the fast time scale T. As was shown in sections 5.3 and 5.4, the x component of exact solution of (5.5) can be written in the form

$$x(T) = C_1e^{-2T}+\varepsilon x_1(T)+R_x(T,\varepsilon). \tag{5.14}$$

Recall that in subsection 5.5.1 we have shown that $|x_1(T)|$ is bounded by a constant $D_x/2$ for all $T \geq 0$, while in subsection 5.5.3 we have shown that $|R_x(T,\varepsilon)| \leq \varepsilon M$ uniformly on expanding time intervals $[0, 1/\varepsilon]$. It follows that (5.14) can be rewritten as

$$x(T) = C_1 e^{-2T} + \phi(T), \tag{5.15}$$

where $|\phi(T)| \leq U\varepsilon$ for all $T \in [0, t_0/\varepsilon]$ and for some constant $U \in \mathbb{R}$ depending only on the initial conditions C and the Lipschitz constant L, since the estimates for $x_1(T)$ and $R_x(T,\varepsilon)$ hold *uniformly* on the expanding time intervals $[0, t_0/\varepsilon]$.

Due to the uniform boundedness of $\phi(T)$ on the interval $[0, t_0/\varepsilon]$ on the fast time scale approximation (5.15) is valid on the interval $[0, t_0]$ on the regular time scale. It follows that

$$x(t) = C_1 e^{-2t/\varepsilon} + \hat{\phi}(t), \qquad t \in [0, t_0] \tag{5.16}$$

where $|\hat{\phi}(t)| < \varepsilon U$. Interpreting the statement (5.16) in terms of original system (5.1), we may say that for $\gamma > 0$ the difference $|v_1(t) - v_2(t)|$ is approximated by $2C_1 e^{-2\gamma t}$ with an error of $O(1/\gamma)$ on any finite time interval $[0, t_0]$, where C_1 denotes $1/2[v_1(0) - v_2(0)]$.

5.5.5 Simplification in the case of conductance-based models

In order to derive approximation (5.16) we used the assumption that $F(\cdot)$ is globally Lipschitz. However, we haven't used any knowledge about the behavior of the exact solutions of system (5.1). It turns out that it is possible to prove that solutions of (5.1) are bounded for all $\gamma \geq 0$ in the case when system (5.1) represents a conductance-based model of a neuron. This statement allows us to weaken the assumption about $F(\cdot)$ being *globally* Lipschitz and to improve the approximation (5.16).

Consider the conductance based-model of an arbitrary neuron having N ionic channels, each governed by the activation variable α_k and the inactivation variable β_k. According to the section 2.2, any conductance-based model has a following general form:

$$\left\{ \begin{array}{rcl} dv/dt & = & i - g_L(v - v_L) - \sum\limits_{k=1}^{N} g_k \alpha_k^{x(k)} \beta_k^{y(k)} (v - v_k) \\ d\alpha_k/dt & = & \lambda_{\alpha,k}(v)[\alpha_{k,\infty}(v) - \alpha_k] \\ d\beta_k/dt & = & \lambda_{\beta,k}(v)[\beta_{k,\infty}(v) - \beta_k] \end{array} \right. , \qquad k = 1 \ldots N \tag{5.17}$$

Consider the gating variables α_k and β_k, $k = 1 \ldots N$ first. Note that functions $\alpha_{k,\infty}(v)$ and $\beta_{k,\infty}(v)$ represent the percent of ionic channels open at steady state

for fixed voltage v, and hence only take values between 0 and 1, while functions $\lambda_{\alpha,k}(v)$ and $\lambda_{\beta,k}(v)$ denote rate constants in time and are strictly positive.

It follows that for any k in $1, \ldots, N$

$$\begin{aligned}
\left.\frac{d\alpha_k}{dt}\right|_{\alpha_k=0} &= \lambda_{\alpha,k}(v)[\alpha_{k,\infty}(v)] \geq 0 \quad \forall v \in \mathbb{R}, \qquad \text{while} \\
\left.\frac{d\alpha_k}{dt}\right|_{\alpha_k=1} &= \lambda_{\alpha,k}(v)[\alpha_{k,\infty}(v) - 1] \leq 0 \quad \forall v \in \mathbb{R}
\end{aligned}$$

Exactly same argument is applicable for β_k. It follows, that if variables α_k and β_k are inside the interval $[0, 1]$ for $t = 0$, they will remain in that interval for all subsequent time $t > 0$.

Consider the equation for dv/dt next. Recall that $x(k)$ and $y(k)$, $k = 1 \ldots N$ are nonnegative integers, g_L and g_k, $k = 1 \ldots N$ are positive constants representing conductances of each ionic channel, while v_L and v_k, $k = 1 \ldots N$ are equilibrium potentials for each ionic channel and are not necessarily positive.

Let $M > 0$ be some constant. Rearranging terms in the first equation of (5.17), and using the fact that $0 \leq \alpha_k(t), \beta_k(t) \leq 1$ for all $t \geq 0$, we obtain that at $v = M$

$$\begin{aligned}
\left.\frac{dv}{dt}\right|_{v=M} &= i + g_L v_L + \sum_{k=1}^{N} g_k \alpha_k^{x(k)} \beta_k^{y(k)} v_k - \left[g_L + \sum_{k=1}^{N} g_k \alpha_k^{x(k)} \beta_k^{y(k)} \right] M \\
&\leq i + g_L v_L + \sum_{k=1}^{N} g_k |v_k| - g_L M
\end{aligned}$$

On the other hand, at $v = -M$ we have that

$$\begin{aligned}
\left.\frac{dv}{dt}\right|_{v=-M} &= i + g_L v_L + \sum_{k=1}^{N} g_k \alpha_k^{x(k)} \beta_k^{y(k)} v_k + \left[g_L + \sum_{k=1}^{N} g_k \alpha_k^{x(k)} \beta_k^{y(k)} \right] M \\
&\geq i + g_L v_L - \sum_{k=1}^{N} g_k |v_k| + g_L M
\end{aligned}$$

Let $M_0 = \max\left(\left[i + g_L v_L + \sum_{k=1}^{N} g_k |v_k| \right] / g_L, \left[\sum_{k=1}^{N} g_k |v_k| - i - g_L v_L \right] / g_L \right)$. Then for any $M > M_0$ we will have that $dv/dt|_{v=M} < 0$ and $dv/dt|_{v=-M} > 0$, which implies that variable v will be restricted to the interval $[-M, M]$ for all $t \geq 0$.

It follows that all solutions of (5.17) with initial conditions inside the box $[-M, M] \times [0, 1] \times \cdots \times [0, 1] \subset \mathbb{R}^{N+1}$ will remain inside this box for all $t > 0$, as long as we choose $M > M_0$.

Consider the system of two coupled neurons, i.e. system (5.1). For $\gamma = 0$ it has form

$$\begin{cases} \dot{v}_1 = f_1(v_1, a_1, \ldots, a_m) \\ \dot{v}_2 = f_2(v_2, b_1, \ldots, b_k) \\ \dot{a}_i = g_i(v_1, a_i), \qquad i = 1 \ldots m \\ \dot{b}_j = h_j(v_2, b_j) \qquad j = 1 \ldots k \end{cases} \tag{5.18}$$

Note that system (5.18) in fact splits into two independent subsystems - one for variables $(v_1, a_1, ..., a_m)$ and another for variables $(v_2, b_1, ..., b_k)$, and hence consists of two conductance-based models independent of each other. Let us choose M larger than M_0 for each of the subsystems $(v_1, a_1, ..., a_m)$ and $(v_2, b_1, ..., b_k)$. Then all solutions of (5.18) with initial conditions in the set $\mathbb{B} = [-M, M] \times [-M, M] \times [0, 1] \times \cdots \times [0, 1] \subset \mathbb{R}^n$ will remain in $\mathbb{B}$ for all $t \geq 0$.

Finally, it is left to analyze the effect of coupling. It turns out that, for positive γ, coupling cannot force solutions to leave $\mathbb{B}$. Consider the coupled system (5.1). Recall that it has form

$$\begin{cases} \dot{v}_1 = f_1(v_1, a_1, \ldots, a_m) + \gamma(v_2 - v_1) \\ \dot{v}_2 = f_2(v_2, b_1, \ldots, b_k) + \gamma(v_1 - v_2) \\ \dot{a}_i = g_i(v_1, a_i), \qquad i = 1 \ldots m \\ \dot{b}_j = h_j(v_2, b_j) \qquad j = 1 \ldots k \end{cases} .$$

$$\left.\frac{dv_1}{dt}\right|_{v=M} = f_1(M, a_1, \ldots, a_m) + \gamma(v_2 - M) < 0,$$

since $f_1(M, a_1, \ldots, a_m) < 0$ by the choice of M, while $\gamma(v_2 - M) \leq 0$ for all $\gamma > 0$ and $v_2 \in [-M, M]$. On the other hand,

$$\left.\frac{dv_1}{dt}\right|_{v=-M} = f_1(-M, a_1, \ldots, a_m) + \gamma(v_2 + M) > 0,$$

since $f_1(-M, a_1, \ldots, a_m) > 0$ by the choice of M, while $\gamma(v_2 + M) \geq 0$ for all $\gamma > 0$ and $v_2 \in [-M, M]$. Exactly same procedure is applicable to the variable v_2, while boundaries on variables $a_1, \ldots, b_k$ are unaffected by the coupling.

It follows, that for any $\gamma \geq 0$ all solutions of (5.1) with initial conditions in the box $\mathbb{B}$ remain in $\mathbb{B}$ for all $t > 0$, as long as (5.1) represents a system of two electrically coupled conductance based models.

Let $\mathbb{B}'$ denote the image of $\mathbb{B}$ under the linear transformation $x = 1/2(v_1 - v_2)$, $y = 1/2(v_1 + v_2)$. Boundedness of solutions of (5.1) implies that all solutions of

(5.5) with initial conditions in $\mathbb{B}'$ remain inside $\mathbb{B}'$ for all $T \geq 0$ as well. Since the biophysically interesting dynamics occurs inside $\mathbb{B}'$, starting from this point we will consider only initial conditions $C \in B'$.

Knowing that the exact solution of system (5.5), $z(T)$, is bounded for all $T \geq 0$ for positive γ, it is possible to weaken the condition of global Lipschitz continuity. Recall that the Lipschitz inequality was used in order to verify the following transition:

$$\int_0^T \|F(z_0 + \varepsilon z_1 + R) - F(z_0)\|\, ds \leq \int_0^T L\, \|\varepsilon z_1 + R\|\, ds.$$

Since $z_0(T) = (C_1 e^{-2T}, C_1, ..., C_n)^T$ (see section 5.4), $z_0(T)$ remains inside $\mathbb{B}'$ for all $T \geq 0$ as long as $C \in \mathbb{B}'$. On the other hand, $z_0 + \varepsilon z_1 + R$ is an exact solution of the initial value problem (5.5), and is contained inside $\mathbb{B}'$ for all $t \geq 0$ if $C \in B'$. Since both $z_0(T)$ and $z(T)$ are contained in $\mathbb{B}'$ provided $C \in \mathbb{B}'$, it is only necessary to assume the existence of Lipschitz constant for $F(\cdot)$ in $\mathbb{B}'$, which follows from the conditions set on $F(\cdot)$ in section 5.1.

Another advantage of restricting the problem to a closed compact set $\mathbb{B}'$ consists in a fact that the constant U in approximation (5.16) can be chosen the *same* for all $C \in \mathbb{B}'$. Recall that U depends on the Lipschitz constant L and constants D_x, D and $\bar{D}$, which are defined in terms of the following maximums (see subsection 5.5.1):

$$\begin{array}{l} \max\limits_{u\in[0,1]} |p(C_1 u, C_2, \ldots, C_n)| \\ \max\limits_{u\in[0,1]} |q(C_1 u, C_2, \ldots, C_n)| \\ \ldots \\ \max\limits_{u\in[0,1]} |h_k(C_1 u, C_2, \ldots, C_n)| \end{array}$$

However, since $\mathbb{B}'$ is a bounded compact convex set, we may redefine D_x, D and $\bar{D}$ in terms of

$$\begin{array}{l} \max\limits_{C\in\mathbb{B}'}(\max\limits_{u\in[0,1]} |p(C_1 u, C_2, \ldots, C_n)|) \\ \max\limits_{C\in\mathbb{B}'}(\max\limits_{u\in[0,1]} |q(C_1 u, C_2, \ldots, C_n)|) \\ \ldots \\ \max\limits_{C\in\mathbb{B}'}(\max\limits_{u\in[0,1]} |h_k(C_1 u, C_2, \ldots, C_n)|) \end{array},$$

which makes D_x, D and $\bar{D}$ independent of choice of initial conditions C inside $\mathbb{B}'$, and hence makes constant U in the estimate (5.16) to be same for all $C \in \mathbb{B}'$.

Independence of initial conditions and boundedness of solutions inside the compact convex set $\mathbb{B}'$ allows us to use the fact that the system (5.5) is autonomous, and leads to the following final conclusion.

Note: The following conclusion can be applied to any system of the form (5.1) provided that all solutions of that system with initial conditions in some closed bounded set are contained inside that set for all $t \geq 0$ and all $\gamma \geq 0$.

5.5.6 Conclusion

Consider an initial value problem for system (5.1) defined on the time interval $[0, 1]$ and with initial conditions inside the box $\mathbb{B}$. Then the approximation (5.16) provided in subsection 5.5.4 is valid, and we have that

$$x(t) = C_1 e^{-2t/\varepsilon} + \phi(t), \qquad t \in [0, 1],$$

where $|\phi(t)| < U\varepsilon$ for all $t \in [0, 1]$, and U is independent of both ε and the choice of initial conditions $C \in \mathbb{B}'$.

Let us fix an arbitrary $\delta > 0$, and for that δ choose ε_0 such that both of the conditions below hold:

$$U\varepsilon_0 < \frac{\delta}{3} \qquad \text{and} \qquad e^{-2/\varepsilon_0} < \frac{1}{2}. \tag{5.19}$$

According to the approximation of $x(t)$ provided above, we have that

$$|x(1)| \le |C_1| e^{-2/\varepsilon_0} + \frac{\delta}{3}.$$

At this point we may use the fact that system (5.1) is autonomous. Taking vector-solution $\mathrm{x}(1) \in \mathbb{B}$ as the initial condition and applying the approximation (5.16) on the time interval $[0, 1]$ one more time, we obtain that

$$|x(2)| \le |x(1)| e^{-2/\varepsilon_0} + \frac{\delta}{3} \le |C_1| e^{-4/\varepsilon_0} + \frac{\delta}{3}(1 + e^{-2/\varepsilon_0}).$$

Repeating this procedure as many times as we want, we obtain that

$$|x(\ell)| \le |C_1| e^{-2\ell/\varepsilon_0} + \frac{\delta}{3}(1 + e^{-2/\varepsilon_0} + e^{-4/\varepsilon_0} + \cdots + e^{-2(\ell-1)/\varepsilon_0}).$$

Due to the condition $e^{-2/\varepsilon_0} < 1/2$, from (5.19) we have

$$\sum_{n=0}^{\ell} e^{-2n/\varepsilon_0} \le \sum_{n=0}^{\ell} \frac{1}{2^n} \le 2.$$

Finally, it follows that for any $t \in \mathbb{R}$

$$|x(t)| \le |C_1| e^{-2t/\varepsilon_0} + \frac{2\delta}{3}.$$

It is obvious that first summand approaches zero as $t \to +\infty$ for any $C \in \mathbb{B}'$, and hence, starting at some time $t_1 \ge 0$, $|x(t)|$ becomes less than δ and remains less than δ for all subsequent t. Reformulating the final conclusion in terms of the original system (5.1), we obtain the following statement.

For any $\delta > 0$ there exists $\gamma_0 > 0$, such that for all $\gamma > \gamma_0$ and for any solution of (5.1) with initial conditions inside the region of interest $\mathbb{B}$, the difference

$|v_1(t) - v_2(t)|$ becomes less than δ at some time $t_1 \geq 0$ and remains less than δ for all subsequent time $t > t_1$.

Reformulating the statement above in terms of fixed γ, we may say that for any fixed $\gamma_0 > 0$ large enough there exists small $\delta_0 > 0$, such that $|v_1(t) - v_2(t)|$ becomes less than δ_0 at some time and remains less than δ_0 for all later time for any initial conditions in the region of interest $\mathbb{B}$. The larger the value of γ_0, the smaller the corresponding δ_0.

5.6 Unbounded growth in the case of negative γ

Consider the case of $\gamma < 0$ next. Subsection 5.5.1 implies in that for $\gamma < 0$ the order one solution is given by $x_0(T) = C_1 e^{2T}$. Since $x_0(T)$ is growing unboundedly as $T \to +\infty$, there is no convenient way to estimate integrals for $z_1(T)$, and we have to restrict ourself to analysis of the finite time intervals on the fast time scale instead of expanding time intervals $[0, 1/\varepsilon]$.

Let us fix some $T_0 > 0$. The initial value problem (5.7) satisfies the conditions of the theorem of existence and uniqueness of solutions, and hence $z_1(T)$ is bounded by a constant on the finite time interval $[0, T_0]$. Precisely, there exists $K_- \in \mathbb{R}$ such that $|z_1(T)| < K_-$ for all $T \in [0, T_0]$.

The norm of $\|R(T, \varepsilon)\|$ can be estimated by the same procedure as in subsection 5.5.2. Note that we don't need $F(\cdot)$ to be globally Lipschitz, since both $z(T)$ and $z_0(T)$ are contained in some compact convex set for $T \in [0, T_0]$. Performing the same steps as in subsection (5.5.2), we can write the analog of inequality (5.10) on the time interval $[0, T_0]$:

$$\|R(T, \varepsilon)\| \leq \varepsilon \int_0^T L(\varepsilon \|z_1(s)\| + \|R(s, \varepsilon)\|) ds.$$

Using the fact that $z_1(T)$ is bounded by K_-, we obtain that

$$\|R(T, \varepsilon)\| \leq \int_0^T \varepsilon^2 L K_- + \varepsilon L \|R\| ds,$$

which can be resolved using Gronwall's argument as in subsection 5.5.2. Finally, we obtain that

$$\|R(T, \varepsilon)\| \leq \varepsilon K_- (e^{\varepsilon L T} - 1).$$

Function $e^{\varepsilon L T}$ is bounded on $[0, T_0]$ as well, and hence $\|R(T, \varepsilon)\| \leq \varepsilon U_1$ for $T \in [0, T_0]$, where $U_1 \in \mathbb{R}$ is some constant. It follows that $R(T, \varepsilon)$ is of $O(\varepsilon)$ on the finite time interval $[0, T_0]$. Therefore,

$$\|z_1(T) + R(T, \varepsilon)\| < U_2 \varepsilon, \quad \text{for some } U_2 \in \mathbb{R} \text{ and } T \in [0, T_0]. \tag{5.20}$$

Comment: Using a different argument, it can be shown that $\|R(T, \varepsilon)\|$ actually is of order ε^2 on finite intervals (see [30] pages 150-153). However, we don't need

$O(\varepsilon^2)$ accuracy in the error estimate since it is impossible to estimate $z_1(T)$ better than $O(\varepsilon)$. Thus, we choose to use the same method as before in order to simplify notation.

The inequality (5.20) implies that for $\gamma < 0$

$$x(T) = C_1 e^{2T} + O(\varepsilon), \qquad \text{on any finite time interval } [0, T_0]. \tag{5.21}$$

Using (5.21), it is impossible to track the behavior of solutions within finite time intervals on the regular time scale $t = T/\varepsilon$, since the finite time interval $[0, T_0]$ corresponds to the expanding time interval $[0, T_0/\varepsilon]$ on the regular time scale. The smaller we make ε, the longer becomes the interval $[0, T_0/\varepsilon]$, since $T_0/\varepsilon \to +\infty$ as $\varepsilon \to 0$. However, it is possible to show that $|x(T)|$ grows unboundedly on the fast time scale for ε small enough, or, equivalently, that $|x(t)|$ becomes unbounded as $t \to +\infty$.

Choose an arbitrary constant $M > 0$. For any $C_1 \neq 0$ there exist $T_0 > 0$, such that $|C_1|e^{2T_0} > 2M$. Consider the solution of the initial value problem (5.5) on the time interval $[0, T_0]$. Due to the estimates (5.20) and (5.21), there exists $\varepsilon_0 > 0$, such that for all $\varepsilon < \varepsilon_0$

$$|\varepsilon x_1(T_0) + R_x(T_0, \varepsilon)| \leq \|z_1(T_0) + R(T_0, \varepsilon)\| < U_2\varepsilon < M.$$

Finally, consider the x component of the exact solution of (5.5) which is equal to $x(T) = C_1 e^{2T} + \varepsilon x_1(T) + R_x(T, \varepsilon)$. We may rewrite the latter equality as $C_1 e^{2T} = x(T) - \varepsilon x_1(T) - R_x(T, \varepsilon)$. It follows from the triangle inequality, that

$$|C_1 e^{2T_0}| \leq |x(T_0)| + |\varepsilon x_1(T_0) + R_x(T_0, \varepsilon)| \leq |x(T_0)| + M.$$

On the other hand, $|C_1 e^{2T_0}| > 2M$. Then

$$2M < |C_1 e^{2T_0}| < |x(T_0)| + M,$$

which implies that

$$|x(T_0)| > M, \qquad \text{for all} \quad \varepsilon < \varepsilon_0.$$

Thus, $|x(T)|$ can be made arbitrarily large by appropriate choice of ε.

Since $|x(T)| = 1/2|v_1(T) - v_2(T)|$, unbounded growth of $x(T)$ implies unbounded growth of at least one of $|v_1(T)|$ and $|v_2(T)|$. However $y = 1/2(v_1(T) + v_2(T))$ remains constant to $O(\varepsilon)$ on the fast time scale. It follows, that $v_1(T)$ diverges to $+\infty$ while $v_2(T)$ diverges to the $-\infty$ with nearly the same speed, or vice versa.

5.7 Discussion

In the present chapter we have analyzed a system of two arbitrary electrically coupled conductance-based models. Consider the case $\gamma > 0$ first. We have shown

that choosing $\gamma > 0$ large enough we may make the difference $|v_1(t) - v_2(t)|$ smaller than any arbitrary number $\delta > 0$. However, does it mean that $|v_1(t) - v_2(t)| \to 0$ as $t \to +\infty$?

In general the answer is no. Note that the analysis done in the present chapter is valid only assuming $\gamma(v_2 - v_1)$ is large. However, when the difference $(v_1 - v_2)$ starts taking values of $O(1/\gamma)$, the term $\gamma(v_2 - v_1)$ becomes of order one, and the perturbation analysis fails. Moreover, no matter how large is γ, as long as the difference $(v_2 - v_1)$ is of $O(1/\gamma^2)$, coupling can be considered as weak coupling! Note that neurons synchronize exponentially fast on the fast time scale until difference between voltages v_1 and v_2 becomes small, while the sum of voltages v_1 and v_2 remain constant on the fast time scale.

In particular, this observation implies that $|v_1(t) - v_2(t)| \to 0$ as $t \to +\infty$ only if corresponding *weakly coupled* conductance based model has stable synchronous solution, no matter how large value of γ is under consideration. However, is this necessary condition sufficient for $|v_1(t) - v_2(t)| \to 0$ as $t \to +\infty$ or not?

This question has no determined answer yet. Theoretically, it is possible that regions of validity of the phase model and approximation (5.16) overlap in the following sense:

There may exist $\gamma_0 > 0$, such that compared with the γ_0 the value δ_0 is so small that $\gamma(v_1 - v_2)$ lies in the region of validity of the phase model after $|v_1 - v_2|$ becomes less than δ_0. Here it is necessary to develop a definition of the region of validity of phase model in terms of the relation between the magnitude of the term $\gamma(v_1 - v_2)$ and the magnitude of the term $F(v_1, v_2, a_1, \ldots, b_k)$. However, this assumption is questionable and needs to be verified.

We have established a relationship between phase models and the approximation for large γ, and that motivates us to study this question in more detail. Note that the region of validity of the phase model can always be estimated using the negative values of γ. Analysis of large negative values of γ done in the present chapter showed that both $v_1(t)$ and $v_2(t)$ grow exponentially fast on the fast time scale $T = \gamma t$ with an error of order $O(1/\gamma)$, which implies that predictions of the phase model have to fail for some $\gamma_{lim} < 0$, and hence the relationship between the magnitudes of $\gamma_{lim}(v_1 - v_2)$ and $F(v_1, v_2, a_1, \ldots, b_k)$ can be taken as an estimate of the region of validity of phase model.

To summarize the analysis, we can make the following general conclusions.

1. Consider the case when the neurons are identical (i.e. $m = k$, $f_1 \equiv f_2$, $g_i \equiv h_i$, $i = 1 \ldots m$), and the system describing each single neuron has some globally stable attractor $\Lambda \in \mathbb{R}^m$. By appropriate choice of $\gamma > 0$ the difference between $v_1(t)$ and $v_2(t)$ can be made smaller than an arbitrary tolerance level δ within a finite time t_1 and will remain less than δ for all $t > t_1$.However, the question if $\Lambda \times \Lambda \subset \mathbb{R}^{2m}$ is a global attractor of the coupled system has to be studied in more detail. A necessary condition is that $\Lambda \times \Lambda \subset \mathbb{R}^{2m}$ has to be a stable attractor of the *weakly* coupled system.

In the case of two identical Morris-Lecar neurons this observation has been verified by the phase plane analysis done in chapter 3 and by the numerical simulations done in chapter 4, since the in-phase limit cycle turned to be the only stable equilibrium state for all $\gamma > 0$.

2. The case of different neurons, or even the same neurons receiving different input signals is even more interesting. Assume that the first neuron has a global attractor $\Theta \subset \mathbb{R}^{m+1}$ with $v_1(t) = \phi(t)$ while the second neuron has the global attractor $\Upsilon \subset \mathbb{R}^{k+1}$ with $v_2(t) = \xi(t)$, where $\phi(t) \neq \xi(t)$. Analysis done in the present chapter suggests that for $\gamma > 0$ large enough voltages of both neurons have to be δ close, which implies that neither Θ nor Υ will be the global attractor for each of the neurons in the coupled system, and the coupled system hence will approach some new attractor $\Gamma \subset \mathbb{R}^n$. However, the difference $|v_1 - v_2|$ will not converge to zero. Γ cannot satisfy condition $v_1 \equiv v_2$ since weakly coupled neurons have to stay each on its own attractor Θ and Υ.

   For example, consider the case of first neuron being the Morris-Lecar neuron with an input corresponding to a stable equilibrium point and the second neuron being the Morris-Lecar neuron with an input corresponding to a stable limit cycle. The corresponding numerical simulations are provided in figures (5.1)-(5.2). Despite the fact that the voltages approach each other very close, magnification shows that, in fact, $|v_1 - v_2|$ does not approach zero.

To conclude, it is worth mentioning that the analysis done in section 5.5 contributes to the general theory of nearly linear systems. In [30] Murdock has shown that the error term is $O(\varepsilon^2)$ for all $t \geq 0$ in the case when all eigenvalues of the matrix A are negative, is of $O(\varepsilon)$ uniformly on expanding time intervals $(0, 1/\varepsilon)$ when both e^{At}, $z_0(t)$, $z_1(t)$ and $z(t)$ are bounded for all $t \geq 0$, and is of order ε^2 on the finite time intervals $(0, t)$ for an arbitrary matrix A.

We have extended the analysis of the case when eigenvalues of A are non-positive. In section 5.5 we have shown that the error along coordinates corresponding to the negative eigenvalues is of order ε uniformly on expanding time intervals $(0, 1/\varepsilon)$. An assumption of $z_1(t)$ being bounded for all t was not used. We have studied only the case of A being diagonalizable. However, the estimation procedure can be generalized for the case of the arbitrary matrix A with non-positive eigenvalues.

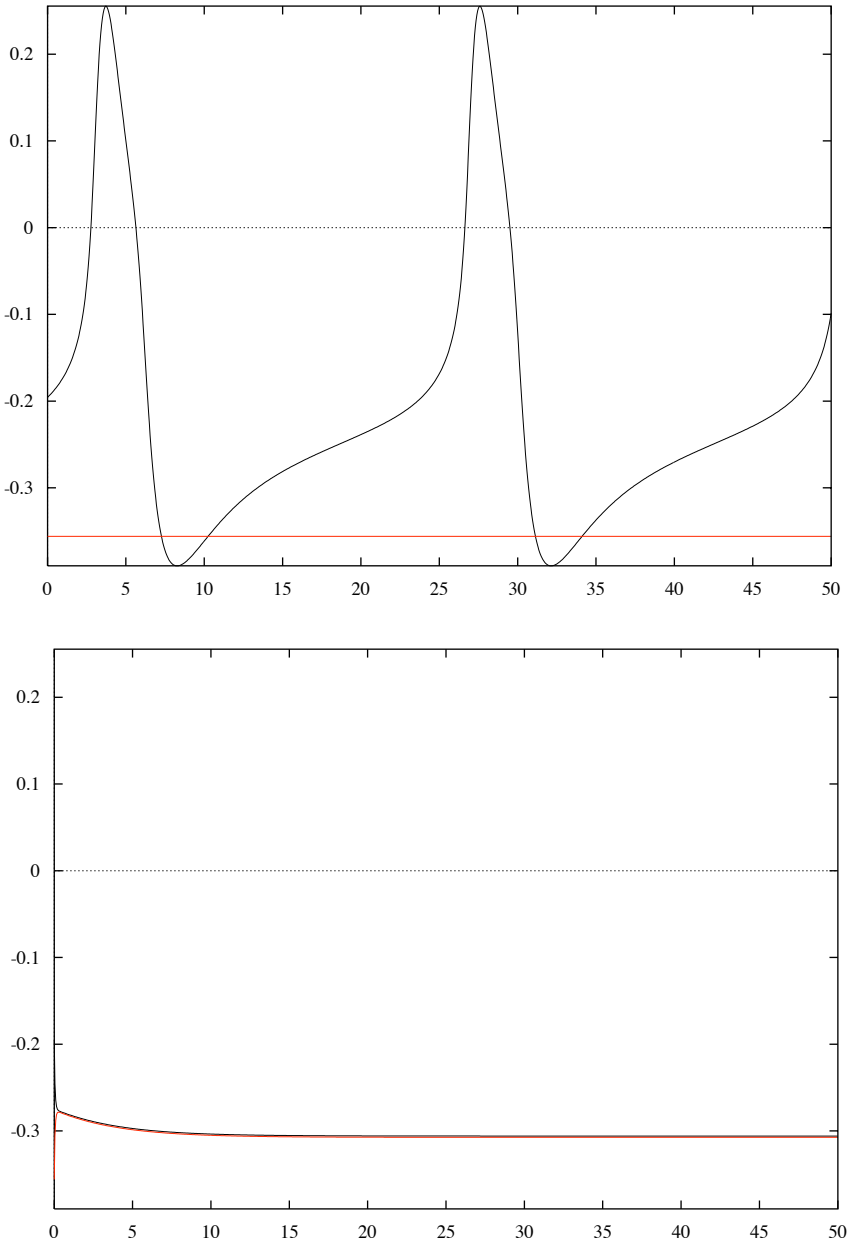

Figure 5.1: Graphs of voltages v_1 and v_2 for decoupled(upper graph) and coupled with coupling strength $\gamma = 10$(lower graph) type I Morris-Lecar neurons with inputs of $i_1 = 0.09$ and $i_2 = 0.06$

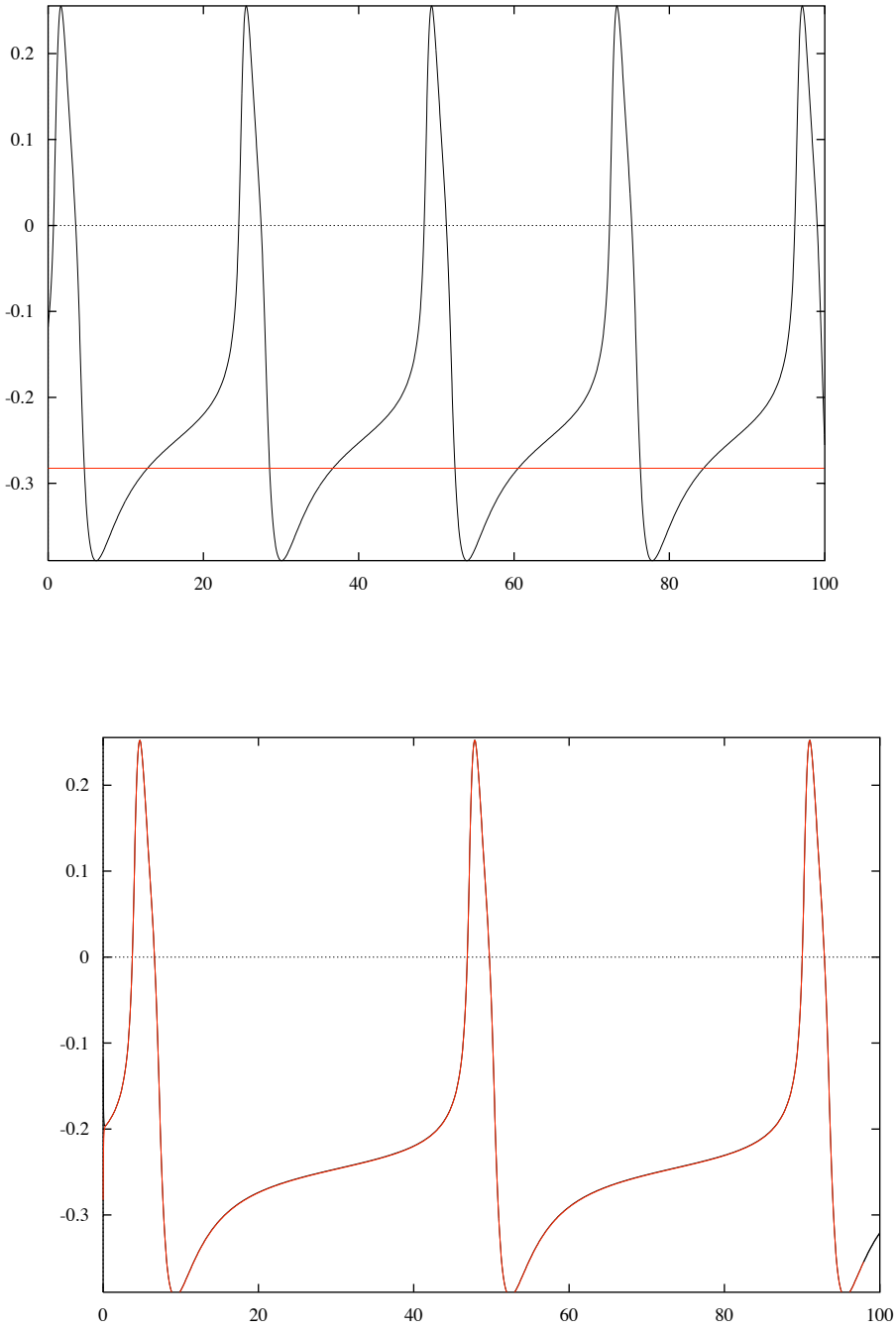

Figure 5.2: Graphs of voltages v_1 and v_2 for decoupled(upper graph) and coupled with coupling strength $\gamma = 10$(lower graph) type I Morris-Lecar neurons with inputs of $i_1 = 0.09$ and $i_2 = 0.08$

Chapter 6

Conclusion

In chapter 2 we introduced the Morris-Lecar model which is a second order conductance-based model that represents the behavior of the barnacle giant muscle fiber. This system exhibits oscillations over a wide parameter range; moreover, both type I and type II oscillators can be modeled using the Morris-Lecar system. The transition between type I and type II behavior can be obtained by variation of the single parameter g_{Ca}.

In order to study the effects of the strength of electrical coupling γ and the coupling time delay τ, we chose to analyze a network of two identical electrically coupled Morris-Lecar neurons of type I, and a network of two identical electrically coupled Morris-Lecar neurons of type II. The applied current i in each network was set close to the onset of oscillations in order to magnify the difference between type I and type II behavior.

In the case of weak coupling we developed a phase model which allowed us to determine the stable periodic solutions of the system. In the non-delayed case for both type I and type II parameter sets the synchronous in-phase solution was stable for physically relevant positive values of γ, while for $\gamma < 0$ the anti-phase solution was stable.

For small enough values of τ, we showed that the phase model (3.36) with a phase shift due to the delay is applicable. Analysis of (3.36) for both type I and type II parameter sets and for $\gamma > 0$ suggested that for small values of τ oscillators synchronize their behavior, while as τ is increased stability switches between in-phase and anti-phase solutions occur. These results are qualitatively the same as the results of the analysis of a coupled Fitzhugh-Nagumo system done by Smith in [34].

We showed that the values of the scaled delay, $\eta = \Omega\tau$, where stability switches occur for type I and type II parameter sets were very similar. Hence, type I oscillators require larger changes in τ to switch stability, since the inherent frequency of oscillations Ω is smaller for oscillators of this type. It follows that the absolute value of τ is unimportant for stability switching, only the relationship between Ω and τ matters.

The numerical analysis done in chapter 4 verified the predictions of the phase model and analyzed the behavior of the system beyond the region of weak coupling. The construction of bifurcation diagrams in both delayed and non-delayed cases was based on the structure of the equilibrium points with respect to γ and τ, obtained in section 4.2. Analysis of the stability along the branches of equilibrium points allowed us to find the Hopf bifurcation points and hence construct periodic orbits. Bifurcation analysis and numerical simulations showed that the neurons synchronized for large $\gamma > 0$, while for large $\gamma < 0$ solutions diverged. This observation motivated the asymptotic analysis done in chapter 5.

Analysis of electrically coupled conductance based models for large $\gamma > 0$ showed that for each $\gamma_0 > 0$ there exists $\delta_0 > 0$, such that voltages of the neurons become δ_0 close in finite time and remain δ_0 close for all subsequent time. As γ_0 is increased, δ_0 becomes smaller. However, for any $\gamma > 0$ the difference $|v_1(t) - v_2(t)| \to 0$ as $t \to +\infty$ only if the corresponding *weakly coupled* system has a stable synchronous state, since as $|v_1(t) - v_2(t)|$ gets small enough coupling can be considered as *weak*.

In order to study the case of $\gamma \to +\infty$ we have extended the theory of nearly linear systems developed by Murdock in [30]. We have shown that for nearly linear systems with non-positive eigenvalues the first order approximation to the solution along directions corresponding to the negative eigenvalues is $O(\varepsilon)$ uniformly on expanding time intervals $(0, 1/\varepsilon)$.

Part of the work done in the present thesis was devoted to estimation of the regions of validity of the phase models. The boundary between "weak" and "strong" coupling with respect to γ was estimated by finding the value, γ_{lim}, where predictions of the non-delayed phase model failed. Numerical simulations showed that $\gamma_{lim} \approx -0.213$ for type I parameter set, and $\gamma_{lim} \approx -0.3065$ for type II parameter set. The asymptotic analysis showed that for large enough $\gamma < 0$ the voltages of the neurons, $v_1(t)$ and $v_2(t)$, both diverge as $t \to \infty$ for any initial condition with $v_1(0) \neq v_2(0)$. Thus, negative values of γ can be used to estimate the boundary between *strong* and *weak* coupling for any conductance-based model, since due to the divergence of $v_1(t)$ and $v_2(t)$ for $\gamma < 0$ the predictions of the phase model have to become invalid for some $\gamma_{lim} < 0$.

In the region where coupling can be considered as weak, the region of validity with respect to γ and τ of the phase model (3.36) with a phase shift was estimated in subsection 3.4. Due to the fact that the transition from the delayed phase model to the simplified phase model with a phase shift due to the delay was done assuming that the term $\gamma\tau\Omega$ is small, we made a conjecture that the region of validity of the phase model (3.36) should depend not on the individual values of γ and τ, but on the product $\gamma\tau\Omega$.

Comparison of the theoretical and numerical values of the time delay τ corresponding to the stability switching showed that the error was nearly constant along the curves $\gamma\tau = Const$ for both parameter sets, which agreed with the estimate done in subsection 3.4. The smaller the value of $\gamma\tau$, the more accurate the predictions of the phase model. The prediction that the error would remain constant along the

lines $\gamma\tau\Omega = Const$ cannot be checked by comparison of the results for type I and type II models, since type I and type II parameter sets lead to the different phase models which may have different regions of validity.

6.1 Future work

Our asymptotic analysis has revealed a possible link between the behavior of the weakly coupled system and the synchronization of the system with strong coupling. The following question is particularly interesting:

• If a weakly coupled network has a stable synchronous state does this imply that, for large enough coupling $v_1(t) \to v_2(t)$ as $t \to +\infty$?

Moreover, since numerical analysis has shown that the in-phase periodic solution is stable for all $\gamma > 0$, it is reasonable to assume that in the case when only electrical coupling is present synchronization for weak coupling (i.e. small $\gamma > 0$) implies synchronization for all $\gamma > 0$. However, this argument is hard to verify analytically.

Another possible direction of future work consists in development of the estimates of the regions of validity of phase models. Finally, the influence of delay beyond the region of validity of the phase model with a phase shift can be studied.

Bibliography

[1] M.V.L. Bennett, *Seeing is relieving: electrical synapses between visualized neurons*, Nature Neuroscience vol. 3, no. 1 (2000), pp. 7-9 1

[2] M.V.L. Bennett and S. Zukin, *Electrical coupling and neuronal synchronization in the mammalian brain*, Neuron 41 (2004), pp. 495-511 1

[3] M. Blatow, A. Rozov, I. Katona, S. G. Hormuzdi, A. H. Meyer, M. A. Whittington. A. Caputi and H. Monyer, *A novel network of multipolar bursting interneurons generates theta frequency oscillations in neocortex*, Neuron 38 (2003), pp. 805-817 1, 27

[4] N. Buric, I. Grozdanovic amd N. Vasovic, *Type I vs. type II excitable systems with delayed coupling*, Chaos, Solitons and Fractals 23 (2005), pp. 1221-1233 2

[5] S. A. Campbell, *Introduction to delay differential equations*, Department of Applied Mathematics, University of Waterloo, 2007 71

[6] S. A. Campbell, *Time delays in neural systems*, Handbook of Brain Connectivity, editors R. McIntosh and V.K. Jirsa. Springer-Verlag, 2007 2

[7] P. Dayan and L. F. Abbott, *Theoretical neuroscience. Computational and mathematical modeling of neural systems*, The MIT Press, Cambridge, Massachusets, 2001 4, 10, 12, 13, 15

[8] L. Edelstein-Keshet, *Mathematical models in biology*, McGraw-Hill, New York, 1988 20

[9] K. Engelborghs, T. Luzyanina, G. Samaey *DDE-BIFTOOL v. 2.00: a Matlab package for bifurcation analysis of delay differential equations*, Department of Computer Science, K. U. Leuven, 2001 70

[10] B. Ermentrout *Simulating, analyzing, and animating dynamical systems*, Society for Industrial and Applied Mathematics, Philadelphia, 2002 46, 64

[11] B. Ermentrout *Type I membranes, phase resetting curves, and synchrony*, Neural Computation 8 (1996), pp. 979-1001 12

[12] T. Fukuda and T. Kosaka, *Gap junctions linking the dendritic network of GABAergic interneurons in the hippocampus*, The Journal of Neuroscience 20(2000), pp. 1519-1528 1

[13] M. Galarreta and S. Hestrin, *A network of fast-spiking cells in the neocortex connected by electrical synapses*, Nature 402(1999), pp. 72-75 1, 27

[14] J. R. Gibson, M. Beierlein and B. W. Connors, *Functional properties of electrical synapses between inhibitory interneurons of neocortical layer 4*, The Journal of Neurophysiology 93 (2005), pp. 467-480 1

[15] J. R. Gibson, M. Beierlein and B. W. Connors, *Two networks of electrically coupled inhibitory neurons in neocortex*, Nature 402 (1999), pp. 75-79 1, 27

[16] T. Heimburg and A. D. Jackson *On soliton propagation in biomembranes and nerves*, PNAS, vol 102, no. 2., 2005 12

[17] M. W. Hirsch, C. G. Pugh and M. Shub, *Invariant manifolds*, Springer-Verlag, New York, 1977 37

[18] A. L. Hodgkin *The local electric changes associated with repetitive action in a non-medullated axon*, Journal of Physiology 107 (1948), pp. 165-181 10, 12

[19] A. L. Hodgkin and A. Huxley *A quantitative description of membrane current and its application to conduction and excitation in nerve*, Journal of Physiology 117 (1952), pp. 500-544 10, 12

[20] F. C. Hoppensteadt, E. M. Izhhikevich *Weakly connected neural networks*, Springer-Verlag, NY, 1997 32, 33, 34, 36, 37

[21] L. Iannelli, K. H. Johansson, U. Jonsson, F. Vasca *Practical stability and limit cycles of dithered relay feedback systems*, European Control Conference (2003), pp. 384-389 33

[22] E. M. Izhikevich *Phase models with explicit time delays*, Physical Review E 58 (1998), pp. 905-908 37, 42

[23] C. Koch *Biophysics of computation*, Oxford University Press, New York, Oxford, 1999 7, 10, 13, 14, 28, 29

[24] Y. A. Kuznetsov, *Elements of applied bifurcation theory*, Applied Mathematical Sciences 112, Springer-Verlag, NY, 1995 64

[25] H. Lecar, *Morris-Lecar model*, Scholarpedia, 2(10):1333, 2007 4

[26] R. Llinas, *Neuron*, Scholarpedia (in review), 2008 4, 6

[27] J. G. Mancilla, T. J. Lewis, D. J. Pinto, J. Rinzel and B. W. Connors, *Synchronizaton of electrically coupled pairs of inhibitory interneurons in neocortex*, The Journal of Neuroscience 27 (2007), pp. 2058-2073 1, 27

[28] E. B. Merriam, T. I. Netoff and M. I. Banks *Bistable network behavior of layer I interneurons in auditory cortex*, The Journal of Neuroscience 25 (2005), pp. 6175-6186 1, 27

[29] C. Morris and H. Lecar *Voltage oscillations in the barnacle giant muscle fiber* Biophysical Journal 35 (1981), pp. 193-213 4, 10, 15, 18, 20, 23, 30

[30] J. A. Murdock, *Perturbations. Theory and methods*, A Wiley-Interscience Publication, NY, 1991 iii, 2, 83, 84, 89, 98, 101, 105

[31] R. E. Plant and M. Kim. *On the mechanism underlying bursting in the Aplysia Abdominal Ganglion R 15 Cell*, Mathematical Biosciences 26 (1975), pp. 357-375 18

[32] J. Rinzel and B. Ermentrout *Analysis of neural excitability and oscillations* Methods of Neural Modeling, MIT Press, 1989, pp. 135-169 4, 20, 23, 30

[33] F. K. Skinner *Conductance-based models*, Scholarpedia, 1(11):1408, 2006 4, 13

[34] A. Smith *Phase models with time delay: coupled Fitzhugh-Nagumo oscillators*, University of Waterloo Master's Essay, 2006 2, 104

[35] Tikhonov A.N. *On systems of differential equations containing parameters (in Russian)*, Matematicheskii Sbornik 27 (1950), pp. 147-156 18

[36] K. Tsumoto, H. Kitajima, T. Yoshinaga, K. Aihara, H. Kawakami *Bifurcations in Morris-Lecar neuron model*, Neurocomputing 69 (2006), pp. 293-316 23

[37] J. Wu, *Introduction to neural dynamics and signal transmission delay*, Walter de Gruyter, Berlin, New York, 2001 4

[38] M. Yoshioka, *Chaos synchronization in gap-junction-coupled neurons*, Physical Review E - Statistical, Nonlinear, and Soft Matter Physics, vol. 71, no. 6 (2005), pp. 1-4 1